ESTABLISHING A BASELINE DAMAGE INDEX FOR RELIABLE DAMAGE DETECTION: FULL SCALE VALIDATION

A Thesis

Submitted to the Faculty

of

Purdue University

by

Sriram Sivaram Krishnan

In Partial Fulfillment of the

Requirements for the Degree

of

Master of Science in Mechanical Engineering

August 2012

Purdue University

West Lafayette, Indiana

ACKNOWLEDGEMENTS

I would like to start by acknowledging my advisor, Professor Shirley Dyke, for providing me with the opportunity and guiding me through the process. Prof. Dyke gave me the freedom to explore new ideas, provided focus, direction and motivation over the two years. I would also like to thank Professor Ayhan Irfanoglu for providing valuable input during testing and during our weekly meetings. Also, I would like to thank Professor Douglas Adams and Professor Irfanoglu for their time and effort in reading, revising my thesis and being a part of my thesis committee.

I would like to thank all my team mates for a wonderful time working at Bowen labs. I would like to extend my special thanks to Charlie for working on the project, Gaby, Xiuyu and Wei for being supportive and helping me with the many technical discussions over the two years. I would also like to express my appreciation to Bowen lab staff, Kevin Brower and Harry Tidrick, for their assistance in setting up the experiments.

Finally, I would like to thank my family. Their patience and understanding has been important to my success.

TABLE OF CONTENTS

LIST OF TABLES

LIST OF FIGURES

Figure Page

Figure Page

Figure Page

Figure Page

Appendix Figure

Figure Page

ABSTRACT

Krishnan, Sriram Sivaram, M.S.M.E., Purdue University, August 2012. Establishing a Baseline Damage Index for Reliable Damage Detection: Full Scale Validation. Major Professor: Shirley J. Dyke, School of Mechanical Engineering.

There is a need to develop effective, fast, automatic and cost-effective structural health monitoring system in the near future to assist in managing our aging infrastructure. The concept of damage is not meaningful without a comparison between two different states of the system, one of which is assumed to represent the initial, and often undamaged state. In general, the modal properties estimated from the multiple sets of data from a real structure show variation in its estimates due to ambient noise, environmental variation and nonlinearities. Hence, it is important to differentiate the change in properties due to damage and environmental variables to demonstrate the robustness of the damage detection method. A drawback of most damage detection methods is that when two sets of acceptable information is passed to a global damage detection algorithm, output damage indices for the structure is obtained without providing information about the acceptability of the results obtained. To detect damage reliably in the presence of these variations, a baseline damage index needs to be established to quantify the change in the damage index due to noise in the structure. It is demonstrated that for a certain noise level in the data, when the damage indices are above a baseline damage index, the damage localization results can be trusted.

A graphical representation is used to provide a background for the proposed method. Two damage detection methods: the Angle-between-String-and-Horizontal (ASH) flexibility method and Axial Strain (AS) flexibility method are used to demonstrate the baseline damage index concept. Numerical simulation of a one dimensional beam model and three dimensional truss is used to demonstrate the development of baseline damage index and demonstrate the method. A numerical benchmarking of damage detection method is also proposed using the same concept.

Tests conducted on a 17.5-m long experimentally full-scale highway sign support truss were used to demonstrate the effectiveness of the proposed method. A series of detailed tests was used to fully characterize the vibration response of the truss in three orthogonal directions at 44 locations on the structure. Multiple input excitations such as white noise excitation using a shaker to simulate ambient vibration and hammer excitation in multiple directions, were used to excite the structure. Five damage cases are studied that replicate scenarios observed during inspection of trusses in the field. A multiple damage case has also been performed in the study. The results demonstrated successfully the applicability of the baseline damage index for reliable damage detection.

CHAPTER 1. INTRODUCTION

Over the last four decades structural health monitoring has branched out from non-destructive testing (NDT) and diversified into a very broad and rich research field in its own merit. In case of NDT testing, the approximate location of damage in complex structure needs to be known and the structure is analyzed locally to detect the damage. In the field of NDT, the requirement of damage detected methods are for localized and small damages which serve a different objective than the methods addressed in this chapter. Some of the examples of NDT techniques are Eddy current technique, acoustic or ultrasonic damage detection technique and radio graph technique. Traditionally, NDT methods are developed for a specific purpose and detect certain types of predefined damage cases.

Structural health monitoring (SHM), this new paradigm offers an automated method for tracking the health of a structure by combining damage detection algorithms with structural monitoring systems [1]. The scope of global damage detection in SHM as defined by Rytter[2]is as follows

Level 1: Determination that damage is present in the structure

Level 2: Determination of the geometric location of the damage

Level 3: Quantification of the severity of the damage

Level 4: Prediction of the remaining service life of the structure

Hence, global SHM is developed to assist detection, locating, quantifying, and predicting the life of more complex structures, where damage is defined in a more general term as change in characteristics of a structure from its initial state.

SHM techniques are used for a variety of structures such as composites, aerospace and space crafts, bridges and sky scrapers, rotating machinery. The use of various sensor technologies like static and dynamics strain gauges, accelerometers, laser vibrometry, optical sensors and piezo-sensors have extended the scope of applicability to various types of damage and structures. The uses of these types of sensors are based on application, access to damage, scale, level and type of damage. Each of these sensors, provide different types of data such as vibration signature, acoustic data, strain, deflections diffraction images. The analysis of these data differs for each type of sensor and signal measured. In civil large scale global methods, the use of accelerometer and strain sensors has gained acceptance as one of the primary methods for instrumenting structures.

With civil infrastructure the technology has many obstacles to deal with including:

1) The structures are generally very complex and large scale. Structures such as bridges have a variety of structural components like deck, tower, cables etc. which form very complex dynamics systems..

2) The need to detect damage by change in global properties rather than measuring localized changes in data signature.

3) The material property variation is less controlled than applications in composite materials and aerospace structures.

4) The effects of larger variation in the structures stiffness, mass etc. due to changes in environmental conditions such as moisture, temperature etc. that are difficult to control.

5) The inability to have a measured reference input excitation to determine the properties of the structure restrict the model development and structural assessment. This issue necessitates the modal identification from very low vibration levels from ambient excitation.

6) There is a need to apply this technology to variety of structures with similar characteristics; the method must be applicable without the use of an accurate model based on tuning and modal updating

7) The need to be able to introduce this technology cost beneficially with low maintenance costs.

The modal data obtained from all types of sensors (accelerometer, dynamic strain sensors) or any other method can be used to track the changes to the structure. Methods developed to use modal properties detect damage by investigating changes in extracted dynamic characteristics such as natural frequencies, mode shapes, damping ratios or their derivatives such as curvature mode shapes, strain mode shapes, frequency response function, transmissivity functions, flexibility matrices.

The scope of this thesis will be in analyzing modal properties of the structure from acceleration data and the methods put forward here are restricted to the specific application to global damage detection methods. The vibration response based methods are categorized according to various criteria such as level of damage detection, requirement of numerical model, physical property of the model that is tracked to

determine damage. Also, the fidelity of the methods and ease of implementation of each of the methods is an important factor to classify them.

Some of the damage detection methods are monitoring changes in modal parameters, matrix update methods, neural network based methods, pattern recognition methods, Kalman filter based methods and methods based on statistical approach.

Natural frequency of a structure is the function of stiffness and mass of the structural members. Any damage occurred in the structure causes loss of stiffness whereas the mass of the structural members remains the same resulting in the loss of the natural frequency of the structure. Thus, a decrease in a natural frequency of the structure can be used as an indicator of damage in the structure. As a natural frequency of a structure is a global property of the structure, it cannot give spatial information about damage in the structure and thus only indicate the occurrence of damage and only can be used as a level 1 damage detection technique. When the change in natural frequencies are used with the aid of accurate models of the structure level 2 damage detection is possible. Numerical sensitivity methods and damage location assurance criteria are examples for these methods. Exception to this is, modal response at higher natural mode frequencies as the mode shapes are associated with local responses at higher modes.

Mode shape information can be used to locate damage in a structure and this technique can be implemented as Level 3 damage detection technique. Damage present in structure causes change in a mode shape and relative change in the mode shape can be graphically monitored to locate damage in the structure.

Modal updating techniques use a structural model and the structural model parameters, i.e., mass, stiffness and damping, are calculated from the equations of motion

and the dynamic measurements. The matrices for mass, stiffness and damping in the model are formulated in such a way that the model response will be almost similar to the measured dynamic response of the structure. The matrices are updated with new dynamic measurements and the updated stiffness as well as damping matrix can be compared to the original stiffness and damping matrix respectively to detect the location and intensity of damage in a structure.

Another method in practice is using experimentally measured flexibility matrix. The flexibility matrix of the structure is defined as an inverse of stiffness matrix and each column of the flexibility matrix of the structure corresponds to the displacement pattern of the structure when subjected to unit force at a particular degree of freedom. The flexibility matrix can be derived by calculating mass-normalized mode shapes and natural frequencies. An advantage of these methods are the need for only lower natural frequency modes and their corresponding natural frequencies.

1.1 Purpose

The global higher transportation network operates about 2.5 million bridges. The current bridge management systems are rating them by various methodologies. This results in very inhomogeneous figures for bridge health and structural ratings. The U.S. Federal Highway Agency[3] stated in 2001 that 28% of their 595.000 bridges are rated deficient. Only a portion of it (about 15%) has structural reasons. In Europe this figure varies around 10%. No figures are available from the Asian networks. Nevertheless if we consider an average of 10% deficiency, there are about 250.000 bridges that definitely require structural health monitoring. ASCE Report Card for America's Infrastructure[4,5] gave a "D" grade for the overall infrastructure system (by ASCE grade scale, a "C" is

average), and estimated a cost of $ 2.2 trillion needs to be invested over 5 years to bring the condition to “B”; a good condition[4]. Structural health monitoring and damage detection is important to maintain safety and integrity of structures, to increase their life span, and to reduce total life-cycle maintenance costs[4].

There is a need to develop an effective, fast, automatic and cost-effective structural health monitoring and damage detection system due to the failures of bridges around the world such as the I-35W highway bridge over the Mississippi River in Minneapolis, Minnesota, US. The need for global SHM system is to assist the current existing practices of visual inspection and quantification. For a large bridge, it is quite difficult to perform visual inspection quickly and in limited time duration due to the need for safety inspectors to inspect the structure visually. Hence, the global monitoring system will assist the visual inspection to decide when visual inspection needs to be performed and which locations needs to be checked for damage. Also, in general, routine inspections on structure are performed at fixed intervals depending on the life cycle evaluation and recommendation of the inspectors based on safety guidelines. But there is a need to have inspections on a need-to basis to reduce maintenance costs and life. The implementation of online SHM systems will enable quick preventative maintenance, monitoring and timely decision-making for critical structures.

The SHM community is addressing some of the issues to move the technology from laboratory to real world. The use of wireless sensors to reduce cost of implementation for large scale structures is an important undertaking to move in this direction. With the size, complexity and variety of structure present in the field, the need to develop cost effective strategies to instrument structures has gained importance in civil

engineering. With the implementation of wireless sensors, to tackle the issues or data synchronization, sampling, data correlation between sensors, new branches of computational SHM and electronics has emerged. This implementation has introduced a multidisciplinary area where SHM, networking and electronics come together to implement the damage detection scheme. Such wireless monitoring systems are assembled from low-cost wireless sensors that collocate sensing, communication and computing in a single device. Wireless sensors for structural health monitoring application has progressed with the initial contributions of Kiremidjian[6], Lynch[7]; Spencer[8].

In the recent past, there has been a drive to instrument real structure and study the responses from these real structures. One of the first field studies performed was by Farrar et.al.[9, 10] on the Alamosa Canyon bridge in New Mexico in 1996. Multiple tests were conducted to study the variation in modal properties with environmental effects and detailed in a number of papers. Figure 1.1 shows the frequencies of the first mode and temperature differential between the east and west side of the bridge against the 24 hour completion time of the field test. The modes shapes vary by approximately 5% during the 24 hour time period[10].

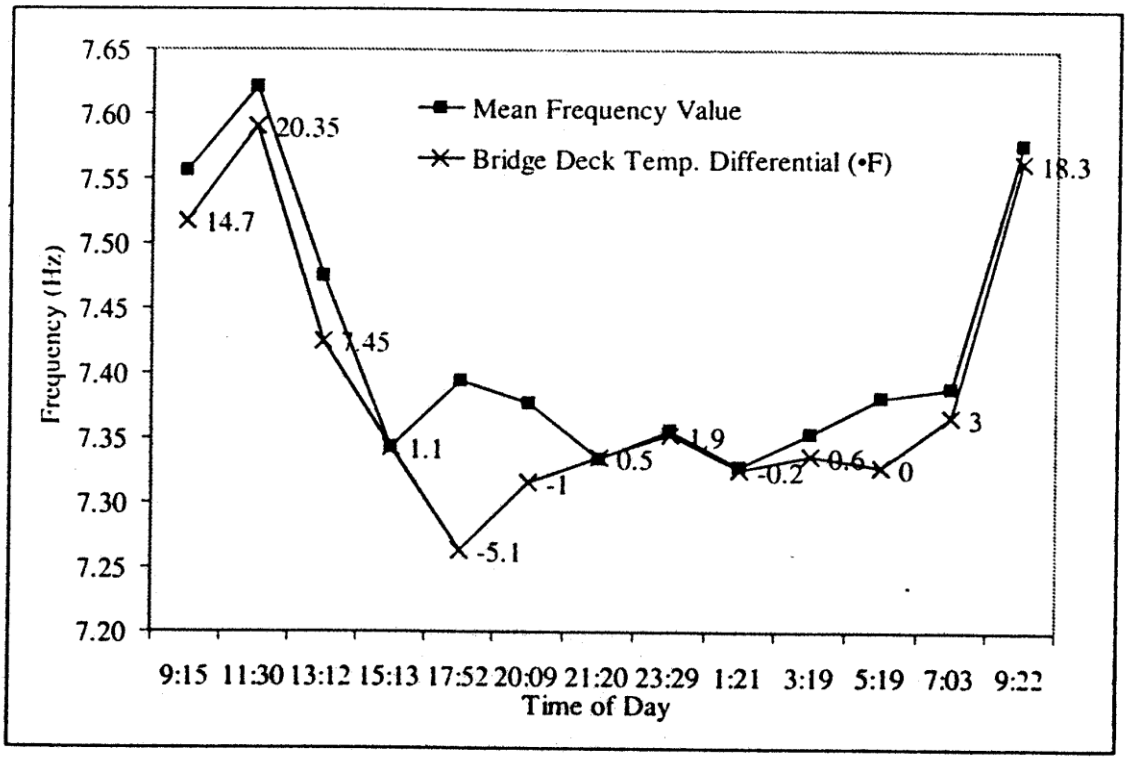

Figure 1.1: Variation of the frequencies over 24hr period from the Alamosa canyon bridge.

In another study, the Donghai Bridge[11,12,13] was instrumented with sensors to automatically collect the data of displacement, force, acceleration of the structure throughout the construction and initial life of the structure. The SHM system installed on the bridge has collected data to describe the healthy condition of the bridge under different types of loadings (wind, ground motion, wave and etc.), different types of environmental variations (such as temperature, moisture and etc.). Data mining performed on the data between the dates of January 1st and August 31st 2007. Figure 1.2 (a) show the variation of the natural frequency of the 3rd mode with respect to temperature during this period. This large variation is not caused by damage but due to changes to the structure due to ambient temperature changes and other unmeasured

factors. The correlation obtained between the modal properties and temperature can applied to compensate for the change in temperature but it is difficult to reduce the noise due to other environmental variations, if they are not measured. Figure 1.2 (b) shows the correlation between temperature and frequency.

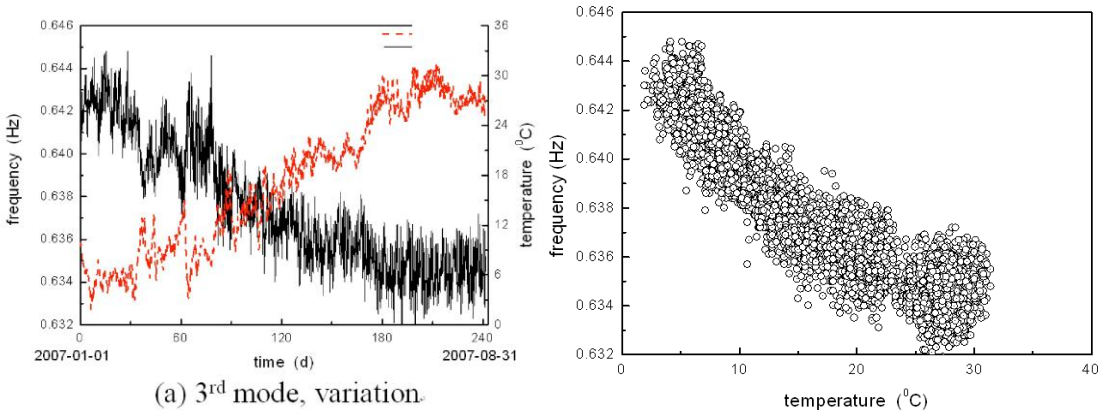

Figure 1.2: Donghai bridge data for the 8 month period (a) Variation of estimated frequencies and temparature, (b) Correlation of frequency and temperature.

Some of the other examples of implementation in real world are Z-24 bridge near Zurich[14], Golden Gate bridge, Jindo bridge in S. Korea, Guangzhou New TV Tower, Henry Hudson Bridge in New York City and many newer projects around the world.

The SHM methods are still in its infancy and the industry is still not convinced of the robustness of damage detection methods for civil infrastructure with the current cost to benefit ratio. Previous work done on instrumenting real world structures, has only been used for model updating or model identification, and full damage detection validation is still restricted to experimental laboratory based environmentally controlled structures.

To push this technology into the next phase the method applied must satisfy a few more criteria as described. Non-model based damage detection methods have a very direct easy to use, easy to implement, scalable architecture that satisfies many of the criteria. Some of the limitations are that they are based on generally uniform structures,

comparing relative change in parameters (necessary to have peaks), user based decision making, does not have criteria to accept or reject the damage indices. The damage indices is scaled to have the maximum value to be 1 or with respect to the baseline modal properties. Also in literature, there are no cases as of yet reported where damage detection was used to find damage in real structures, most damage detection implementation is to detect damage in prior known damage, created for verification.

1.2 Scope

A major setback to validation of a damage detection algorithm is that the results are not presented for repetitions of multiple data sets for the same cases to establish that the accurate localization (level 2 damage detection) results were not an artifact of the specific modal realization due to extraneous noise in the system from various environmental factors and modal estimation methods.

To a degree, all damage detection methods have consistent theoretical basis and can be proved numerically with perfect ideal systems, but problems and issues begin when testing the robustness of the method using experimental data. Hence, the question is whether or not a method can operate successfully with quality of information that can be collected in the field[15]. Also, it is important to know an estimate of the smallest damage that can be detected for a certain baseline or threshold limit predicted. Hence, it is necessary to demonstrate that the damage detection methods insensitive to changes in modal estimates from the same structure due to noise and highly sensitive to damage to all parts of the structure.

Another issue is that even though a threshold is determined from the assumption of the noise levels in the final modal estimated used for the damage detection, this varies

depending on modal estimation method used and other parameters of the estimation process. Therefore, the use of a standard threshold or baseline damage index from experience or intuition could lead to constraining or relaxing the results.

In this thesis, some of these concerns are addressed by developing a baseline damage index determined from data to improve the reliability of the damage detection results and demonstrate a method to benchmark a damage detection method numerically.

Chapter 2 presents a graphical representation of the concept and the method to evaluate the baseline damage index from the data. The chapter presents a guideline to benchmark a damage detection method to amount of damage that can be reliably localized relative to the noise in the data. Numerical validation of the method is performed on two models: A one dimensional beam model and three dimensional beam model of the experimental highway sign support truss.

Chapter 3 presents the full scale highway sign support truss, the testing framework and the damage cases studied. The modal identification scheme used to evaluate the modal properties and its variation is presented. Lastly, the damage detection method and results for five damage cases are presented.

Chapter 4 presents a summary of the baseline damage index developed and key results from the numerical and experimental validation.

CHAPTER 2. THEORETICAL ANALYSIS

2.1 Introduction

The field of damage identification is very broad and encompasses both local and global methods. Here, the focus is restricted to global methods that are applicable to large scale structures and use changes in vibration characteristics of the structure to detect damage. These vibration characteristics, commonly measured modal parameters (notably frequencies, mode shapes, and modal damping) are dependent on the physical properties of the structure (mass, damping, and stiffness). Hence, changes in the physical properties, such as reductions in stiffness resulting from change in elastic modulus due to cracks or material degradation will cause detectable changes in these modal properties. Doebling et. al.[16] noted that because changes in modal properties are being used as indicators of damage, they need to be determined accurately for good damage detection results. Many different issues are critical to the success of using the observed changes in vibration characteristics of a structure for damage identification and health monitoring. Among the important issues are excitation and measurement considerations, including the selection of the type and location of sensors, and the type and location of the excitations.

From past literature it was observed that there is a large selection of methods developed to perform global damage detection. Numerous studies on damage

detection are performed using numerical models to describe the applicability, performance and benefit of the damage detection algorithm. Some classes of methods studied are based on change in curvature[17], mode shapes[18], natural frequencies[19] and dynamically measured flexibility[20] Also, there are a class of methods based on updating structural model parameters classified as optimal matrix update method[21,22], sensitivity based update[23,24], eigen-structure assignment method[25] and many more.

One specific class of methods, the dynamic measured flexibility based method, is considered in this thesis. In this chapter, a guide to benchmarking of various damage detection algorithms is constructed to establish the baseline damage index for damage detection. The evaluation of the baseline damage index is described and the method is demonstrated numerically using a one dimensional beam model and a three dimensional space truss.

2.2 Flexibility Based Methods

Flexibility based damage detection methods have gained popularity in recent past due to the following definitive features of the flexibility matrix. The dynamic flexibility matrix can be calculated accurately using a subset of the lower modes of the structure. Hence, only the lower modes need to be estimated accurately. For civil infrastructure, this approach is very helpful. Ambient vibration or low power shakers can be used to excite the lower modes of a civil structure more readily than higher modes. Research on how to construct the complete structural flexibility from the measured modes have been conducted by some researchers[20].

The flexibility based method is also easy to implement. These methods may not require a prior accurate model or known approximate material properties and machine

learning or dynamic model updating to estimate the location of damage. The interpretation of the result from these methods is also straight forward and has excellent scalability[26]. Flexibility based method are also data centric. Some of the methods can determine damage location without the external information about the structure but use only the basic wireframe models.

Based on the fact that the presence of damage in many classes of structures reduces structural stiffness, and hence increases structural flexibility, the change in structural flexibility between the pre- and post-damaged states can be used to detect damage. The flexibility matrix of the structure is defined as an inverse of stiffness matrix and each column of the flexibility matrix of the structure corresponds to the displacement pattern of all the Degrees of Freedoms (DOFs) of the model when subjected by a unit force at a particular DOF. A method developed by Yan et.al.[27,28] uses similar concept of classical flexibility and defines the Angle-between-String-and-Horizontal (ASH) flexibility and the Axial-Strain (AS) flexibility method depending on the assumed unit load on the structure. These two methods will be used to demonstrate the concepts presented in the rest of the thesis.

2.2.1 Angle between String and Horizontal Flexibility Damage Detection Method

The ASH flexibility is defined for beam-type structures. The components in the *ith* column of this flexibility matrix represent the ASHs of all elements resulting from a unit moment applied at the two nodes of element *i* (as a couple with opposing forces applied at the two end nodes of element *i*), and no force or moment on the other elements.

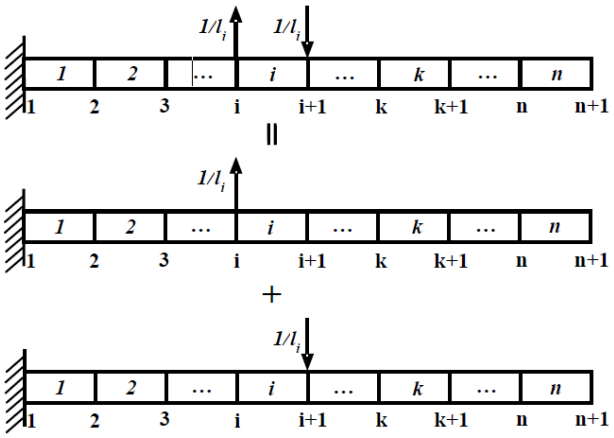

Figure 2.1:Superimposition of loads.

This moment can be split into two forces acting at adjacent nodes *i* and *i+1*. The *ith* column of the classical flexibility matrix represents the deflection of all of the DOFs resulting from a unit force applied to *ith* DOF and no force or moment on other DOFs. Hence, from the definition of classical flexibility and the superposition of the unit load as shown in Figure 2.1, the ASH flexibility at all DOFs is evaluated as

$$F_{\theta\,k,i} = \frac{1}{l_k}\frac{\left[\left(F_{k+1,i+1} - F_{k+1,i}\right) - \left(F_{k,i+1} - F_{k,i}\right)\right]}{l_i} \tag{2.1}$$

where, l_i is the length of the *i*th element and $F_{k,i}$ is the deflection at node *k* resulting from a unit force at node *i*, is the classical flexibility matrix, which can be evaluated using modal information of mode shapes and natural frequencies obtained from dynamics testing as shown in

$$F = \Phi\Omega^{-1}\Phi^T = \sum_{r=1}^{n}\frac{1}{\omega_r^2}\varphi_r \cdot \varphi_r^T \tag{2.2}$$

where, φ_r and ω_r are the *r*th mode shape and circular natural frequency of the structure; *n* is the number of modes used, which is given by

$$\varphi_j = \begin{Bmatrix} \varphi_{y1j} \\ \varphi_{y2j} \\ \vdots \\ \varphi_{yij} \\ \vdots \\ \varphi_{ynj} \end{Bmatrix}. \quad (2.3)$$

Damage detection using the ASH flexibility matrix is performed by calculation of the difference between the damaged and undamaged ASH flexibility as shown in

$$\Delta F_\theta = F_\theta^d - F_\theta^u. \quad (2.4)$$

The damage indices for each of the elements is taken as maximum absolute values or diagonal values of the components in each column of ΔF_θ and elaborated as

$$\Delta F_{\theta\,d} = [\Delta F_{\theta 11} \quad \Delta F_{\theta 22} \quad \cdots \quad \Delta F_{\theta ii} \quad \cdots \quad \Delta F_{\theta n-1n-1} \quad \Delta F_{\theta nn}] \quad (2.5)$$

or,

$$\Delta F_{\theta\,m} = [\max(\Delta F_{\theta 1}) \quad \max(\Delta F_{\theta 2}) \quad \cdots \quad \max(\Delta F_{\theta i}) \quad \cdots \quad \max(\Delta F_{\theta n})]. \quad (2.6)$$

2.2.2 Axial Strain Flexibility Damage Detection Method

The ASH flexibility damage detection method is extended to structures with axial load bearing members. In the method proposed by Yan et. al [28] a more feasible flexibility for damage detection is proposed for truss-like structures with primarily axial strain deformation . This Axial Strain flexibility matrix is evaluated from the three dimensional mode shapes and natural frequencies of complex structures. The elements in the *ith* column of the AS flexibility represent the axial strains of all elements or members resulted from a pair of axial forces with equal amplitudes, which are equal to the reciprocals of the length of the *ith* member, but opposite directions applied at two nodes of the *ith* member. This definition is based on the force-bearing characteristics of this kind of structure[28].

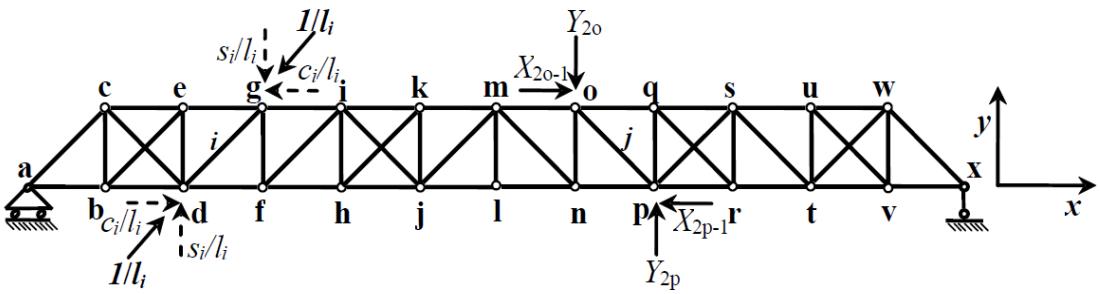

Figure 2.2:The definition of Axial Strain Flexibility.

From Figure 2.2, the opposing axial forces pair on the ith element can be separated into their *X* and *Y* components. The pair of forces in the *x* and *y* direction are dependent on the orientation of the member being evaluated. The contribution of the pair of forces in the *Y* direction to the axial deformation flexibility matrix can be evaluated similar to the ASH flexibility discussed above using the *Y* direction classical flexibility matrix evaluated from the *Y* direction mode shapes and natural frequencies. Similarly the contribution of the *X* component pair forces to the axial deformation flexibility can be evaluated from the *X* direction mode shapes and circular natural frequencies as

$$\delta X_j = \frac{c_i}{l_i}\left[\left(F_{2o-1,2d-1} - F_{2o-1,2g-1}\right) - \left(F_{2p-1,2d-1} - F_{2p-1,2g-1}\right)\right] + \frac{s_i}{l_i}\left[\left(F_{2o-1,2d} - F_{2o-1,2g}\right) - \left(F_{2p-1,2d} - F_{2p-1,2g}\right)\right] \tag{2.7}$$

$$\delta Y_j = \frac{c_i}{l_i}\left[\left(F_{2p,2d-1} - F_{2p,2g-1}\right) - \left(F_{2o,2d-1} - F_{2o,2g-1}\right)\right] + \frac{s_i}{l_i}\left[\left(F_{2p,2d} - F_{2p,2g}\right) - \left(F_{2o,2d} - F_{2o,2g}\right)\right]. \tag{2.8}$$

where, $F_{2o-1,2d-1\ to\ 2o,2d}$ are the deflection for both *X* and *Y* directions at *dth* DOF when a unit load is applied in the *X* and *Y* direction at the *oth* DOF.

The classical flexibility matrix, which can be evaluated using modal information of mode shapes and natural frequencies obtained from dynamics testing as shown in

$$F = \Phi\Omega^{-1}\Phi^T = \sum_{r=1}^{n} \frac{1}{\omega_r^2}\varphi_r\varphi_r^T \tag{2.9}$$

where,

$$\varphi = \begin{Bmatrix} \varphi_{x1} \\ \varphi_{y1} \\ \varphi_{x2} \\ \varphi_{y2} \\ \vdots \\ \varphi_{xi} \\ \varphi_{yi} \\ \vdots \\ \varphi_{xn} \\ \varphi_{yn} \end{Bmatrix}. \tag{2.10}$$

Finally, the axial deformation in the direction of the members is evaluated from the axial deformation in the *X* and *Y* direction by resolving the components in the orientation of the member as shown in

$$\delta l_j = c_j \delta X_j - s\delta Y_{.j.} \tag{2.11}$$

The Axial Strain flexibility is evaluated by dividing each of the members by its length to get the strain associated with the unit axial load applied, as described in

$$ASF_{ji} = \frac{\delta l_j}{l_j} = \frac{c_j \delta X_j - s_j \delta Y_j}{l_j}. \tag{2.12}$$

Damage detection using the AS flexibility matrix is performed by calculating the difference between the damaged and undamaged AS flexibility matrices as

$$\Delta ASF = ASF^d - ASF^u. \tag{2.13}$$

The damage index for each of the elements is taken as diagonal values of the components in each column of ΔASF as shown in

$$\begin{aligned} &\Delta ASF_d \\ &= [\Delta ASF_{11} \quad \Delta ASF_{22} \quad \cdots \quad \Delta ASF_{ii} \quad \ldots \quad \Delta ASF_{n-1n-1} \quad \Delta ASF_{nn}]. \end{aligned} \tag{2.14}$$

2.2.3 Advantage of ASH Flexibility and AS Flexibility Method

The damage detection methods presented above have many advantages over classical flexibility methods. These methods have been proven to be robust in detecting multiple damages at once accurately with relative insensitivity to the boundary conditions. The classical flexibility methods have been shown to fail at detection of multiple damage locations in cantilevered structures [27].

Directly project the damage index to the correct element rather than to adjacent nodes or degree of freedom.

1) One feature of the ASH flexibility is that the components in the ASH flexibility matrix are associated with elements instead of nodes or DOFs.
2) Only lower frequency modal behaviors are required to evaluate the flexibility matrix accurately.

2.3 Proposed Benchmarking Scheme for Damage Detection Methods

In this section, the geometrical interpretation of the modal properties space is established. Also, the reasoning behind and need for a data-intensive-baseline to assist any damage detection method is discussed. The data-intensive baseline will facilitate the benchmarking of damage detection algorithm using numerical simulation. This data-intensive baseline will also remove some of the dependence on human decision making once the damage detection algorithm presents the damage indices.

The structure that is used for the numerical analysis is an important consideration when one studies a damage detection algorithm. Therefore, it is necessary to develop a benchmarking scheme to rate structures. This approach is necessary because when numerically validating damage detection algorithm on a variety of structure, some

parameters need to be defined to establish the complexity of the structure and sensitivity of the measured DOFs to damage in the structure. From the literature related to damage detection algorithms, there are no standard structures that are used to benchmark the new damage detection algorithms being developed. Most researchers design the numerical models to replicate the experimental structure used for the experimental validation. Hence, there is no way to directly compare different methods. Separate studies by other researchers are being conducted to compare the different methods on ASCE benchmark structure now.

In the numerical study presented in the next sections, a simple one dimensional beam and a complex three dimensional space truss are studied. The ASH flexibility damage detection algorithm is applied to both structures with various damage elements. The numerical analysis of the AS flexibility method is not discussed here but has been applied to the experimental structure in the next chapter.

2.3.1 Modal Properties Space Concept

The graphical representation of the change in modal properties and the evolution of the properties of the structure is presented. Let us assume that we have a structure under consideration. The main modal properties of a structure that are used are natural frequencies, mode shapes and modal damping. The exact realization of the modal properties of the structure at a nominal environmental condition is represented by a point in an n dimensional modal properties space. The realization of the same intact structure when estimated from real world data with noise results in points in the modal property space that is other than the exact realization. Every set of data acquired with varying environmental conditions have different quantities of systemic and random noise present

in the vibration data at all sensor location. This data is then processed using any of the modal estimation processes to evaluate the modal properties. Since the environmental parameters are different and ambient noise is present in the data, the modal properties estimated are not exactly same every time. During modal estimation if we perform averaging and zero padding etc. we can reduce the noise but never fully eliminate it.

When all these modal realizations are graphically presented on the n dimensional modal properties space as points they form a cluster around the perfect ideal case.

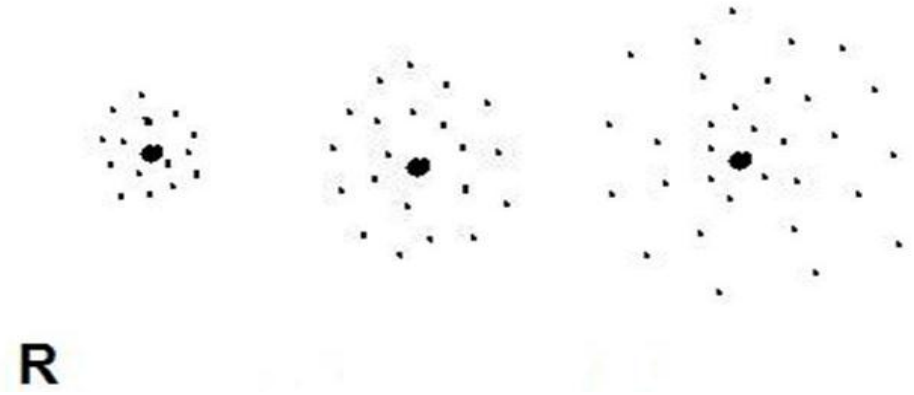

Figure 2.3: Graphical representation of modal realization of intact structure with noise.

Figure 2.3 shows the size of the cluster depending on the amount of variance in the data due to various factors. As the noise in the system increases, the "radius" of the cloud increases, assuming the modal estimation process, number of averages and filtering, are kept the same.

Damage in the structure also causes change to the modal properties of the intact structure and can be graphically represented. In this study, damage is assumed to be linear, i.e. the vibration response of the structure can be modeled by a linear system of equation. Assuming the *n* dimensional space is chosen such that the modal realizations of increasing extent of the same damage are along a vector in the modal properties space.

Assuming noise is present, when multiple sets of data and their modal realizations are graphically represented on the same modal properties space we obtain a cloud around the perfect realization of the damaged location as well. Similarly, various cases of damage to the structure can be assumed to lie on vectors orthogonal to each other in the same modal properties space. This is a valid assumption because of the assumption of linear damage.

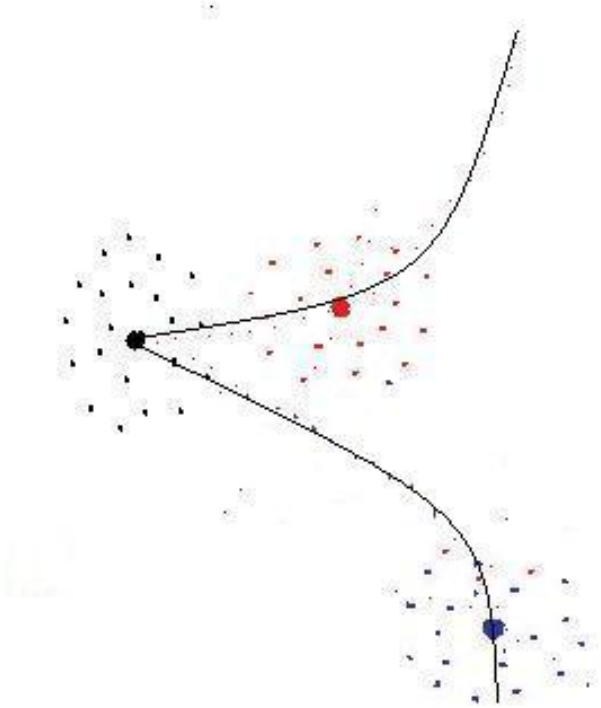

Figure 2.4: Intact and Damage realization in modal properties space

In Figure 2.4, black points represent the intact structure, blue points- damage 1 and red points- damage 2. The two solid lines show the damage progression for the two damage cases with increasing damage. Also, it is assumed that the noise level is consistent in all the data cases, resulting in similar cluster size of the modal realization of all cases. When the damage extent is small, the clusters of the damage cases are very close to the intact case and overlap, making the modal realizations of the damaged cases

indistinguishable from each other and the intact case. This graphical representation serves to describe the structure in the modal properties space.

The damage detection method in the modal space is assumed to be a *n* dimensional sphere centered at the ideal exact damage estimate, within which all modal points will represent a particular damage location. Damage detection method, localizes damage to a particular node, element or sub-structure, i.e., the damage detection methods are not continuous, but detect damage only to discrete entities. Hence, it can be assumed that the damage detection method has a "region of influence" about a damage estimate. Hence, when the region of influence of a damaged location contains points from other damages, the damage detection method will still locate the damage to the correct region of influence.

Hence in the case of high noise or low level of damage, the modal estimates for intact and damaged cases could overlap in the modal properties space and the damage could be located to an incorrect location.

With the concept, the baseline damage index is established as developing a radius for the cloud of the modal estimates. As described above, for a certain noise level the structure is represented as a cloud of points in the modal space. Hence, when the damage is small, the clouds of points for the intact and damaged cases intersect and points in this intersection cannot be distinguished. Hence, when the damage is large enough the two clouds separate and the damage index between the intact and damage cases will be larger than the established baseline damage index and the damage will be reliably detected to the correct location. In this chapter, this idea will be demonstrated numerically and a

framework is established to use this method as a method to benchmark damage detection methods.

2.3.2 Method to Rate the Structure and Damage Extent

When performing a numerical study of damage detection algorithm on different structures, the effect of change in property of an element of the structure or damage needs to be understood to be able to compare results and evaluate various damage detection methods. We need a measure to compare the damage extent on different structure.

Consider two structures, one dimensional beam and a complex space truss. Damage is induced on similar elements in both structures by reducing the elastic modulus of the elements. This damage is clearly of different magnitude from the context of the global stiffness of the structure. Hence, there is a need to evaluate and rate the complexity of the structure when benchmarking different structures.

Many studies are being performed by various researchers to evaluate the optimal set of sensors required to be placed on the structure to reduce cost and detect various locations of damage[30] These studies are performed to find the best distribution of sensors to have highest observable of the change in structure due to damage.

When the structure is complex and the sensors are placed in a few locations on the structure, the experimental realization of the structure is reduced to the measured DOFs. Therefore, it is necessary to quantify the effect of change in material property or damage at different locations of the structure at the measured DOFs. In this study, the mode shapes and natural frequencies are used to characterize the observability of the various damages.

2.3.2.1 Global Stiffness Change

The governing system of equation for the small oscillation of structures can be represented by

$$[M]\{\ddot{u}\} + [C]\{\dot{u}\} + [K]\{u\} = \{f\} \tag{2.15}$$

where,$[K]$, $[M]$ and $[C]$ are the global stiffness, global mass and global damping matrices of the discretized system. The only non-trivial solution for solving the homogeneous equation of motion (without damping) is evaluating the determinant to be zero, as shown in

$$\left[-[M]\omega^2 + [K]\right]\{u\} = 0. \tag{2.16}$$

This equation is recognized as the familiar eigenvalue problem. ω^2 are the eigenvalues and $\{\tilde{u}\}$ are the eigenvectors. There are as many eigenvalues as the order of the system of equations. Hence, the solution yields *N* eigenvalues (ω_{1-N}) and *N* corresponding ($\{\phi\}_{1-N}$) eigenvectors. The system of equation can be diagonalized by pre-multiplying by the transpose of modal matrix and post-multiplying with the modal matrix. This diagonalization separates the *N* variable system of equation to *N* single variable equations to solve for the eigenvalues or natural frequencies of the system as

$$[\Phi]^T[M][\Phi]\omega^2 = [\Phi]^T[K][\Phi] \tag{2.17}$$

$$\begin{bmatrix} M_1 & \cdots & 0 \\ \vdots & \ddots & \vdots \\ 0 & \cdots & M_N \end{bmatrix}\{\omega^2\} = \begin{bmatrix} K_1 & \cdots & 0 \\ \vdots & \ddots & \vdots \\ 0 & \cdots & K_N \end{bmatrix} \tag{2.18}$$

where, M_{1-N} are the modal masses and K_{1-N} are the modal stiffnesses for the system. Hence, the natural frequencies are given by

$$\omega_{1\ to\ n} = \sqrt{\frac{K_{1\ to\ N}}{M_{1to\ N}}}\ rad/s. \tag{2.19}$$

Damage throughout this study is considered to be a change in the stiffness property of the structure without change in mass distribution. The natural frequencies of the damaged structure can be evaluated similarly and can be represented as

$$\omega^{d}_{1\ to\ n} = \sqrt{\frac{{K_{1\ to N}}^{d}}{M^{d}_{1to\ N}}}\frac{rad}{s}. \tag{2.20}$$

To obtain a numerical estimate of the damage in various locations and for comparing damage in different structure, the percentage change in global stiffness or modal stiffness can be evaluated from the change in natural frequencies between the healthy and damaged cases, as shown

$$\frac{{K_{1\ to\ N}}^{d} - {K_{1\ to\ N}}^{u}}{{K_{1\ to\ N}}^{u}} = \frac{(\omega^{d}_{1\ to\ n})^2 - (\omega^{u}_{1\ to\ n})^2}{(\omega^{u}_{1\ to\ n})^2}. \tag{2.21}$$

2.3.2.2 Modal Assurance Criteria (MAC)

The modal assurance criterion (MAC) can be defined as the correlation coefficient between two mode shapes. It defines the consistency in the shapes of the mode shapes from the two cases considered. If the coefficient is equal to 1.0, then the two shapes are perfectly correlated. If the coefficient is any value less than 1.0, then there is some degree of inconsistency in the mode shapes being compared and to some degree, proportional to the value of the factor. MAC is evaluated between two modes as

$$MAC = \frac{|\{\varphi_1\}^T\{\varphi_2\}|}{|\{\varphi_1\}^T\{\varphi_1\}||\{\varphi_2\}^T\{\varphi_2\}|} \tag{2.22}$$

where, φ_1 and $\varphi_2$are two mode shapes that are evaluated to check their consistency.

This inconsistency can be caused by either damage in structure (change in stiffness characteristics) or the presence of noise and nonlinearities in the measured data.

The MAC is calculated in the current study to evaluate the change in the mode shapes between healthy and damaged states when the damage is increased in the structure and is calculated as

$$MAC_i^{hd} = \frac{([\Phi_m]^{h^T}[\Phi_m]^d)_{ii}}{([\Phi_m]^{h^T}[\Phi_m]^h)_{ii} \cdot ([\Phi_m]^{d^T}[\Phi_m]^d)_{ii}} \tag{2.23}$$

where, h and d represent healthy and damaged state, i refers to the mode shape being compared and $[\Phi_m]^h$ is the modal matrix at the measured DOFs for the healthy case and $[\Phi_m]^d$ is the measured modal matrix for the damaged case.

In general, for global damage detection methods, another concern is reducing the number of sensors used to instrument the structure. Hence, the MAC is estimated only at the measured degree of freedom. This gives a relative evaluation of the extent of change in mode shapes projected on the measured degree of freedom. Damage to any part of the structure will change the modal properties of the structure, but if this change is not reflected at the measured DOF then the damage is not observable.

Two numerical examples are evaluated to validate and demonstrate the methodology presented above. The structures are compared using the global stiffness change and MAC to compare the similar extent of damage in both structures. Also, with the aid of these parameters, it is shown that the quality of the damage detection method is independent of the structure.

2.4 Numerical Demonstration - One Dimensional Structure

This one dimensional truss is modeled using 12 nodes, 11 beam elements to construct a finite element (FE) model. Cylindrical geometry was assumed for all the members. A FE model of the test beam was developed in MATLAB using the toolbox developed by

Caicedo. Fixed conditions for all DOF were defined both at the left support and right end supports. Finally, mass proportional damping was introduced in the homogeneous equation of motion. The exact values of the first 25 natural frequencies and corresponding mode shapes of the truss are calculated from the state space realization of the FE model. The properties of all elements are given in the Table 2.1.

Table 2.1: Material and Cross-sectional properties of the 1D beam model

	E (N/m^2)	G (N/m^2)	Rho (Kg/m^3)	
Material	6.96E+10	2.62E+10	2.71E+03	
	Ixx (m^4)	Iyy (m^4)	Area (m^2)	J (m^4)
Section	9.79E-06	8.52E-07	3.76E-03	1.06E-05

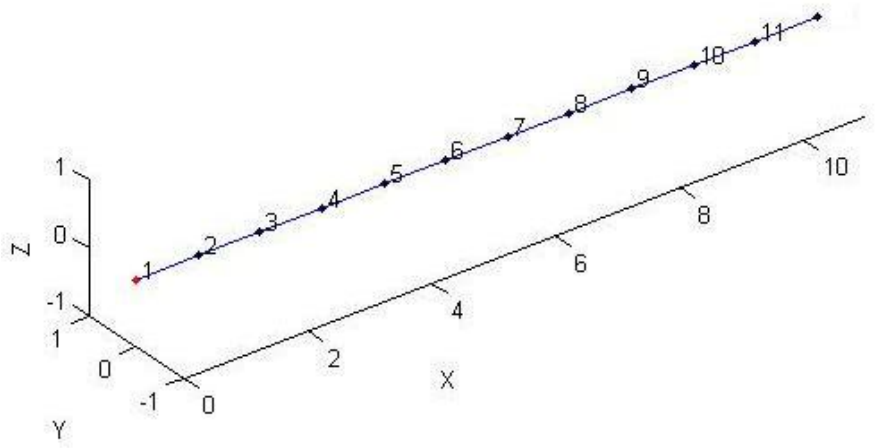

Figure 2.5: One dimensional fixed-fixed beam model.

2.4.1 Setup of the Cases

The numerical simulation of the beam described above is performed with various modifications to the structure to evaluate the effects of system noise, damage extent and damage location. In this section, the various cases studied to evaluate the damage detection method on the healthy structure is described. To distinguish between the damaged location and the detected locations, in the future discussions, Element, is used to refer to the discretized element of the numerical model that are damaged for the various

cases and damage is localized to a certain bay location. In the present case the element numbers and bays are one and the same. The damage to an element of the structure is induced by reducing the elastic modulus by a certain percentage. In the one dimensional numerical validation the elastic modulus is reduced by 10%, 50% 90% and 99%.

The ASH flexibility and AS flexibility damage detection methods are developed based on linear damage models and can track only changes to linear behavior of the structures. Noise in this study is classified as any variation in the measurement that cannot be modeled by the ideal perfectly linear model of the structure. Hence, noise includes any variable that changes the property other than the control variable: damage to the healthy linear model of the structure. Hence, noise can arise from environmental noise, environmental variation like temperature and humidity variation and its associated nonlinearities in material properties, variation due very small changes in mass distribution, environmental degradation, noise from data acquisition system and other nonlinearities in the structure. To replicate this noise, random noise is added to the numerical simulation at various stages when performing the study. The system identification process reduces the noise in the data traces for the acceleration response by using filters and windowing. All modal estimation schemes reduce the random noise by filtering, averaging, tuning etc. But, it is never possible to fully eliminate noise in the final modal properties estimated. The process of system identification for data compression is a computationally intensive process. For this study a large number of cases need to be evaluated and to reduce the need to performing large amount of system identification repeatedly, for simplicity, random noise of 1% 5% and 10% of absolute magnitude of the mode shape vectors are added as shown.

$$\varphi_{noise} = \varphi + \%noise \cdot rand(-1,1) \cdot avg(|\varphi_i|) \qquad (2.24)$$

2.4.2 Damage detection results for 1D model – no noise

Damage detection with perfect data, with no added noise, needs to be presented before analysis with noise is performed. For the 1D fixed- fixed beam structure case with 11 elements, damage indices is indicated in these three dimensional bar plot. This strategy is used to describe a large amount of cases in a single plot and to interpret the results effectively. The method to interpret the plots is described. Each element of the numerical model is damaged (elastic modulus reduced) and the damage indices for the 11 bays are evaluated. The damage indices for each of the elements damaged is shown using a different color as each column of the bar plot. For example, the damage indices at the 11 elements for stiffness reduction at first element is shown in the first column in blue and similarly stiffness reduction at element 7 is shown in the yellow bar plot at column 7.

Also, varying levels of damage to the elements are induced by reducing the elastic modulus by 10%, 50%, 90% and 99%. It has to be mentioned that no noise has been added to the mode shapes in this analysis. Hence, this obtained distribution and accuracy of damage detection is the best possible result that can be obtained with the level of damage in the elements using the ASH damage detection method. Perfect results for the damage indices would be when the maximum indices for each column corresponds to the same bay as the damaged element, i.e. the bar plot forms a diagonal with the tallest bars. As observed in Figure 2.6 (a) the taller bars for each of the damaged elements have a diagonal pattern, but are at the correct bay or the adjacent bay at 10% reduction in modulus. Hence, damage is localized to within the adjacent bay with 10% reduction in elastic modulus. Hence, it can be concluded that the “domain of influence” for this

damage detection method for a certain location at 10% damage also contains the adjacent elements. Similarly, this pattern can be observed in Figure 2.6 (b) and Figure 2.6 (c) for 50%, and 90% reduction in stiffness property. In Figure 2.6 (d) with 99% reduction in elastic modulus the damage is localized to the correct bay and the magnitude of the maximum damage index is significantly larger than the average value and detects the damage to the exact bay.

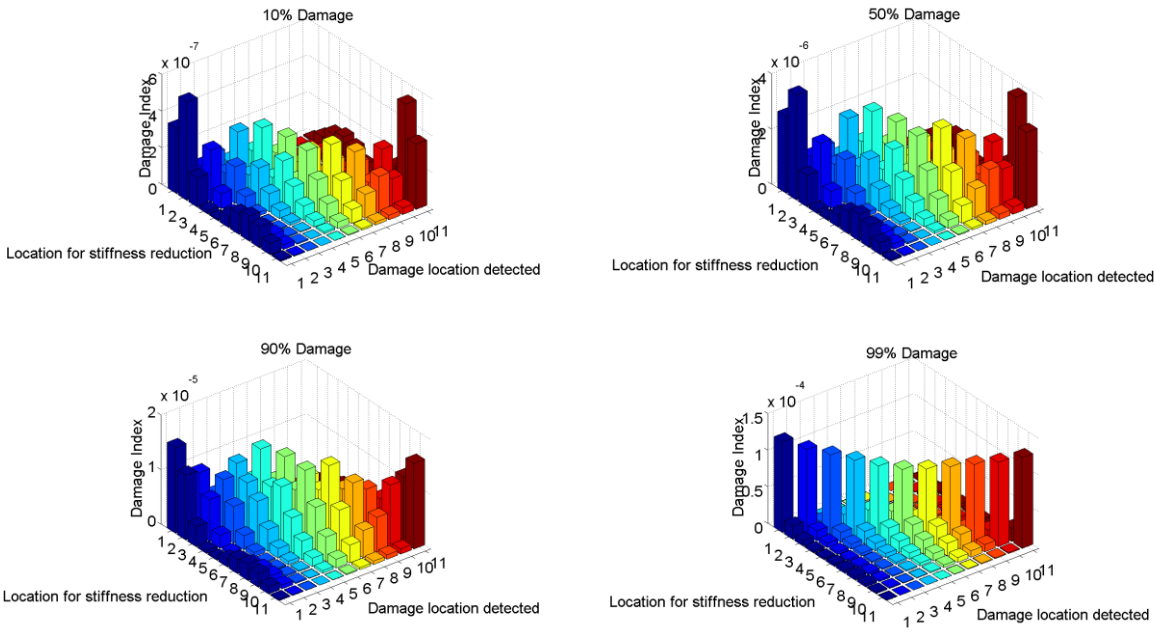

Figure 2.6: Damage indices for all 11 elments damaged to (a) 10% damage; (b) 50% damage; (c) 90% damage; (d) 99% damage.

The value of the maximum damage indices and damage localization for the different damaged elements is further reduced to a single plot. The information of interest in damage localization is to determine the bay at which the maximum damage indices occurs and determine the value of the damage indices. The maximum damage indices, its corresponding location and mean value of the damage indices for each of the damage locations is calculated and shown in plot below. Figure 2.7 condenses the essential information from the above three dimensional bar plots into 2 plots. Figure 2.7 (a) shows

the damage localization for each of the damaged elements with varying levels of damage and Figure 2.7 (b) plots the variation of maximum damage index for all damaged elements for various extents of damage.

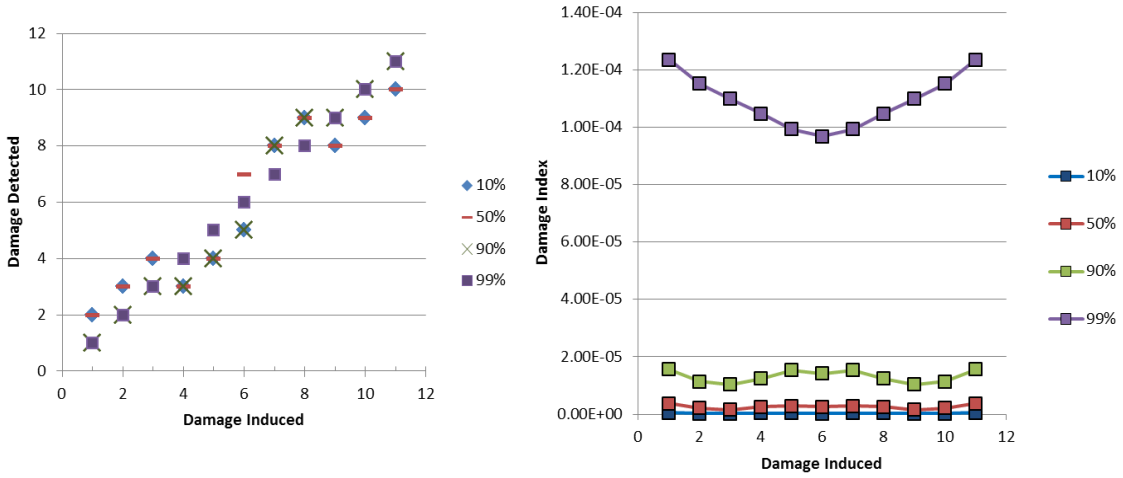

Figure 2.7: Damage detection results for all elements with perfect data (a) Damage localized vs. damaged element; (b) Damage index vs. damaged element.

From the Figure 2.7, we observe that the damage index increases with reduction in elastic modulus of the elements from 10% to 99%.

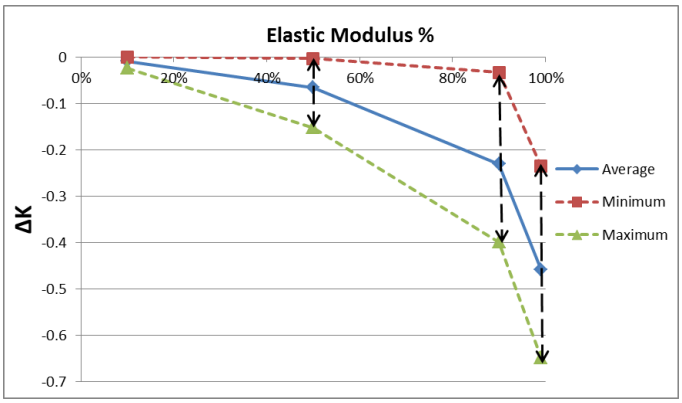

Figure 2.8: Average global stiffness variation with % change in elastic modulus.

The plot shows the change in global stiffness with increasing damage level from 10% to 99% damage. The damage index trend from Figure 2.7 shows similarity with the change is stiffness value plot shown in Figure 2.8. The general trend of quadratic increase

in damage indices with increase in damage can be correlated to the global stiffness change.

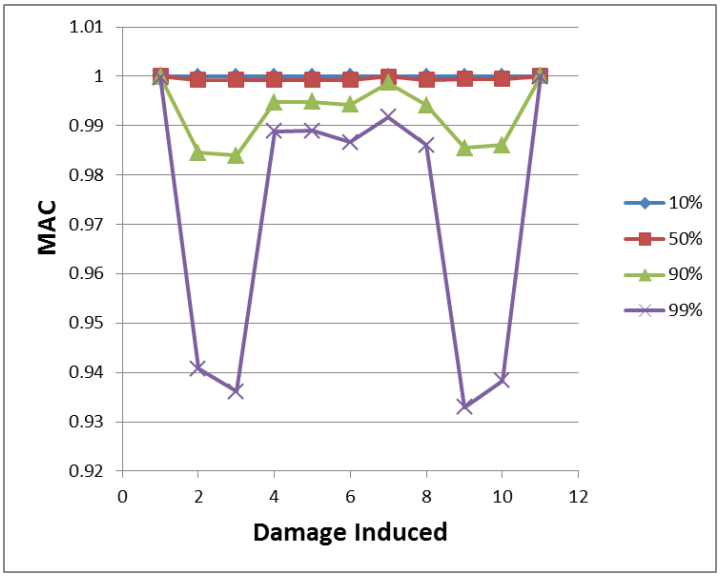

Figure 2.9: Average MAC variation with % change in elastic modulus.

Figure 2.9 shows the change in reduction in the MAC between the intact and damaged mode shapes with reduction in elastic modulus of the elements. Since, the mode shapes are used to evaluate the flexibility matrix and finally the damage indices, the damage to the structure needs to be reflected in the modeshapes to detect damage effectively.

2.4.3 Damage Detection Results for 1D Model – With Noise

The numerical simulation with noise is performed to simulate experimental data obtain from real world structures. The performance of the damage detection method to noise is studied here. The damage detection results of the study with noise are analyzed to understand the minimum extent for damage that can be reliability localized with a certain amount of noise.

Multiple cases of intact and damage modal properties are input the damage detection algorithm to perform a statistical analysis of the effect of noise The numerical study is performed at different noise levels to study the degradation in damage detection quality with noise. Due to limited computer resources and time, only five repetitions are performed for each of the cases of damage level, noise level and damage location. In all, five repetitions of four damage levels, three noise levels and 11 damage elements are evaluated. A similar strategy, as that established in the section, is used to condense the large amount of cases into essential information.

In hindsight, performing limited number of cases with noise is in keeping with application of the method to experimental data in the field and laboratory. With the general issue of time and resources for experimental testing, it is not possible to take a large number of sets of data for the structure to perform a thorough statistical study of the noise in the system and understand its effects to the damage detection method.

2.4.3.1 Establishing a Baseline

The baseline is determined by evaluating the damage detection method between two intact cases, i.e multiple sets of data collected from the same healthy structural configuration. When there is no noise in the system and it is an linear structure, damage detection results with repeated sets of data would result in zero damage index at all bays. But, when noise is present in the data or random noise is added to numerical system the damage indices are no longer zero. This property is inherent in all global damage detection algorithms. If two valid sets of data are provided all damage detection algorithm will generate a result.

The damage indices obtained is an artifact of the noise in the structure and not due to damage. Hence, five repetitions of the damage detection algorithm are performed at three different noise levels, 1%, 5% and 10%, to evaluate the resulting maximum damage indices. The maximum value obtained from the analysis is used as the baseline (radius of influence) for a certain noise level.

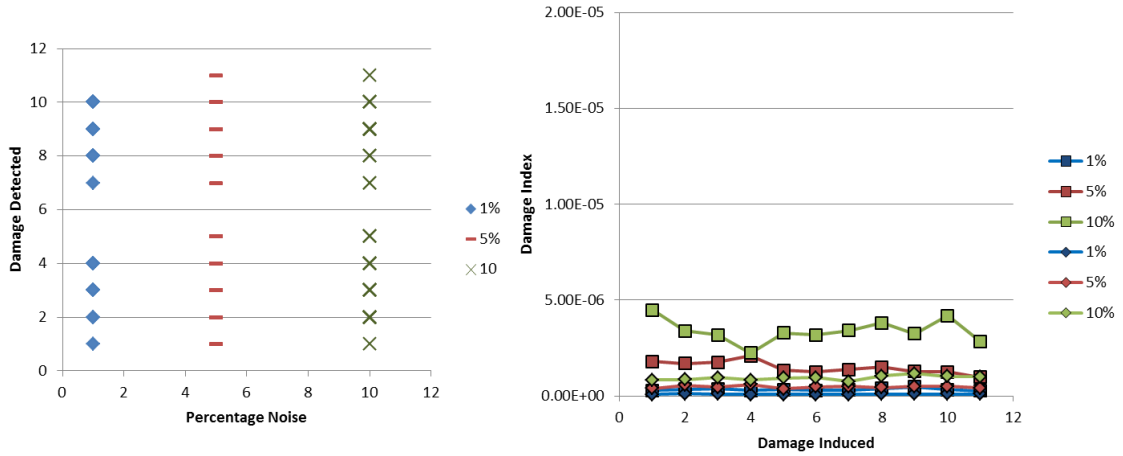

Figure 2.10: Baseline results for all elements with noise (a) Damage localized vs. % noise; (b) Damage index vs. damaged element.

The data compression is similar to the method described in the previous section. Each pair of case that is input to the damage localization method returns damage indices for all 11 bays. The information of interest, damage localization, is determined by the bay at which the maximum damage indices occurs and determine if this value is significantly higher than the damage indices for the other bays. Hence, the data is reduced to just 3 units of information: The maximum value of the damage indices, the mean value of the damage indices and bay number at which the maximum occurs. Since, there is no specific location where the structure is damaged for these baseline cases, the values obtained are a byproduct of the noise. The Figure 2.10 condenses the essential information for the 55 cases into 2 plots. Figure 2.10 (a) shows the baseline localization for each of the noise

levels in *X* axis and bay location on *Y* axis. From Figure 2.10: Baseline results for all elements with noise (a) Damage localized vs. % noise; (b) Damage index vs. damaged element it can be observed that, there is no discernable pattern to the damaged location and the predicted localization. Figure 2.10 (b) plots the variation of maximum and mean damage index with bay location estimated for the various noise level. From Figure 2.10 (b) it is observed that there is a slight variation from bay to bay, but the baseline indices for all bays are taken at the same level for a certain noise level.

Table 2.2: Baseline limit for 3 noise levels.

	1.0%	**5.0%**	**10%**
Baseline value	4.71E-07	2.08E-06	4.48E-06

The Table 2.2 shows the values for each of the noise levels that are used as baseline for the rest of the analysis. The values for each of the noise levels are obtained by taking the average of the maximum indices for all bays.

2.4.3.2 Damage to 1D Beam Model

In this section, the results for damage detection quality with variation in noise and damage extent for all elements of the structure are presented. Damage is created at every element of the structure successively to different extent and the modal parameters are estimated. Five repetitions of the damage detection method are evaluated for each of the damaged locations with different noise added to each of the repetitions. Each pair of case which is input to the damage localization method returns damage indices for 11 bays. The data is reduced to just 3 units of information: The maximum value of the damage indices, the mean value of the damage indices and bay number the damage is predicted to be. The Figure 2.11 condenses the essential information for the 165 cases into 2 plots. Figure 2.11

(a) shows the localization for 10% damage (10% reduction in elastic modulus) at each of the elements with varying levels of noise. Each column represents an element that was damaged and contains 5 data points for each noise level (1% , 5% and 10%) indicating the bays detected by the damage detection. Different marker styles are used for the 3 noise levels as shown. Figure 2.11 (b) plots the variation of maximum and mean damage index with damage location and noise level for 10% reduction in stiffness property of the corresponding elements. Square and diamond markers are used to represent the maximum and mean value of the damage indices for each of the noise levels. Horizontal hashed lines are color coded for each of the baseline limits set at 4.71E-7, 2E-6 and 4.48E-6.

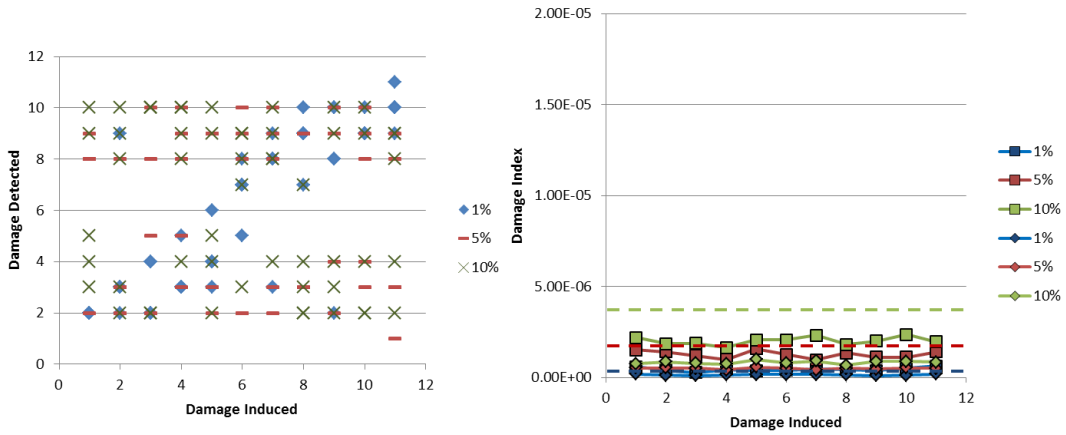

Figure 2.11: Damage detection results for all elements with 10% damage (a) Damage localized vs. damaged element; (b) Damage index vs. damaged element.

As observed in Figure 2.11 (a), with the reduction of the noise, the damage localization bay for each of the damaged element is at the correct bay or adjacent bay. The blue diamond markers for 1% noise cases align in a diagonal pattern. From Figure 2.11 (b) it is observed that the line for the maximum damage index for 1% noise (blue line with square markers) is very close to the baseline limit whereas the lines for the other noise levels are well below the baseline limit. Hence, for the higher noise levels there is no

observable correlation between the damaged element and the predicted damage location. From the no noise study performed in the Section 2.4.2; with perfect damage detection with 10% damage, it was shown that, the best damage localization possible was to the exact or adjacent bay. Hence, the best possible damage localization is observed for the lower noise levels of 1% with 10% damage.

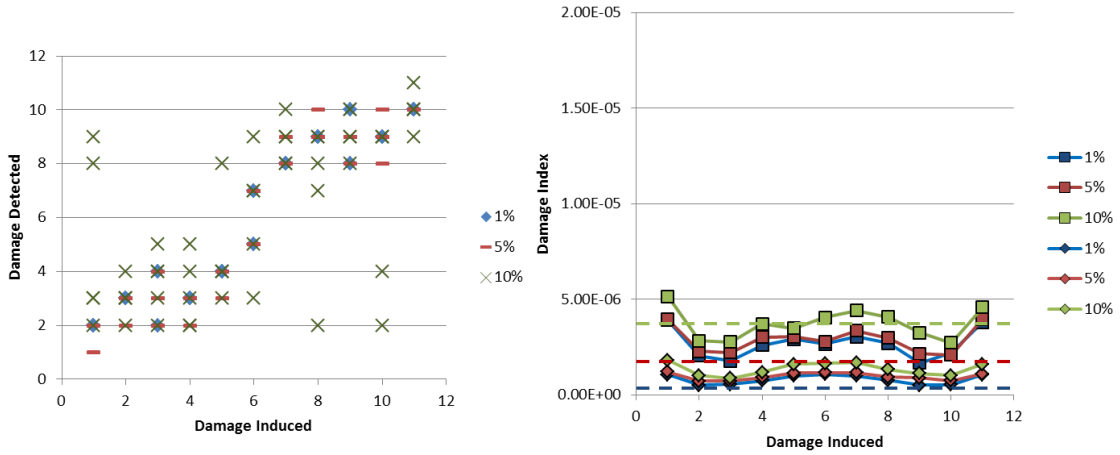

Figure 2.12: Damage detection results for all elements with 50% damage (a) Damage localized vs. damaged element; (b) Damage index vs. damaged element.

As the damage extent induced on the structure increases to 50%, a more pronounce diagonal pattern emerges, as shown in Figure 2.12 (a). The diagonal pattern can be correlated to the fact that, from Figure 2.12 (b) it is observed that the average value of the maximum indices for 1% noise level is well above the baseline limit and 5% and 10% noise level are very close to the baseline limit. Some of the damage locations are observed to have the maximum damage indices above the baseline limit at 5% and 10% noise as well.

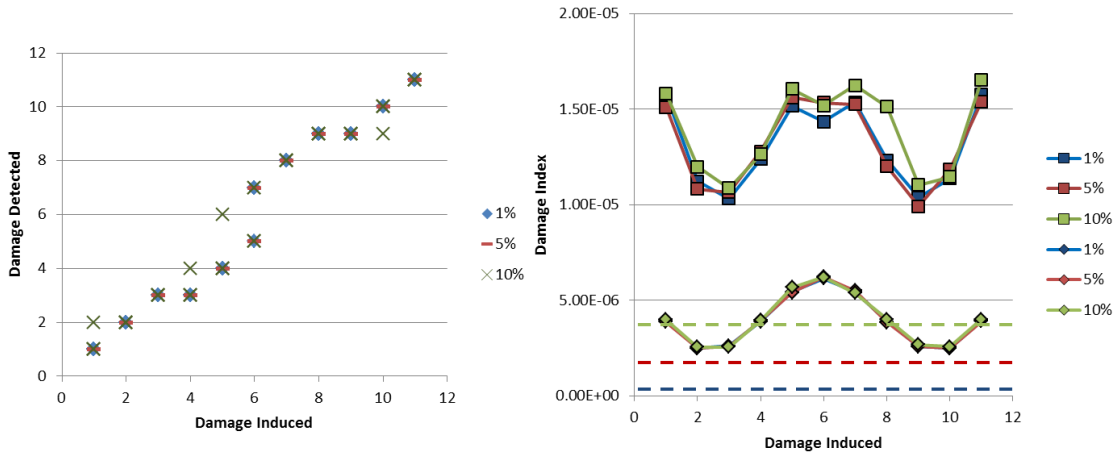

Figure 2.13: Damage detection results for all elements with 90% damage (a) Damage localized vs. damaged element; (b) Damage index vs. damaged element.

In the next sequence, Figure 2.13 with 90% damage, the average of the maximum damage indices are 1.25E-5 which is above the baseline limits for all noise levels and as a result the damage localization is to the correct bay or adjacent bay at all noise levels. From the no noise study with 90% and no added noise, it was shown that the best damage localization possible was to the exact or adjacent bay, shown in Figure 2.7 (a).

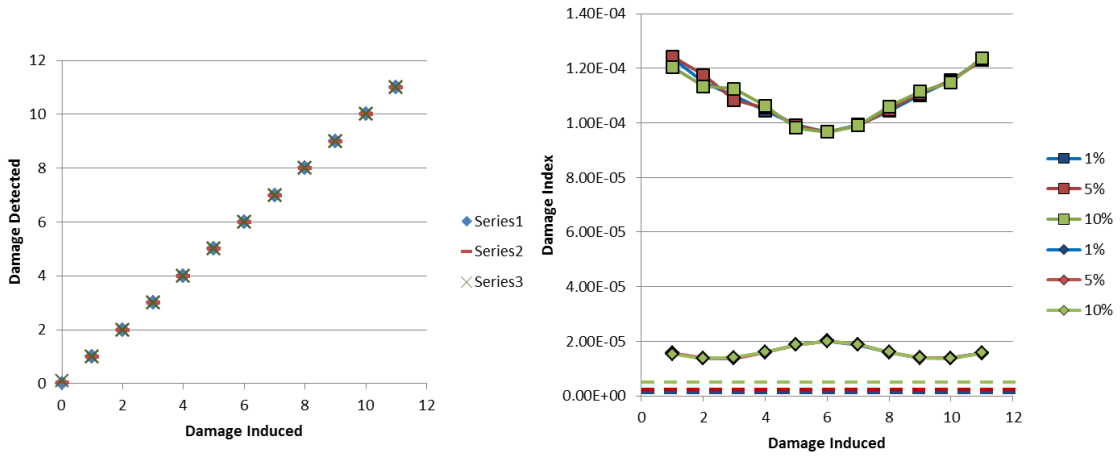

Figure 2.14: Damage detection results for all elements with 99% damage (a) Damage localized vs. damaged element; (b) Damage index vs. damaged element.

Finally, when the damage is increased to 99% reduction in elastic modulus, damage is detected to the exact bay at all noise levels.

The results from the previous figures is condensed to a high level representation in Table 2.3 with color coded values to depict the reliability of the results obtained based on the average of the maximum damage indices for all elements over the baseline (average value of all damage indices). The quality of the damage localization is shown using green yellow and red.

Table 2.3: Maximum damage indices with respect to percentage reduction in modulus and noise.

	1.0%	5.0%	10%
Baseline value	**4.71E-07**	**2.08E-06**	**4.48E-06**
10%	6.21E-07	1.56E-06	2.34E-06
50%	3.9E-06	3.95E-06	5.13E-06
90%	1.58E-05	1.56E-05	1.65E-05
99%	1.24E-04	1.24E-04	1.24E-04

In the Table 2.3, green depicts the damage results obtained from the damage detection method can be accepted as accurate damage detection for that particular noise level and damage extent. Yellow depicts the cases where maximum damage indices are close to the baseline and the results are good in most cases but cannot be fully accepted for that particular noise level and damage extent. Red depicts the cases where maximum damage indices are lower than the baseline and the results cannot be guaranteed to detect damage reliably for that particular noise level and damage extent.

2.5 Numerical Demonstration - Three Dimensional Structure

There are three main purposes of this study. 1) Study the damage detection capability of the ASH flexibility damage detection method and validating the methodology proposed in the chapter. 2) Study the use of limited number of sensors in detecting damage in a

complex structure and 3) compare the one dimensional beam and three dimensional structure results to demonstrate the independence of the methods to the structure under consideration.

The modal created in MATLAB is wireframe model of the actual experimental structure studies for this thesis. The structure is full scale highway sign support truss. A finite element model of the three dimensional truss is developed using SHM toolbox in MATLAB to perform numerical evaluation of the methods and to validate the baseline methodology. The FEM model has 48 nodes with 6 DOFs each and 144 beam elements. The boundary conditions at nodes 1, 12, 25 and 36 are assumed to be fixed in all 6 DOFs. The properties used for the elements in the numerical model are the same as that of the undamaged experimental structure. The material properties and cross sectional properties of the elements are given in Table 2.4and Table 2.5. Figure 2.15 shows the configuration the structure.

Table 2.4: Material properties of the 3D model.

Material	E (N/m^2)	G(N/m^2)	Rho (Kg/m^3)
Aluminium (AL-6061)	6.96E+10	2.62E+10	2.71E+03

Table 2.5: Cross-sectional properties of the 3D model.

Section	Ixx (m^4)	Iyy (m^4)	Area (m^2)	J (m^4)
Main chords	9.79E-06	9.79E-06	3.76E-03	1.96E-05
Secondary in-plane diagonals	8.52E-07	8.52E-07	1.38E-03	1.70E-06
Tertiary vertical elements	1.85E-07	1.85E-07	7.03E-04	3.71E-07

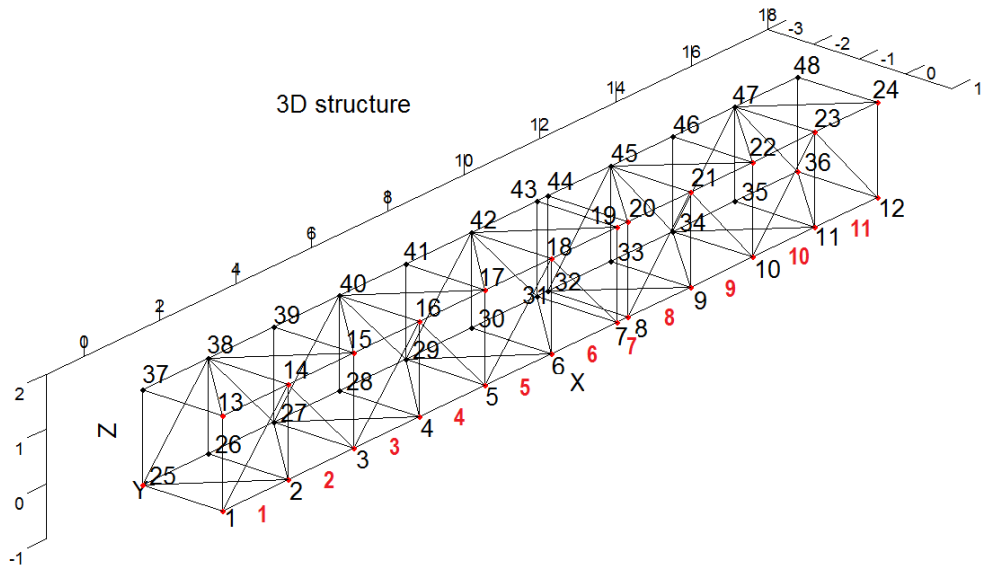

Figure 2.15: Three dimensional highway sign support truss model.

To simulate damage in the numerical model, the elastic moduli of the elements of the model are reduced.

2.5.1 Setup of Cases

The numerical simulation of the truss described above is performed with different variations to the model to evaluate the effects of system noise, damage extent and damage location. In this section, the various changes to the property of the healthy model are described. The damaged locations in the model are referred to as Elements and the location at which the damage is predicted is referred to as Bays. The bays are numbered 1- 11 from left to right as shown in Figure 2.15. To study the effect of using limited sensors to detect damage, it is assumed that the structure is instrumented with only accelerometers at nodes 1- 12 in the Y- direction (shown by red markers in Figure 2.16)

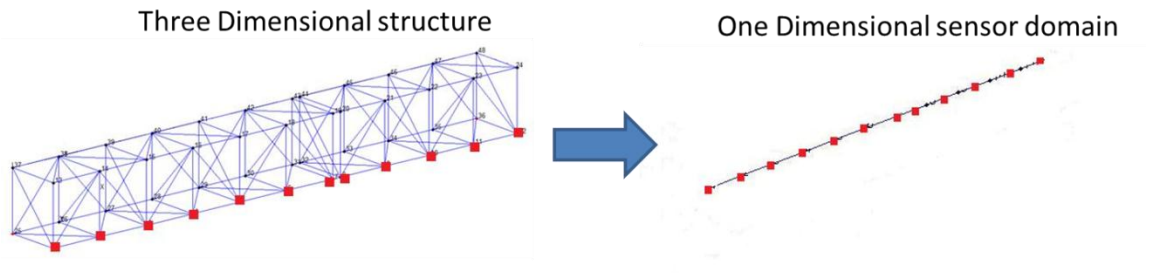

Figure 2.16: Measured DOFs of the model.

This limited sensor information restricts the information available for effective damage detection. Damage to any part of the three dimensional model must be projected onto the sensor domain to be able to detect the damage, i.e. the modal properties at the measured sensors must reflect the change in the model caused by damage to any of the elements. The damage to an element of the model is induced by reducing the elastic modulus by a certain percentage. The damage is created by reducing the elastic modulus of each element by 10%, 50%, 70%, 90% and 99% successively. In total there are 144 beam elements present in this model. The numerical analysis for damage is restricted to 84 primary elements and is conducted in 8 sets. The cases are divided based on the similarity of the elements in a set and relative position of the element being damaged with respect to the sensor locations. The structure is divided into front-bottom chord: elements between nodes 1- 12, front-top chord: elements between nodes 13 – 24, back-bottom chord: elements between nodes 25-36, back-top chord: elements between nodes 37-48, front panel diagonals: secondary elements between node 1-24, back panel diagonals: secondary elements between node 25- 48, bottom panel diagonals: secondary elements between node 1-12 and 25-36 and top panel diagonals: secondary elements between node 13-24 and 37-48.

The definition of noise, in the context of this analysis is presented earlier in the section 2.4.1 of one dimensional beam case. Random noise is added to the numerical simulation, after the system identification process to the mode shapes. Random noise of 0.1%, 0.5%, 1%, 2.5%, 5% and 10% of the average of the component of the measured mode shapes are added at the measured DOFs of the model as shown in Equation 2.25.

$$\varphi_{m,noise} = \varphi_m + \%noise \cdot rand(-1,1) \cdot avg(|\varphi_{m,i}|) \qquad \text{Equation 2.25}$$

Where, $\varphi_{m,i}$ is a component of the mode shape at the measured DOFs.

2.5.2 Damage Detection Results for 3D model – No Noise

Damage to the 8 sets of damaged location with no noise and perfect modal properties are described in this section. The analysis is presented to understand the best possible damage localization possible with the extent of damage to each of the elements. The strategy, illustrated for the 1D model (section 2.4.2), is used to reduce a large amount of cases in a single plot. Each element of the numerical model is damaged (elastic modulus reduced) and the damage indices for the 11 bays are evaluated. As no noise is added in the current analysis, the damage indices distribution obtained is the most accurate result that is possible for a certain level of damage in the elements using the ASH damage detection method. Since, the analysis is reoccurring for the 8 cases only 4 are discussed here. They are Front-bottom chord, Front-top chord, Front panel diagonal and Back panel diagonals.

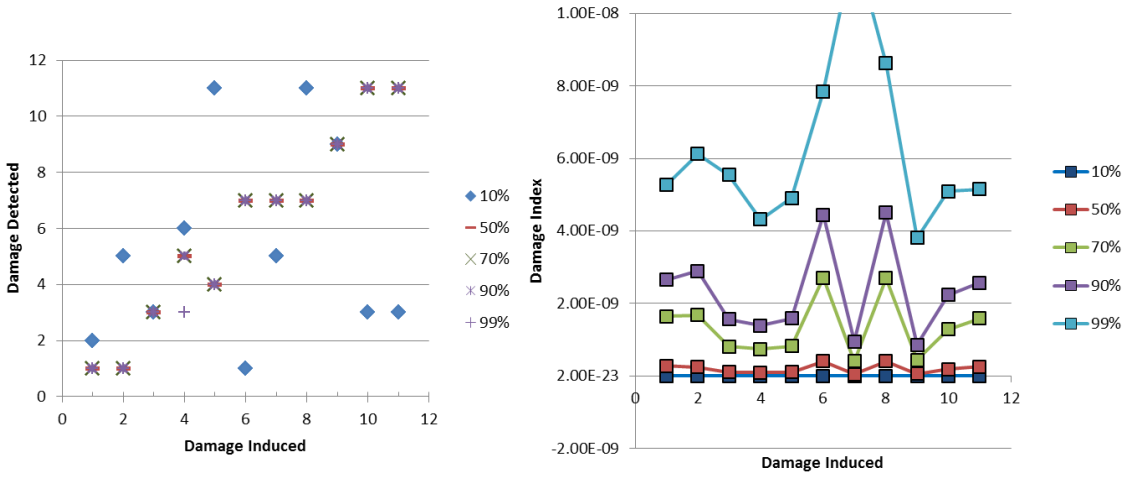

Figure 2.17: Damage detection results for front-bottom chord damaged with perfect data (a) Damage localized bay vs. damaged element; (b) Damage index vs. damaged element.

As observed in Figure 2.17 (a) the markers indicate the damaged bay along the *Y* axis for each of the damaged element for the front-bottom chord along the *X* axis. Hence, damage is localized to within the adjacent bay only above 50% reduction in elastic modulus. From Figure 2.17 (a) we can observe that for 10% reduction to the front-bottom chord elements and measurement DOFs collocated, the damage detection methods cannot detect damage with perfect modal properties. It can be concluded that the "domain of influence" for this damage detection method for a certain location above 50% damage also contains the adjacent elements. Figure 2.17 (b) shows that the maximum damage indices for all the damage cases increase with the decrease in elastic modulus from 10% to 99%.

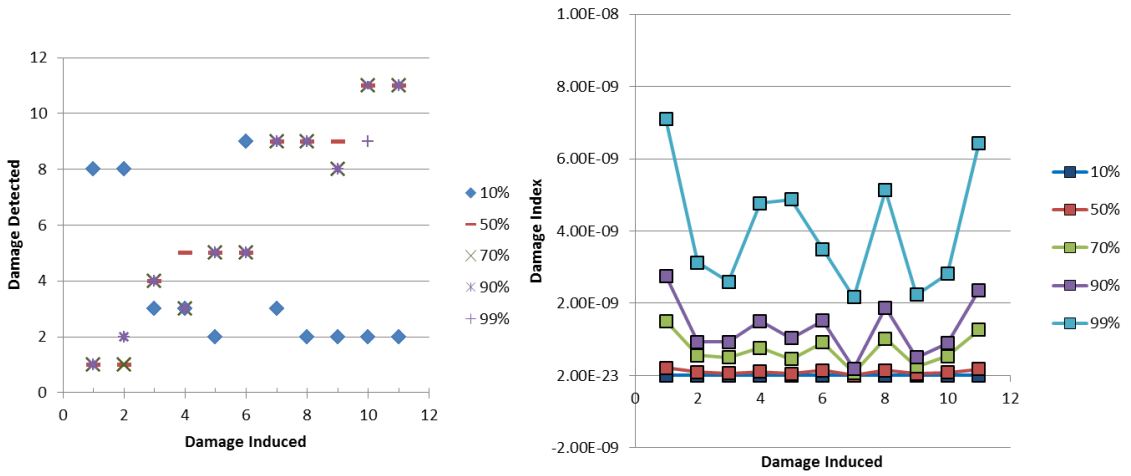

Figure 2.18: Damage detection results for front-top elements damaged with perfect data (a) Damage localized vs. damaged element; (b) Damage index vs. damaged element.

Similar trend is observed in Figure 2.18 (b), with damage index increases for each of the element of the front-top chord being damaged by reducing the elastic modulus of the elements from 10% to 99%.But, the damage indices are lower than that of the front bottom chord damaged.

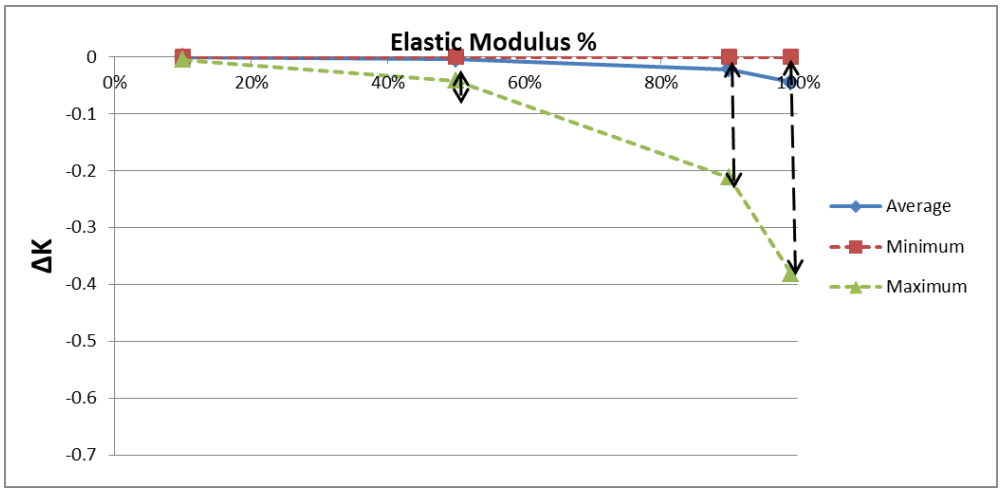

Figure 2.19: Global Stiffness change vs.average percentage change in elastic modulus of the main chords.

The Figure 2.19 shows the change in global stiffness with increasing damage level from 10% to 99% damage for the main chords. The damage index increases from 10%

to 99% and shows similarity with the change is stiffness value plot shown in Figure 2.18 (a). But, unlike the case of the 1D structure, where all the DOFs are measured, for limited sensors used, the change in mode shapes are not large enough to localize damage to the correct bay at 10% damage.

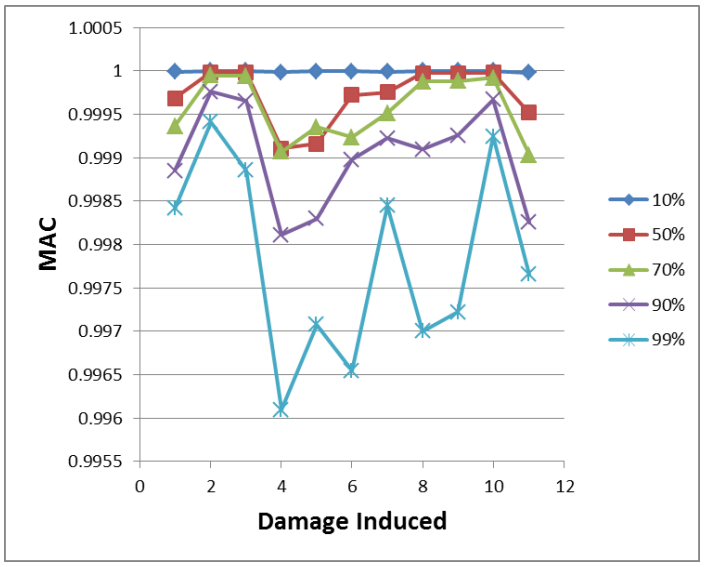

Figure 2.20: Average MAC variation with reduction in chord element stiffness.

The MAC between intact and damaged cases are evaluated only at a few DOFs of the the model; the front-bottom chord in the *Y* direction. The MAC value for the damage to the front-top chord is shown in

Figure 2.20. It is observed that the MAC value for 10% damage is very close to 1 and the modeshape does not have information regarding the change in stiffness.

The damage detection results for the secondary in-panel diagonals are presented. Figure 2.21 (a) shows the damage detection results for damage to front panel diagonals. Note that Bay 7 does not have an in-panel diagonal and damaged location is left blank.in Figure 2.21. The damage is detected to the correct bay for damage above 50% reduction

in modulus. In Figure 2.21 (b) we note that the maximum damage indices for the all the cases increase with increase in damage.

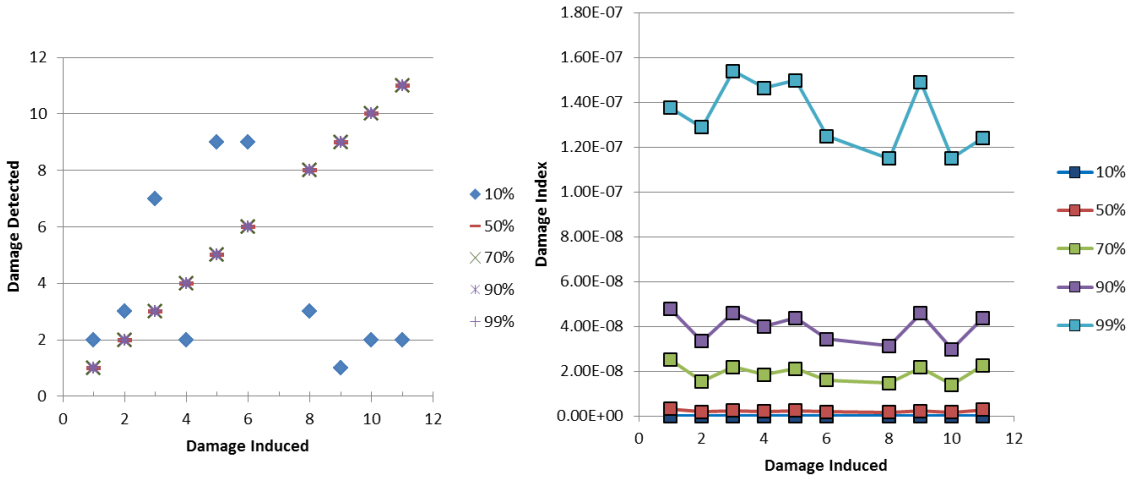

Figure 2.21: Damage detection results for front-panel diagonals damaged with perfect data (a) Damage localized vs. damaged element; (b) Damage index vs. damaged element.

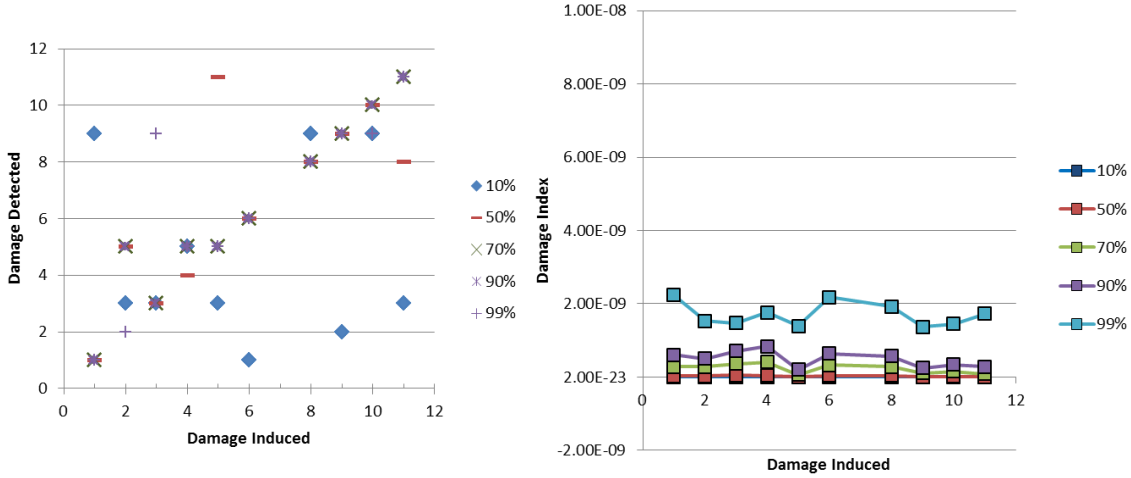

Figure 2.22: Damage detection results for back-panel diagonals damaged with perfect data (a) Damage localized vs. damaged element; (b) Damage index vs. damaged element.

Similar trend is observed for the back-panel damage as well.10% reduction to elastic modulus does not detect damage consistently to the correct bay. The damage is localized to adjacent bay or to the correct bay for all elements damaged except diagonal at the second bay. In this case, the damage is localized to the 5th bay when damage was

induced at element 2. The maximum damage indices for the front-panel diagonals are 100 times larger than the damage indices for the back-panel. The sensors at the front-bottom chord cannot measure a significant change in modal properties when damage is induced at the back-panel diagonals.

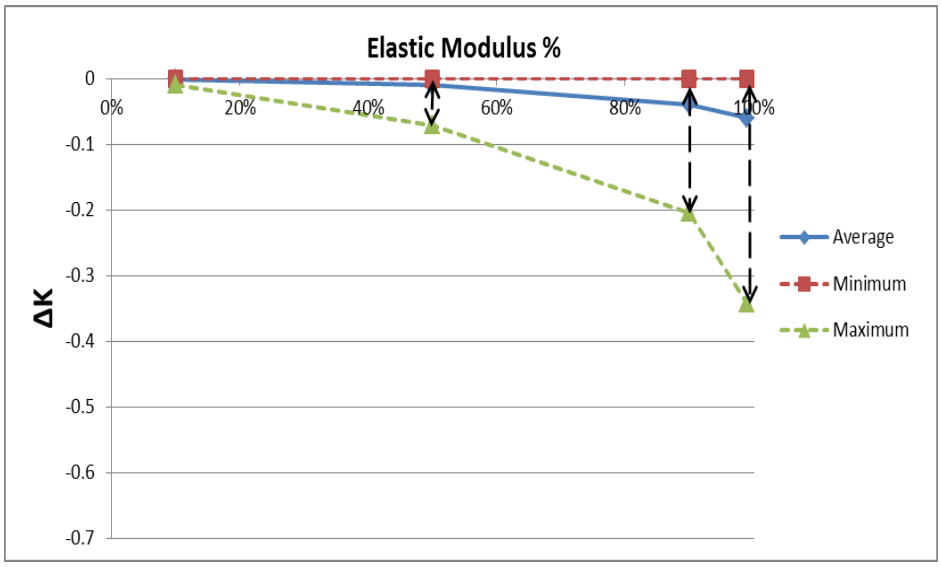

Figure 2.23: Global Stiffness change vs. average percentage change in elastic modulus of the in-panel diagonals.

Figure 2.23 shows that the change in global stiffness due to the diagonals is similar to the main chords, about -0.2 average reduction in stiffness with deviation from 0 to -0.4. But, to localize damage using flexibility based methods the mode shape sensitivity is important.

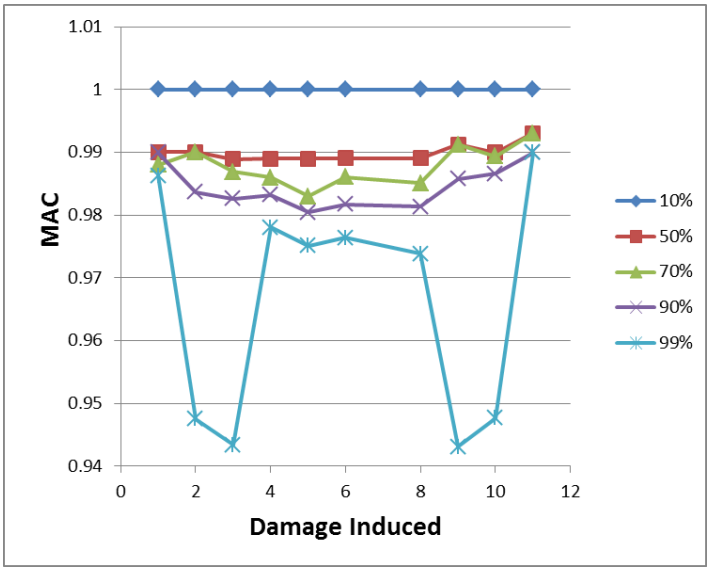

Figure 2.24: Average MAC variation with change in stiffness of in-panel diagonals.

Figure 2.24 shows the comparison of the average change in that the MAC for the main chord and diagonals. The MAC between the intact and damaged structure shows lesser correlation for the damage to the diagonals than that of the main chords. The mode shapes are more sensitive and localized to change in the stiffness of the diagonals than the main chord elements.

2.5.3 Damage Detection Results for 3D model – With Noise

2.5.3.1 Baseline Damage Index

Hence, the next step is to evaluate the damage detection algorithm to noise in the system. The damage detection method is performed on the structure to understand the effect of noise in the modal properties on the damage detection quality. 0.1%, 0.5%, 1%, 2.5%, 5% and 10% random noise is added to the exact realization of the mode shape and natural frequencies.

The process to evaluate the baseline has been detailed in Section 2.4.3.1 and only the results are presented.

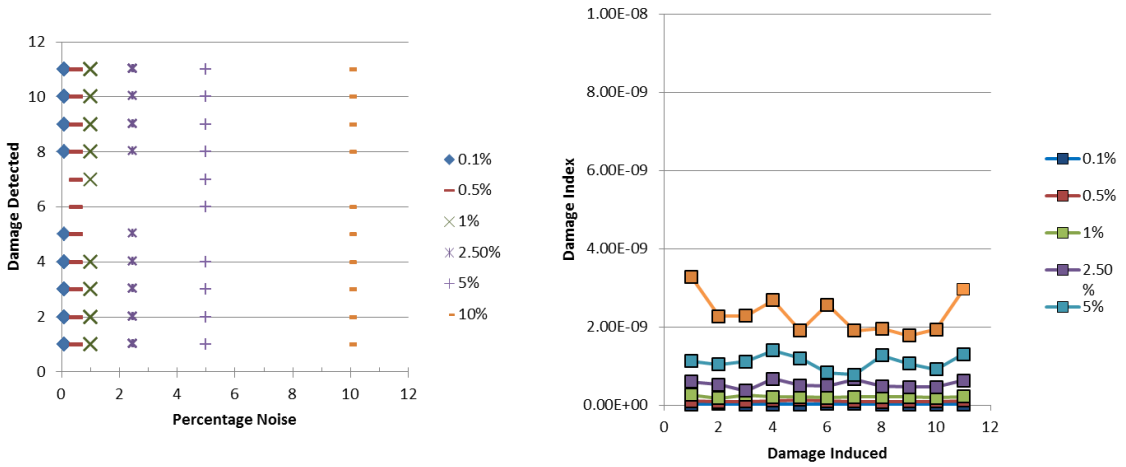

Figure 2.25: Baseline results for measured DOFs at the front-bottom chord with noise (a) Damage localized vs. % noise; (b) Damage index vs. damaged element.

The results of the baseline are presented here relative to the amount of noise added to the modal properties. Figure 2.25 condenses the essential information for the 90 cases (15 repetitions for 6 noise levels) into 2 plots. Figure 2.25 (a) shows the baseline localization for each of the noise levels in *X* axis and bay location on *Y* axis. Figure 2.25 (b) plots the variation of maximum and mean damage index against noise level in the measurements.

Table 2.6: Baseline Values for different noise levels.

Noise	**0.1%**	**0.5%**	**1%**	**2.50%**	**5%**	**10%**
Baseline value	3.4E-11	1.46E-10	3.46E-10	7.86E-10	1.81E-09	3.27E-09

From Figure 2.25. (a), it is observed that there are no set patterns to the baseline prediction. For simplicity, the baseline indices for all bays are taken at the same level for a certain noise level. The Table 2.6 shows the values for each of the noise levels that are used as baseline for the rest of the analysis. The values for each of the noise levels are obtained by taking the average of the maximum indices for all bays. These value are used

for the rest of three dimensional truss analyses as the threshold ffor reliable damage detection.

2.5.3.2 Front-Bottom Chord

In this case, damage is induced by reducing the elastic modulus of the elements between nodes 1-12. Also, the sensors used to perform the ASH flexibility damage detection are also at the front bottom chord node locations. Hence, it is expected that the change is elastic modulus will be easily captured by the sensors as they are collocated.

The data compression is similar to the method described in the previous section 2.4.3.2. The Figure 2.26 condenses the essential information for the 330 cases into 2 plots for each damage extent. The baseline determined from the previous section for sensors at the front-bottom chord are indicated by the hashed lines for the different noise levels. Each column of Figure 2.26 (a) represents an element that was damaged and contains 5 data points for each noise level indicating the bays detected by the damage detection algorithm for that specific damage location. The noise levels are indicated by different marker styles for each damage location. With 10% reduction in stiffness, it can be observed that, only at the lowest noise level of 0.1% (blue diamond markers) the damage can be localized to the correct element or adjacent element.

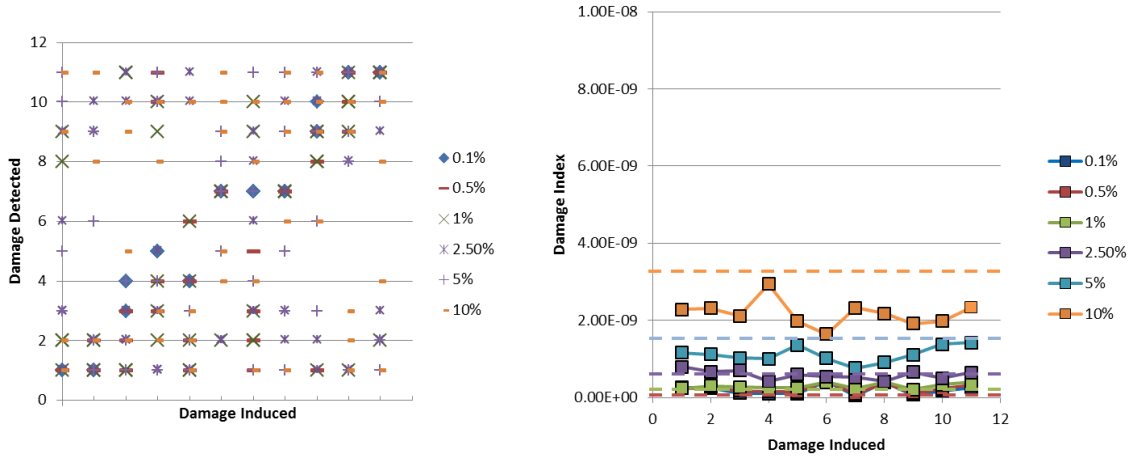

Figure 2.26: Damage detection results for front-bottom chord damaged with 10% reduction and noise (a) Damage localized vs. damaged element; (b) Damage index vs. damaged element.

Figure 2.26 (b) plots the variation of maximum damage index with damage location and noise level for 10% reduction in stiffness property of the corresponding elements. From Figure 2.26 (b) it is observed that the line for the maximum damage index for 0.1% noise (blue line with square markers) is above the baseline limit whereas the lines for the other noise levels are well below the baseline limit. Also, to note is that the maximum damage indices lines are approximately constant for each noise level and implies that the effect of noise and damage extent on the damage indices are uniform. Figure 2.26 (a) shows that there is no observable correlation between the damaged element and damage localization bay (identifiable diagonal pattern to the damage localization) for higher noise levels.

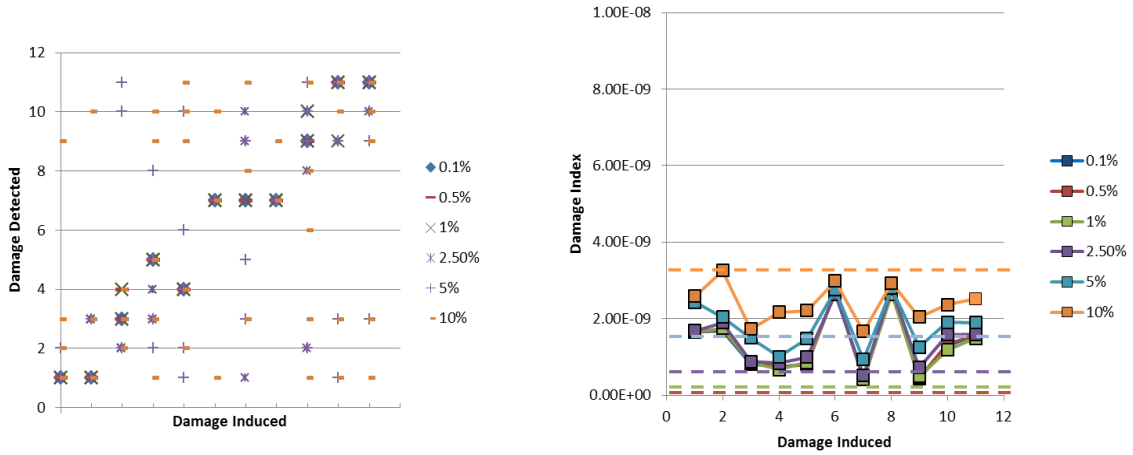

Figure 2.27: Damage detection results for front-bottom chord damaged with 50% reduction and noise (a) Damage localized vs. damaged element; (b) Damage index vs. damaged element.

In Figure 2.27 (a) with 50% damage level, damage can be estimated accurately up to 1% noise level in the system. This is correlated to the Figure 2.27 (b) where the maximum damage indices are above the baseline limit at all the bay locations. It is observed that the at element locations 7 and 9 the indices are below the limit and it affects the quality of the damage detection at this locations.

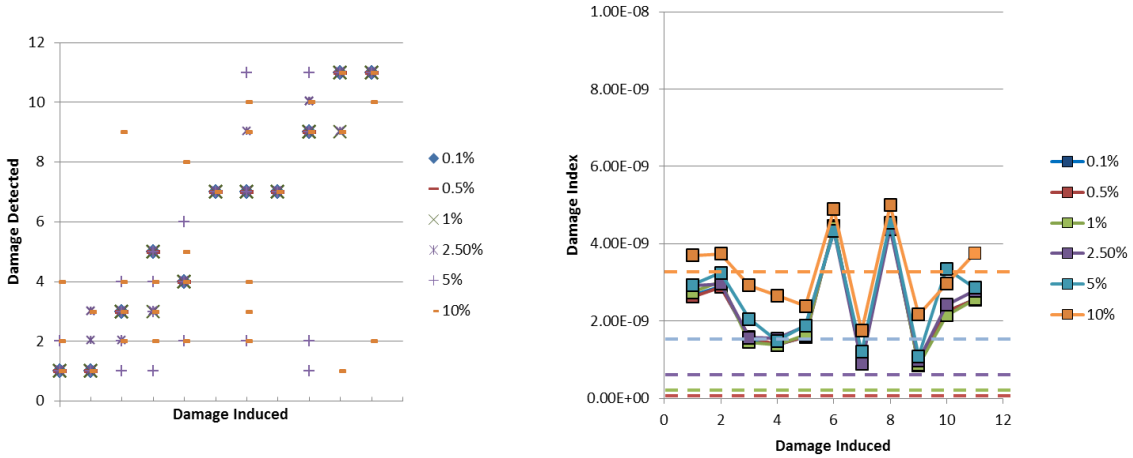

Figure 2.28: Damage detection results for front-bottom chord damaged with 70% reduction and noise (a) Damage localized vs. damaged element; (b) Damage index vs. damaged element.

As the damage extent induced on the structure increases to 70%, a more pronounce diagonal pattern emerges. This can be correlated to the fact that, from Figure 2.28 (b) that the average value of the maximum indices for 2.5% noise level is well above the baseline limit for all locations except for bay 7 and 9 and 5% and 10% noise level are very close to the baseline limit. In the next Figure 2.29, with 90% damage, the average of the maximum damage indices is above the baseline limits for all noise levels and as a result the damage localization is to the correct bay or adjacent bay at all noise levels.

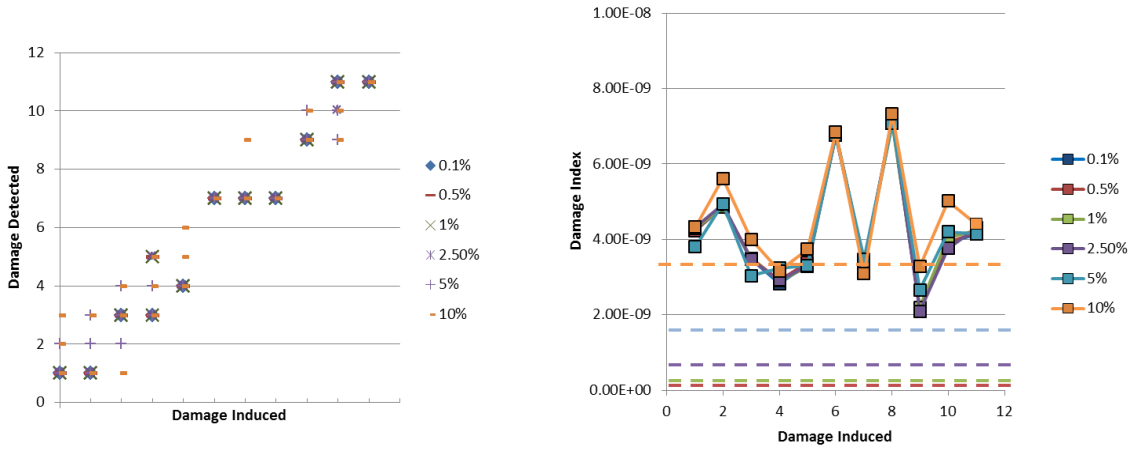

Figure 2.29: Damage detection results for front-bottom chord damaged with 90% reduction and noise (a) Damage localized vs. damaged element; (b) Damage index vs. damaged element.

Finally, when the damage is increased to 99% the damage is localized accurately to the adjacent bay.

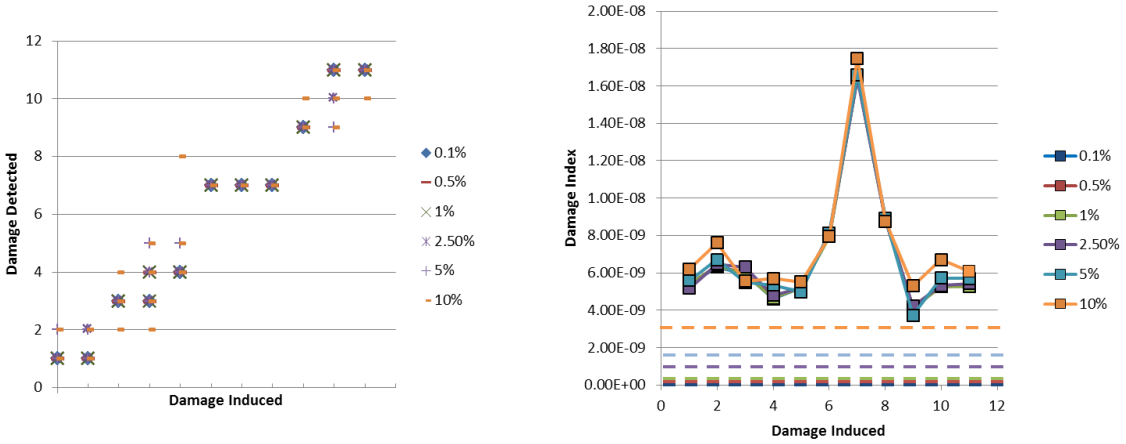

Figure 2.30: Damage detection results for front-bottom chord damaged with 99% reduction and noise (a) Damage localized vs. damaged element; (b) Damage index vs. damaged element.

Also, the information from all the plots is condensed to a high level representation in a table with color coded values to depict the reliability of the results obtained based on the average maximum damage index value over the baseline. Section 2.4.3.2 presents an interpretation of the color coding of the numbers in Table 2.7.

Table 2.7: Maximum damage indices with respect to noise and percentage reduction in elastic modulus.

Noise	0.1%	0.5%	1%	2.50%	5%	10%
Baseline value	**3.4E-11**	**1.46E-10**	**3.46E-10**	**7.86E-10**	**1.81E-09**	**3.27E-09**
10%	2E-10	2.29E-10	2.97E-10	5.87E-10	1.11E-09	2.18E-09
50%	1.35E-09	1.36E-09	1.34E-09	8.46E-10	1.82E-09	2.4E-09
70%	2.33E-09	2.33E-09	2.33E-09	2.42E-09	2.03E-09	3.27E-09
90%	4.21E-09	4.22E-09	4.23E-09	4.22E-09	4.24E-09	4.62E-09
99%	6.86E-09	6.87E-09	6.85E-09	6.92E-09	6.99E-09	7.53E-09

This information can be interpreted in 2 ways. Firstly, if a real world system has a certain amount of noise in the final modal properties stage (say 5% noise), then damage greater than 90% reduction of stiffness property is required to reliability predict the correct damage location. The second interpretation is that to detect a certain damage level

in a system (say 50% damage), then the data acquired from the real world structure needs to be controlled and processed to reduce the noise to less than a certain level to reliably predict the correct damage location (less than 1% noise in the final modal properties estimated for the case presented here).

2.5.3.3 Front Top Chord

In this case, damage is induced by reducing the elastic modulus of the elements between nodes 13-24. The sensors used to perform the ASH flexibility damage detection are at the front bottom chord node locations. It is expected that the damage detection process to reduce in quality as the damage to front-top elements must be projected and observable by the front-bottom measured sensors.

In Figure 2.31 (b) the baseline determined from the previous section for sensors at the front-bottom chord are indicated by the hashed lines for various noise levels. With 10% reduction in stiffness, damage cannot be localized to the correct element or adjacent element even at the lowest noise level of 0.1%. The noise in the system overwhelms the change in modal properties due to 10% reduction in modulus.

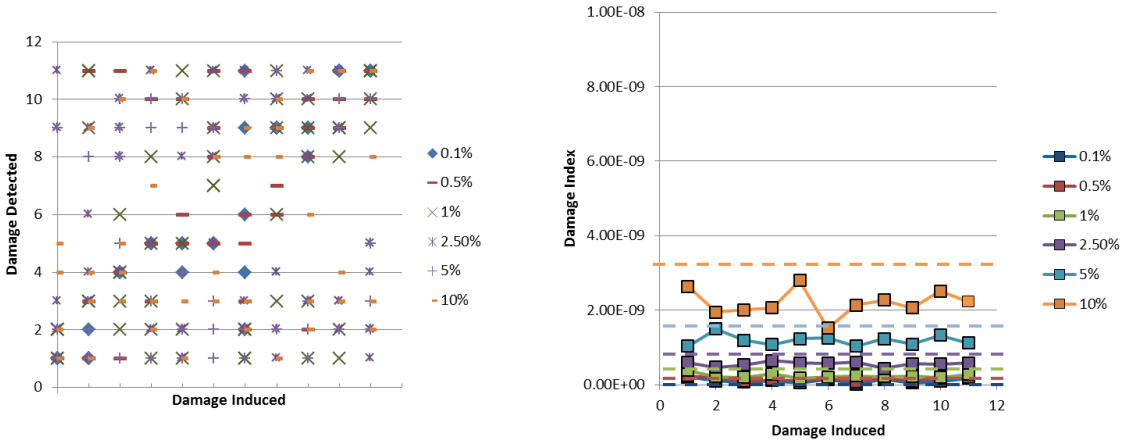

Figure 2.31: Damage detection results for front-top chord damaged with 10% reduction and noise (a) Damage localized vs. damaged element; (b) Damage index vs. damaged element.

Figure 2.31(b) plots the variation of maximum damage index with damage location and noise level for 10% reduction in stiffness property of the corresponding elements. From Figure 2.31 (b) it is observed that the maximum damage indices for all noise levels are below the baseline limit. But it is observable that for lowest noise level the diagonal pattern is starting to emerge.

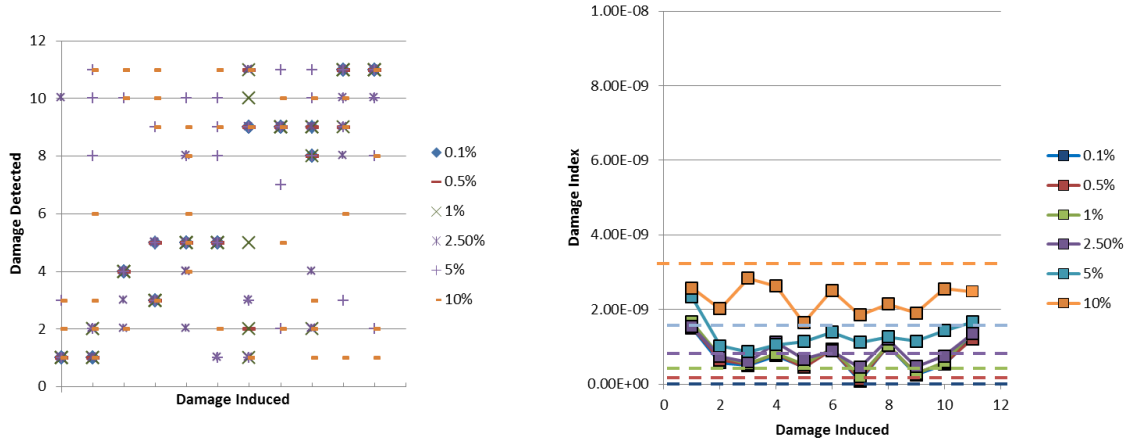

.

Figure 2.32: Damage detection results for front-top chord damaged with 50% reduction and noise (a) Damage localized vs. damaged element; (b) Damage index vs. damaged element.

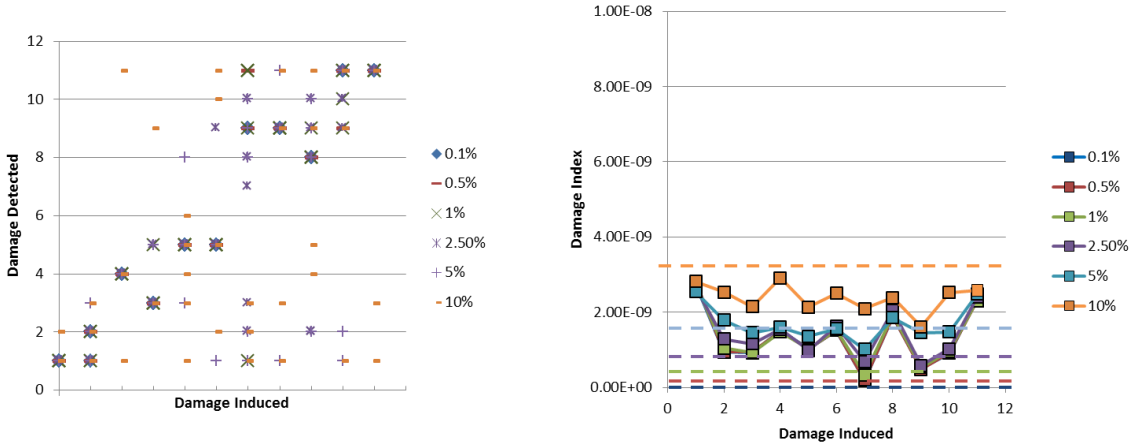

Figure 2.33: Damage detection results for front-top chord damaged with 70% reduction and noise (a) Damage localized vs. damaged element; (b) Damage index vs. damaged element.

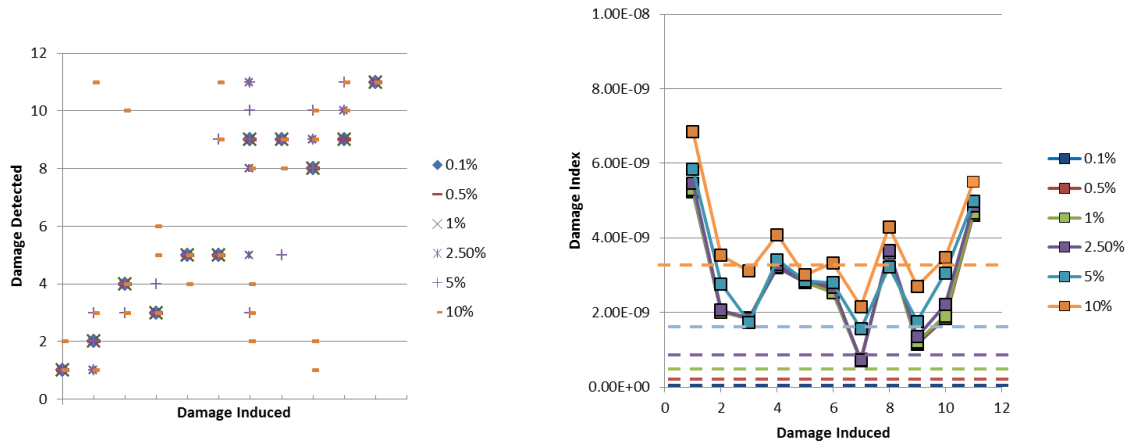

Figure 2.34: Damage detection results for front-top chord damaged with 90% reduction and noise (a) Damage localized vs. damaged element; (b) Damage index vs. damaged element.

As the damage extent induced on the structure increases from 50% to 90%, a more pronounce diagonal pattern emerges. This can be observed in Figure 2.32, Figure 2.33and Figure 2.34. For the 99% damaged case, from Figure 2.35 (b) it is observed that for the highest noise level some damage locations are very close to the baseline limit and this is observable in the damage localization in Figure 2.35 (a).

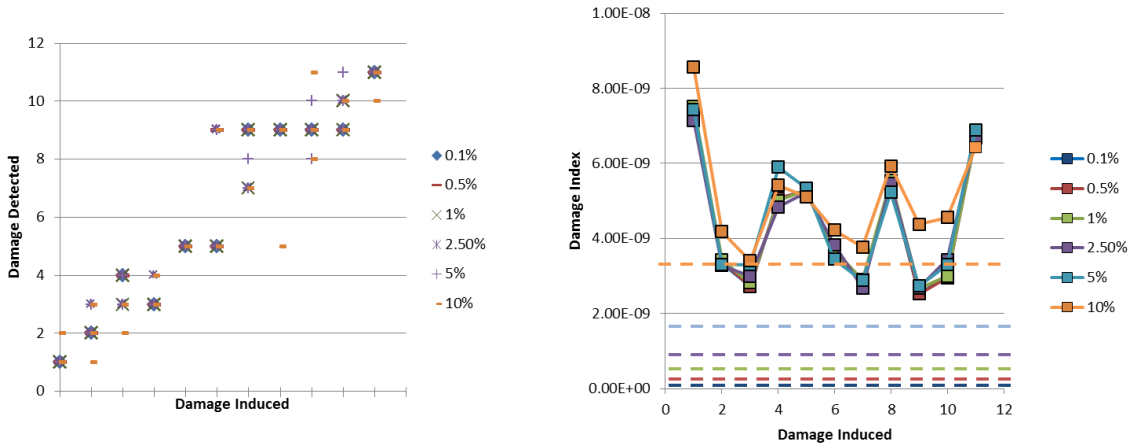

Figure 2.35: Damage detection results for front-top chord damaged with 99% reduction and noise (a) Damage localized vs. damaged element; (b) Damage index vs. damaged element.

Also, the information from all the plots is condensed to a high level representation in a Table 2.8 with color coded values to depict the reliability of the results obtained based on the average maximum damage index value over the baseline.

Table 2.8: Maximum damage indices with respect to noise and percentage reduction in modulus.

Noise	0.1%	0.5%	1%	2.50%	5%	10%
Baseline value	**3.4E-11**	**1.46E-10**	**3.46E-10**	**7.86E-10**	**1.81E-09**	**3.27E-09**
10%	7.05E-11	1.52E-10	2.39E-10	5.58E-10	1.19E-09	2.2E-09
50%	7.15E-10	7.37E-10	7.93E-10	8.88E-10	1.31E-09	2.29E-09
70%	1.32E-09	1.32E-09	1.35E-09	1.46E-09	1.69E-09	2.38E-09
90%	2.7E-09	2.71E-09	2.72E-09	2.82E-09	3.09E-09	3.82E-09
99%	4.36E-09	4.36E-09	4.41E-09	4.39E-09	4.52E-09	5.09E-09

2.5.3.4 Front Panel Diagonals

In this case, damage is induced by reducing the elastic modulus of the elements in the front panel between nodes 1 -24. It is noted that bay 7 (small bay) does not have a diagonal element. The front panel diagonal elements are numbered from 1- 11 without 7 for ease of plotting. Also, the sensors used to perform the ASH flexibility damage

detection are also at the front bottom chord node locations. Hence, it is expected that the change is elastic modulus will be easily captured by the sensors as they are collocated. From the no noise cases, Figure 2.21, damage is detected to the correct bay for damage over 50%.

The data compression is similar to the method described in the previous section. The baseline determined from the Section 2.5.3.1 for sensors at the front-bottom chord are indicated by the hashed lines for various noise levels.

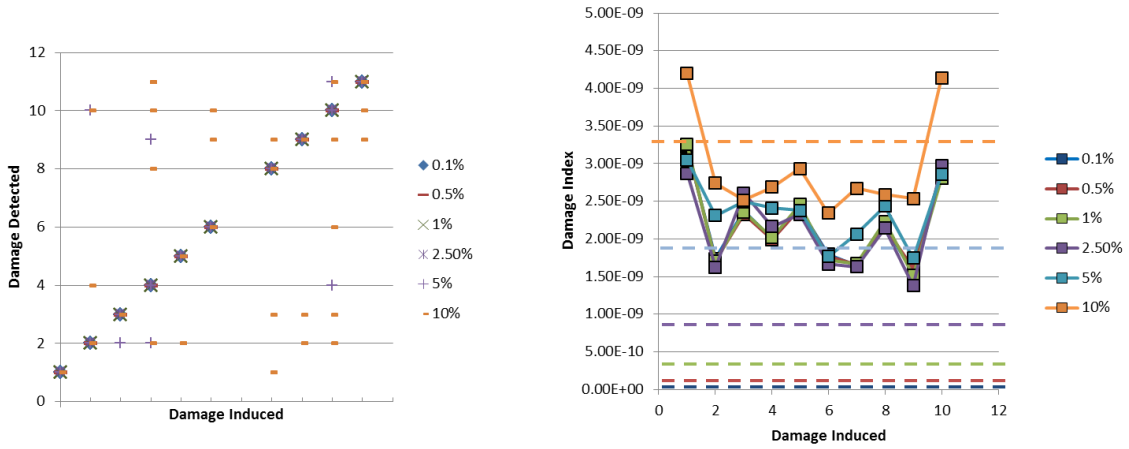

Figure 2.36: Damage detection results for frontpanel diagonal damaged with 10% reduction and noise (a) Damage localized vs. damaged element; (b) Damage index vs. damaged element.

Each column of Figure 2.36 (a) represents an element that was damaged and contains 5 data points for each noise level indicating the bays detected by the damage detection algorithm for that specific damage location. With 10% reduction in stiffness, it can be observed that, only the highest noise level of 10% damage cannot be localized to the correct element.

Figure 2.36 (b) plots the variation of maximum damage index with damage location and noise level for 10% reduction in stiffness property of the corresponding

elements. From Figure 2.36 (b) it is observed that the line for the maximum damage index for 10% noise (orange line with square markers) is the only case below the baseline limit whereas the lines for the other noise levels above the baseline limit. Hence, for the highest noise level in Figure 2.36 (a) there is no observable correlation between the damaged element and damage localization bay. An identifiable diagonal pattern to the damage localization is observed for lowest noise levels.

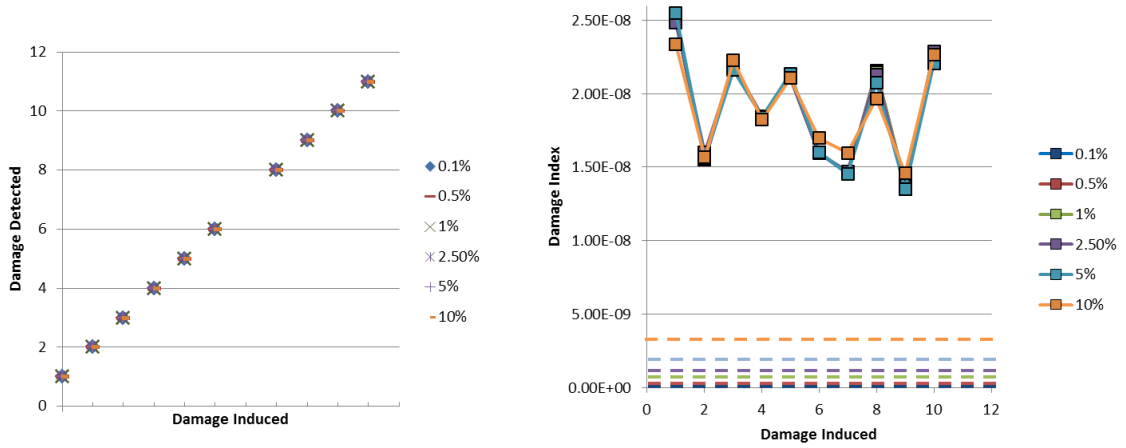

Figure 2.37: Damage detection results for frontpanel diagonal damaged with 70% reduction and noise (a) Damage localized vs. damaged element; (b) Damage index vs. damaged element.

In Figure 2.37 (a) with 50% damage level, damage can be estimated accurately with 10% noise level in the system. This is correlated to the Figure 2.37 (b) where the maximum damage indices are above the baseline limit at all the bay locations. Hence, damage to the diagonal is the most easily detectable damage for this structure. The Table 2.9 shows the maximum indices values and are color coded to show reliable damage detection.

Table 2.9: Maximum damage indices with respect to noise and percentage reduction in modulus.

Noise	0.1%	0.5%	1%	2.50%	5%	10%
Baseline value	**3.4E-11**	**1.46E-10**	**3.46E-10**	**7.86E-10**	**1.81E-09**	**3.27E-09**
10%	2.17E-09	2.18E-09	2.17E-09	2.14E-09	2.35E-09	2.93E-09
50%	2E-10	2.29E-10	2.97E-10	5.87E-10	1.11E-09	2.18E-09

2.5.3.5 Back Panel Diagonals

In this case, damage is induced by reducing the elastic modulus of the elements in the front panel between nodes 25 -48. Also, the sensors used to perform the ASH flexibility damage detection are also at the front bottom chord node locations. It is expected that the damage detection process to reduce in quality as the damage to back panel diagonal elements must be projected and observable by the front-bottom measured sensors.

The data compression is similar to the method described in the previous section. The interpretation of the plots is not described again but more emphasis on the observations is presented.

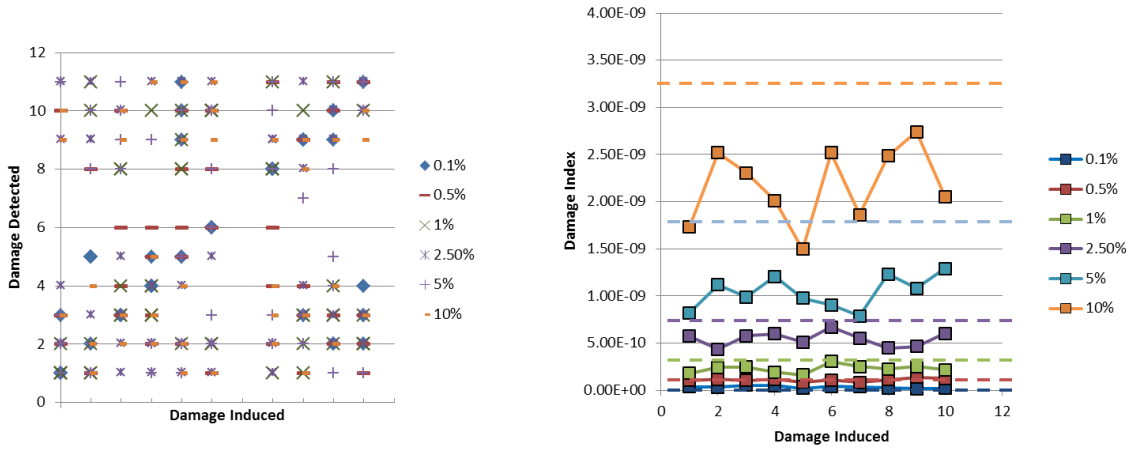

Figure 2.38: Damage detection results for back-panel diagonals damaged with 10% reduction and noise (a) Damage localized vs. damaged element; (b) Damage index vs. damaged element.

Each column of Figure 2.38 (a) represents an element that was damaged and contains 5 data points for each noise level indicating the bays detected by the damage detection algorithm for that specific damage location. With 10% reduction in stiffness, it can be observed that, none of the noise level can localize the damage to the correct element. Hence, for this level of damage to back panel diagonals, in Figure 2.38 (a) there is no observable correlation between the damaged element and damage localization bay.

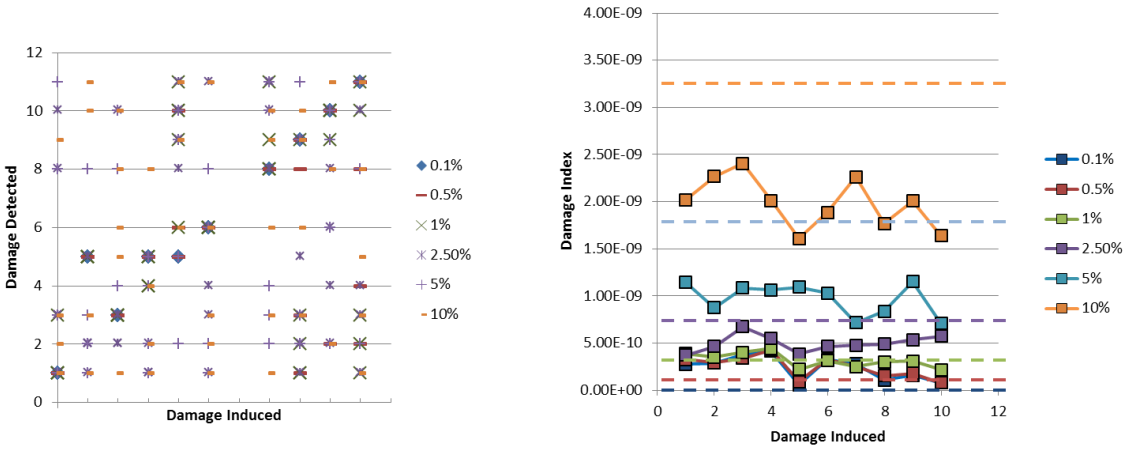

Figure 2.39: Damage detection results for back-panel diagonals damaged with 50% reduction and noise (a) Damage localized vs. damaged element; (b) Damage index vs. damaged element.

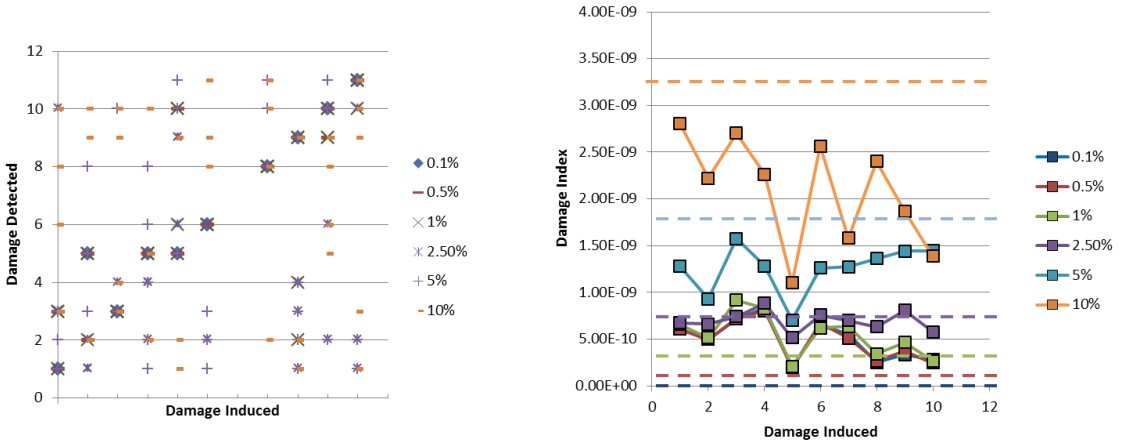

Figure 2.40: Damage detection results for back-panel diagonals damaged with 70% reduction and noise (a) Damage localized vs. damaged element; (b) Damage index vs. damaged element.

An identifiable diagonal pattern to the damage localization is observed for lowest noise levels with 50% and 70% reduction in elastic modulus in Figure 2.39 and Figure 2.40 . This is correlated to the fact that the damage indices for the lower noise levels are moving above the baseline limit.

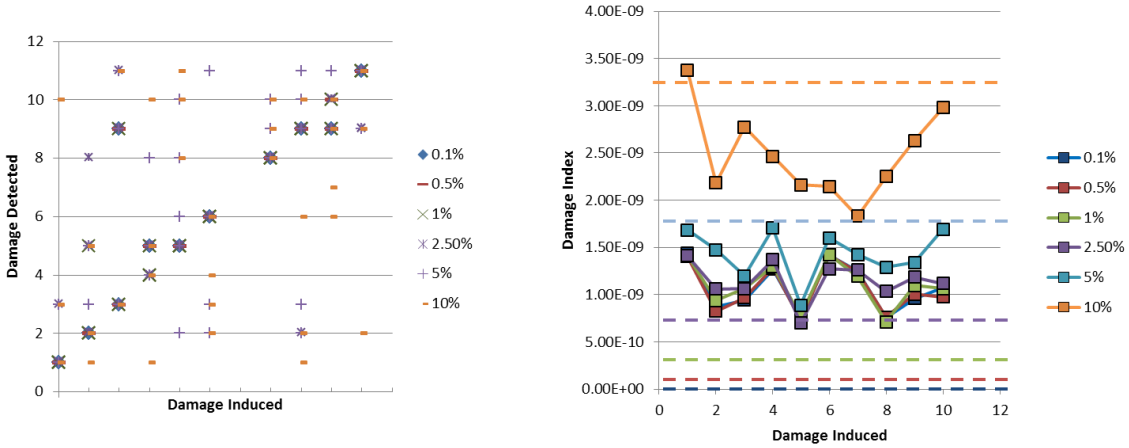

Figure 2.41: Damage detection results for back-panel diagonals damaged with 90% reduction and noise (a) Damage localized vs. damaged element; (b) Damage index vs. damaged element.

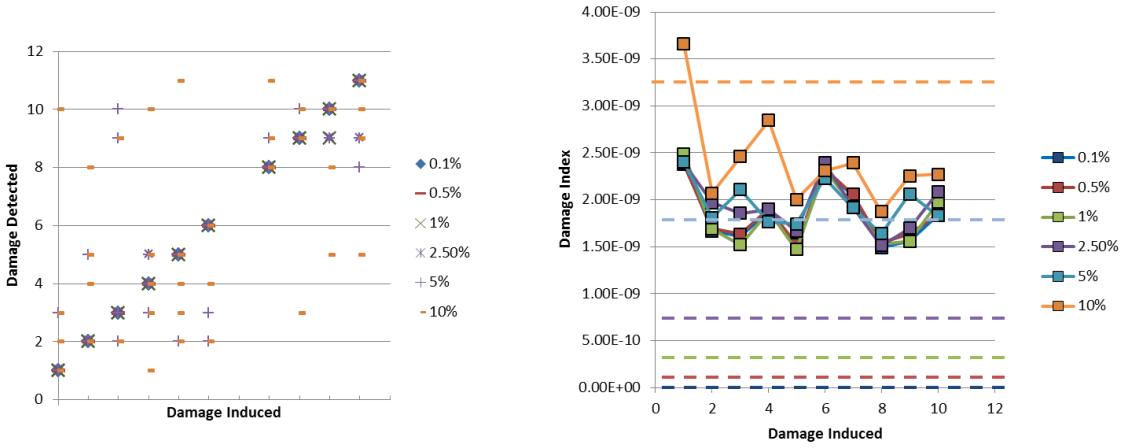

Figure 2.42: Damage detection results for back-panel diagonals damaged with 99% reduction and noise (a) Damage localized vs. damaged element; (b) Damage index vs. damaged element.

Finally with 90% and 99% reduction of modulus, the damage localization has improved for noise levels up to 5% noise. In Figure 2.42 (b) it is observed that the maximum index is very close to the baseline limit for 5% noise.

Also, the information from all the plots is condensed to a high level representation in a Table 2.10 with color coded values to depict the reliability of the results obtained based on the average maximum damage index value over the baseline.

Table 2.10: Maximum damage indices with respect to noise and percentage reduction in modulus.

Noise	**0.1%**	**0.5%**	**1%**	**2.50%**	**5%**	**10%**
Baseline value	**3.4E-11**	**1.46E-10**	**3.46E-10**	**7.86E-10**	**1.81E-09**	**3.27E-09**
10%	3.3E-11	1.08E-10	2.27E-10	5.43E-10	1.04E-09	2.17E-09
50%	2.36E-10	2.46E-10	3.19E-10	4.98E-10	9.7E-10	1.99E-09
70%	4.92E-10	4.89E-10	5.46E-10	6.95E-10	1.25E-09	2.09E-09
90%	1.07E-09	1.06E-09	1.1E-09	1.15E-09	1.43E-09	2.48E-09
99%	1.83E-09	1.85E-09	1.84E-09	1.94E-09	1.95E-09	2.41E-09

2.6 Conclusions

Noise is an important parameter to consider when evaluating the effectiveness of a damage detection method. Also, with added noise, one needs to estimate the amount of damage that needs to be induced on the structure to detect the damage reliably.

It is proven from the one dimensional beam model and the three dimensional space truss that the baseline damage index is an acceptable way to judge the reliability of the results obtained from damage detection. It was also shown that this baseline damage index has some of the necessary indicators to benchmark a structure and different damage detection methods.

CHAPTER 3. EXPERIMENTAL VALIDATION: FULL SCALE STRUCTURE

The method developed in the previous chapter is verified on an experimental full scale structure. In this chapter, a description of the experimental setup and data acquisition is presented. The experiment was performed to characterize the full scale highway sign support truss in three orthogonal directions at 44 nodal locations. The baseline is determined using the data for the intact structure. Five damaged cases for the structure are evaluated using this baseline method to detect damage.

3.1 Description of Full-Scale Structure

An experiment to demonstrate the proposed approaches is performed on a full-scale highway sign support truss at the Robert L. and Terry L. Bowen Laboratory for Large-Scale Civil Engineering Research at Purdue University. The truss is 17.04m long, 1.83m wide and 1.98m high. All members have a cylindrical cross-section. The truss is made of aluminum alloy (6061-T6). The truss studied here was previously mounted over interstate I-29 near Sioux City in Iowa as a sign support to display route information. The truss consists of four three-dimensional space frames sections connected by bolted joints and 2 planar frames for end supports. Two of the four space frames were assembled at the Bowen laboratory for testing. Table 3.1 shows the cross-sectional information for all the elements in its latent state obtained from the drawings.

Some of the nomenclature used to describe the structure for the remainder of the thesis is as follows.

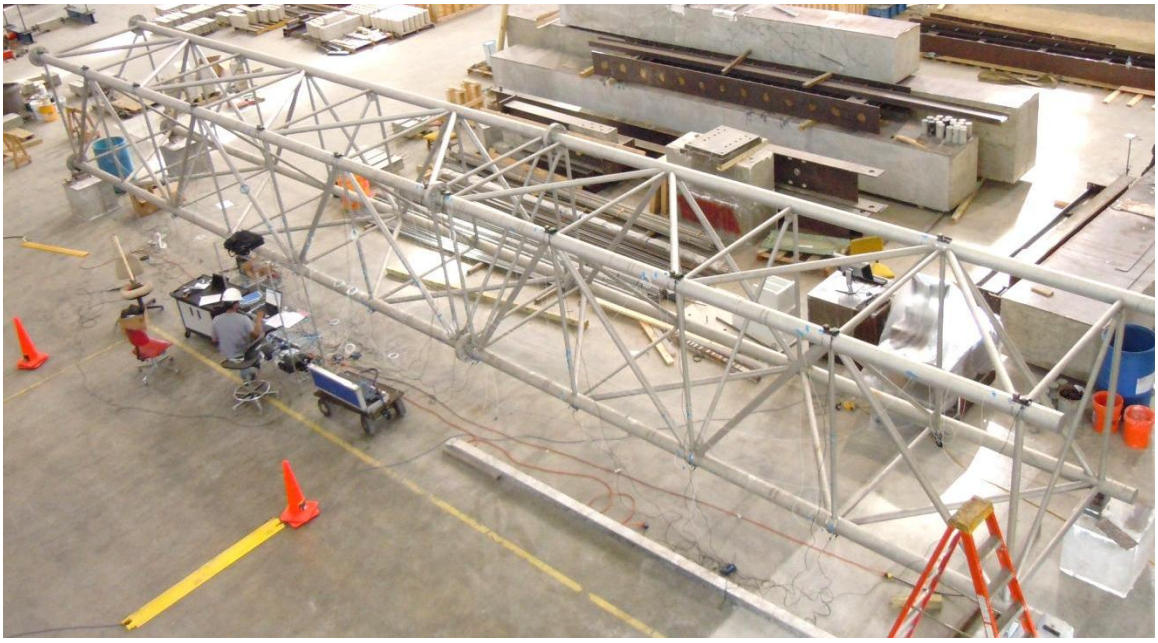

Figure 3.1: Highway sign support truss testing at Robert L. and Terry L. Bowen Laboratory for Large-Scale Civil Engineering Research at Purdue University.

Table 3.1: Properties of the structure from the drawings of the structure.

Outside diameter and thickness of main chords	152.4mm
	79.0mm
Outside diameter and thickness of in-panel diagonals	76.2mm
	6.3mm
Outside diameter and thickness of secondary orthogonal elements and tertiary elements	50.8mm
	4.8mm
Total span length	17.24m
Young's modulus	6.964E10N/m2
Density	2714.47kg/m3
poissons's ratio	0.33

Highway Sign Support Truss and Structure will be interchangeably used to refer to the experimental setup.

Co-ordinate directions: X – The direction along the major dimension of the highway truss

Y – The direction vertical to the baseline ground

Z – The direction out of plane; orthogonal to the vertical and along the major dimension of the truss

Bay: A section along the major dimension of the truss between two adjacent node. The truss has six bays of 1.73 m, one bay of 0.3m at the bolted joint and four bays of 1.68m each from left to right while looking at the truss facing north with bay number from 1-11as shown in Figure 3.2. Node numbers for the front panel are also shown.

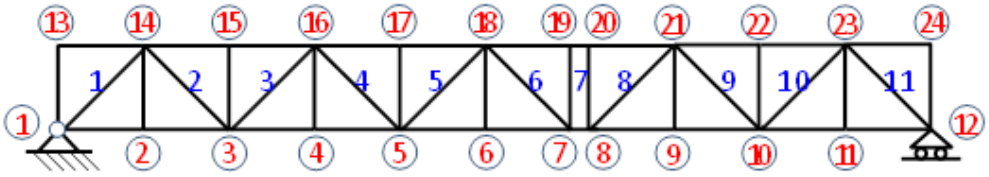

Figure 3.2: geometrical representation of the structure.

Front panel: Looking at the truss facing north, the plane containing the nodes closer to the viewer.

Back panel: Looking at the truss facing north, the plane containing the nodes farther from the viewer.

Bottom panel: The plane containing the nodes on the bottom chord of the front and back panel.

Top panel: The plane containing the nodes on the top chord of the front and back panel.

Top-Front chord, Bottom-Front chord, Top-Back chord, Bottom-Back chord: Looking at the truss facing north, the top and bottom chords of the front panel and top and bottom chords of the back panel

In-panel diagonal: The diagonal members at each bay within each panel. Each bay contains for in-panel diagonal members. These diagonals will be referenced with the panel and bay in which they are located.

In-panel secondary: The secondary members orthogonal to major chord members within each panel. Each of the panel contains 12 in-panel secondary members. The in-panel secondary members at the right end of the truss are of different dimensions to the rest of the secondary elements.

Intra-panel tertiary diagonals: The tertiary diagonal members between the front and back panel. The purpose of these elements is to maintain the ‘squareness’ of the cross-section of the truss. A particular design aspect of the intra-panel tertiary diagonals cylindrical members are that they are connected to the in-panel secondary members via stiffener plates. This joint characteristic increases flexibility of the structure as these plates are welded at about 0.1m from the main chord onto secondary more flexible members.

Figure 3.3: Intra-panel tertiary member detail; stiffener plate.

3.1.1 Setup of the Experiment

The full-scale truss was configured in the Bowen Laboratory with the left ends of the truss simply supported by placing it on metal blocks to simulate a pinned joint and the right ends of the truss were placed on cylinders to simulate roller supports.

Figure 3.4: Boundary condition of experimental setup.

An electro-dynamic shaker (VG-100 from Vibration Test Systems) was used to excite the truss along the Y direction and a modal sledge hammer (PCB 086D50; Sensitivity: (±15%) 1 mV/lbf, Measurement Range: ±5000 lbf) was used to impact the structure in Y and Z direction to fully excited all three dimensional degrees of freedom. Uniaxial accelerometers (PCB model 333B40, ICP accelerometers; Sensitivity: 500 mV/g, Range: ±10 g, Frequency range: 0.5 to 3kHz) and tri-axial wireless accelerometer (IMOTE2, SHM-A boards; Sensitivity: 2mV/g, Frequency range: 0-270Hz) were used to measure the output acceleration data. Three 8-channels, Smart Office analyzer (m+p international, Inc.) with VibPilot front end were used collect the input dynamic force and output acceleration data. Sensor mounts were designed for attaching the sensors on the cylindrical surface. The purpose of the sensor mounts is to provide consistent and

repeatable measurement direction, flat surface to mount the uniaxial wired sensors and platform for mounting the wireless sensors on the cylindrical members.

Figure 3.5: Electro-dynamic shaker.

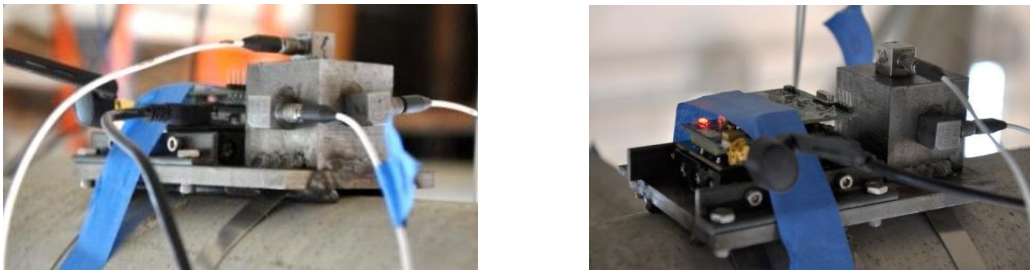

Figure 3.6: Sensor Mount with three wired and wireless sensors.

Figure 3.7: Data acquisition stem, amplifier and laptop.

Figure 3.8: Continued.

3.1.2 Data Acquisition

A 24-channel DAQ system enabled the sensor deployment of a panel of the full structure in any one test. Thus, a comprehensive test strategy was developed to fully characterize the front and back panel of the truss in the *X*, *Y*, *Z* direction; a total of 144 DOFs, using seven tests.

In six of the tests, only a single direction (*X*, *Y* or *Z*) are instrumented with sensors on the front or back panel at 23 node locations using the sensor mounts. For the same configuration of the structure, the sensors were switched from measuring one direction to the other on the front panel and back panel to measure the vibration response at all the nodes. Hence, *X*, *Y* and *Z* vibration traces from the 44 nodes (10nodes on front-bottom chord and back-bottom chord and 12 nodes on front-top chord and back-top chord) are measured. The first channel is used to measure the input excitation: shaker or hammer depending on the excitation and the rest 23 channels are dedicated to measuring vibration responses of 23 nodes.

The data collected in the 6 sets do not contain overlapping DOFs to finally combine the modeshapes to create full three dimensional modeshapes. For this purpose, the seventh test was performed with the 18 sensors attached distributed on the lower

chords at six location measuring in all *X*, *Y* and *Z* directions. Hence, data from this test was used to stitch together the other six tests to obtain complete three dimensional modal properties of the truss.

Multiple single-input excitations are performed to excite all the modes using the shaker and hammer. Data was collected for 320 seconds at sampling frequencies of 512 Hz for all the sensor configurations.

More information on the sensor location and direction, shaker and hammer input location, channel numbering, file format are presented in Appendix B. The complete data described here is made available through the free data repository of Network for Earthquake Engineering Simulation; NEES. The data is available for download at nees.org, project number: 1013, titled: "144 DOF Dynamic Measurement from a 50 foot Full Scale Highway Sign Support Truss in Intact and Damaged Conditions".

3.1.2.1 Shaker Testing

The truss was excited in the *Y* direction with band-limited white noise to simulate ambient excitation in the field. The shaker was located adjacent to node 4 as shown in Figure 3.5. The white noise signal from the signal generator was first amplified using an amplifier before being sent to the electro-dynamic shaker. For each of the test configurations, multiple repeatable data sets are collected. The signal generator was set to a band limited white noise of 0-200 Hz. The baseline noise in the system also was recorded. The noise level of the ambient was found to be of the order ~5 mg and the excitation of the structure created an average 1g level. A sample white noise input excitation and the 20 welch averaged power spectra for the input is shown in Figure 3.9.

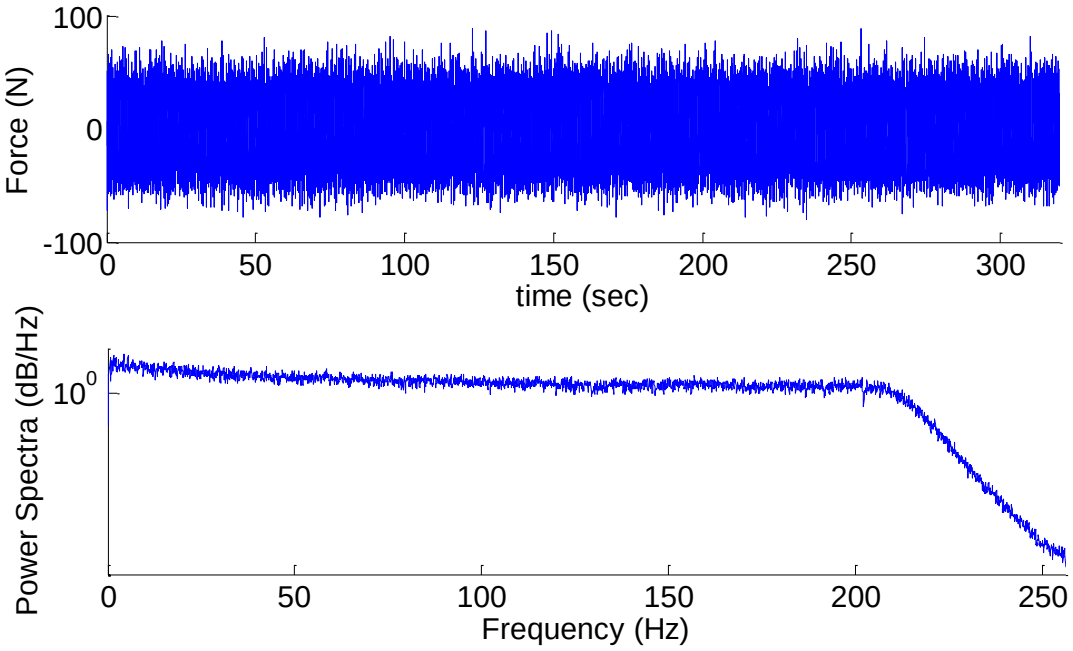

Figure 3.9:Shaker excitation (a) Time domain excitation, (b) Frequency domain.

3.1.2.2 Hammer Testing

The truss was excited with impact force at two locations in both *Y* and *Z* directions using the modal sledge hammer. Since the modal properties were not known at the time of testing and to ensure all the modes were excited, two different locations were tested to ensure that all the modes were fully excited. In total four hammer hit locations were collected for all 144 DOFs. For each DOF, 15 hits were performed to get better averaged frequency response functions. Two directions were tested to ensure all three dimensional modes could be evaluated and captured. Figure 3.10 shows the time history for one of the data sets: hammer input at node 10, *Y* direction and acceleration measurement at node 3 in *X*, *Y* and *Z* direction.

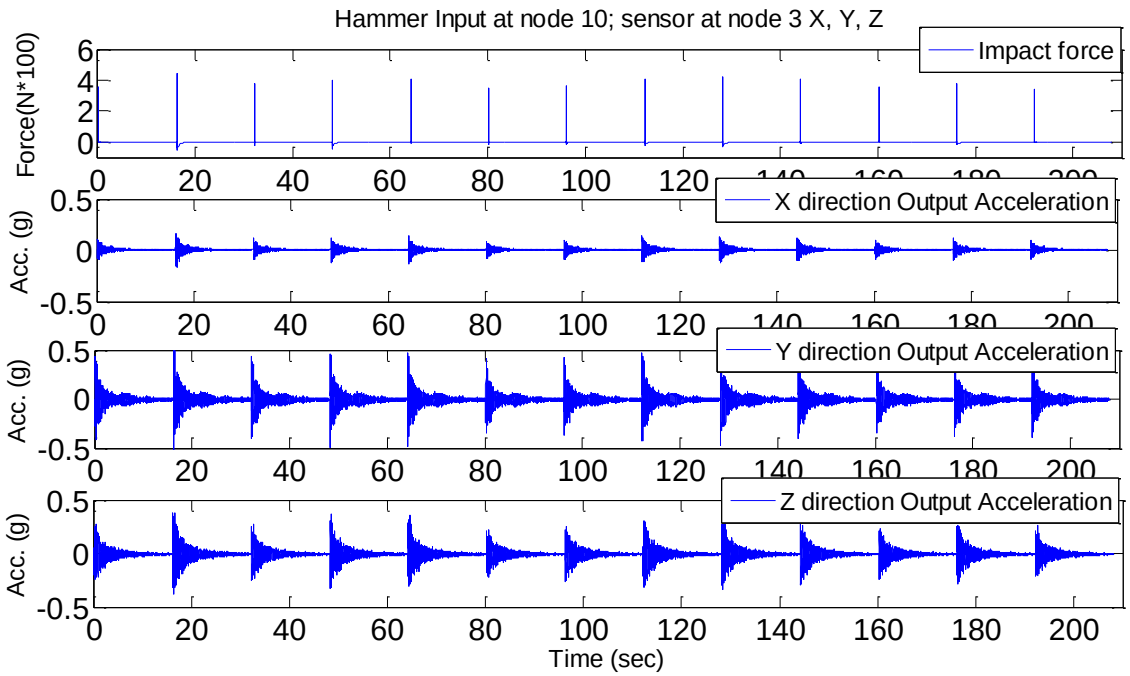

Figure 3.10: Sample time series data for hammer excitation.

Figure 3.11 shows the frequency response function evaluated for the time series shown above using all 15 hits in the averaging process. The sampling frequency is 512Hz but the frequency of interest is reduced to 0-40Hz.

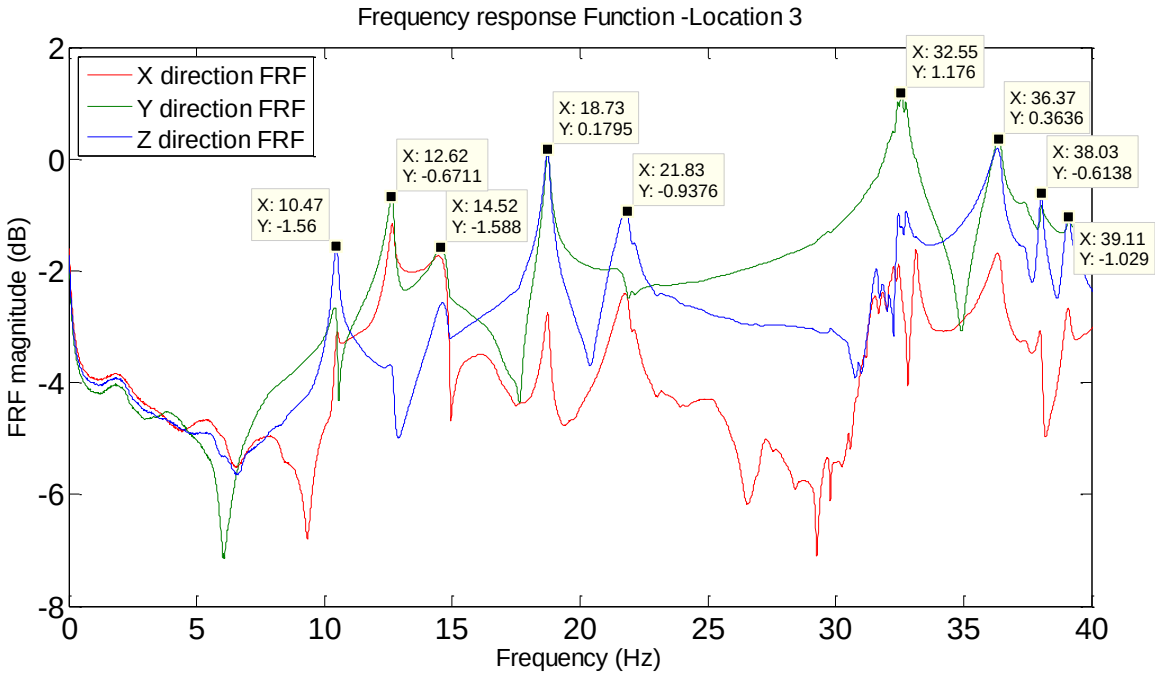

Figure 3.11: Frequency response function for location 3 in *X,Y,Z* direction for hammer excitation.

3.1.3 Damage Cases

Common damage to highway sign support truss is detailed in a technical report by the FHWA[31]. Some of the damages observed in the real world are discussed in this report. The types of damage reported are dents, tears, cracks in regions away from the ends, weld crack in diagonal member joint to the main chord, weld crack at the joint of vertical member and main chord and bolt loosening and splice gap at the flange connection. These field cases are shown in Figure 3.12. An important information to regard is that in an unpublished load test of a four-chord bridge structure by the Iowa Highway Department, the structure was able to carry in excess of its design load even when numerous secondary members were totally cut[31]. Hence, the damages shown in the Figure 3.12 that are prioritized as class 1, (i.e. needing immediate repair) are preventative

measures to restrict the damage progression but are far too small to cause any undesirable change in the ultimate load carrying capability of the structure. This warrants the question of the need to be able to detect these small damages.

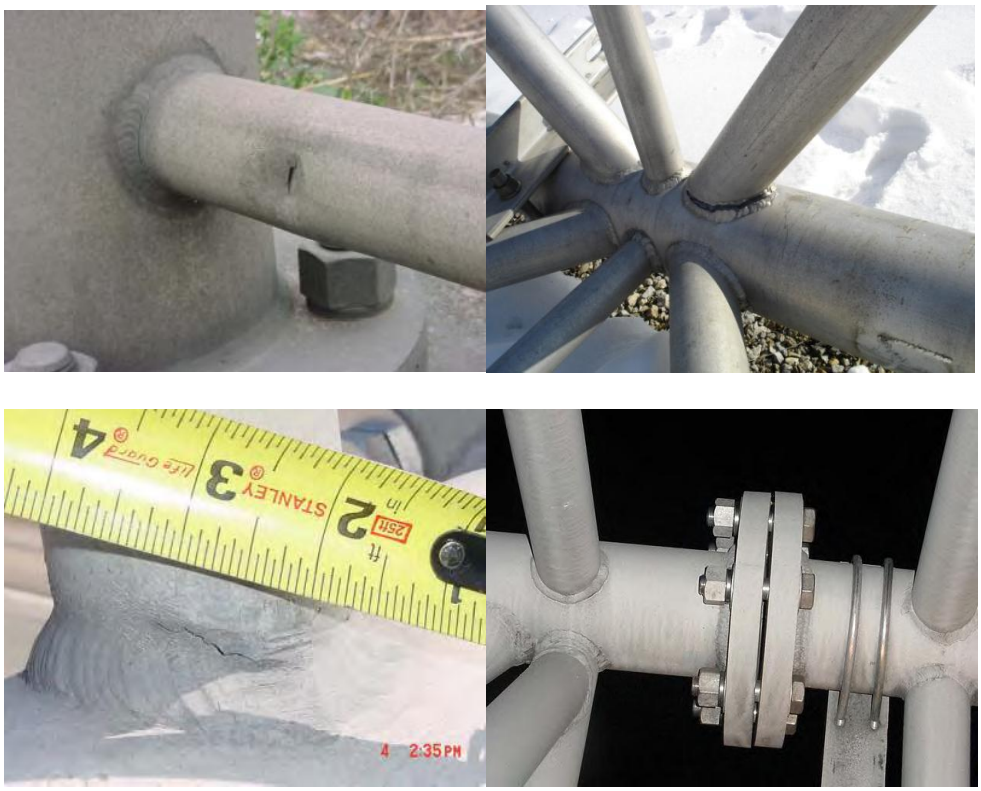

Figure 3.12: (a): Dent, tear, and weld crack in first strut on tower; (b): Weld crack in in-panel diagonal; (c): 1" long weld crack at lower chord; (d): Three loose fasteners that could not be tightened, Gap in chord splice.[46]

3.1.3.1 Damage Cases

To validate the damage detection methodology and study a variety of damages on the structure, multiple damage scenarios were created, instrumented and tested. One difficulty with this real structure was that once damage was created or repaired it cannot be reliably restored to its previous configuration. Therefore, the structure was considered to have evolved from one state to the next.

The structure had been tested before by a previous graduate researcher in February 2010. In the first round of testing only one damage case was studied. The damage was created at the weld located at the intersection of the front panel in-plane secondary diagonal and front-bottom chord at node 4, to replicate weld crack and failure of the in-panel secondary diagonal. It was induced on the structure by a full cut through the member so as to completely disconnect the member. After the testing the structure was disassembled and moved to a different location.

The data analyzed in the thesis is only from the current round of testing from April 2011 to July 2011.In April the structure was reassembled and setup at the lab. Since the structure was moved and reassembled, it is expected that the modal properties of the structure have changed because of the change is boundary conditions. To get as many cases of damage as possible from the structure during the structure's evolution, the damaged case from the previous round of testing was evaluated again. The full cut damage at the secondary diagonal at bay 4 was welded to half the cross section to simulate a smaller damage at the same location. The structure was tested in this configuration to evaluate another damage case. The intact or healthy case of the structure is then evaluated after welding the rest of the cut at bay 5. These damage and healthy cases will be considered as phase 1. Important information to note is that the in phase 1 of testing only 22 sensor mounts was available and the mounts needed to be moved from the front to back panel with the sensors. The mass of each of the sensor mounts is about 1kg. Hence, there is change of about 40kg from front panel to the back panel. This structural change causes a change in the modal properties of the structure from the front to back panel.

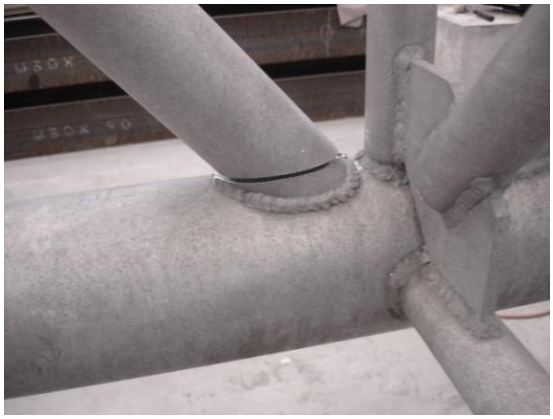

Figure 3.13: Damage case in Phase 1 of testing (a) Full Cut at bay 4 (Damage Case 5).

Figure 3.14: Damage case in Phase 1 of testing Half cut a bay 4 (Damage case 4).

In phase 2 of testing, all the nodes are instrumented with a sensor mount for the full test. Hence, the modal properties are consistent from front and back panel, and there are no issues regarding change in mass distribution. The intact structure data is collected again in the new 44 sensor mount configuration. Damage was created at a different location: middle of the back-panel diagonal at bay 9 was cut. The cut was about a third in depth of the full cross-section. For the next case, the same damage to the back panel diagonal was extended to about 90% across the cross section, to study the evolution of damage. The data was collected again as the next damaged set. The last case that was studied was a multiple damage case. Damage was created by cutting the bottom panel

diagonal at bay 5 by 90%. The damage in this case was created to study 3 dimensional damage. The multiple damages are present in orthogonal panels at the back and bottom panel.

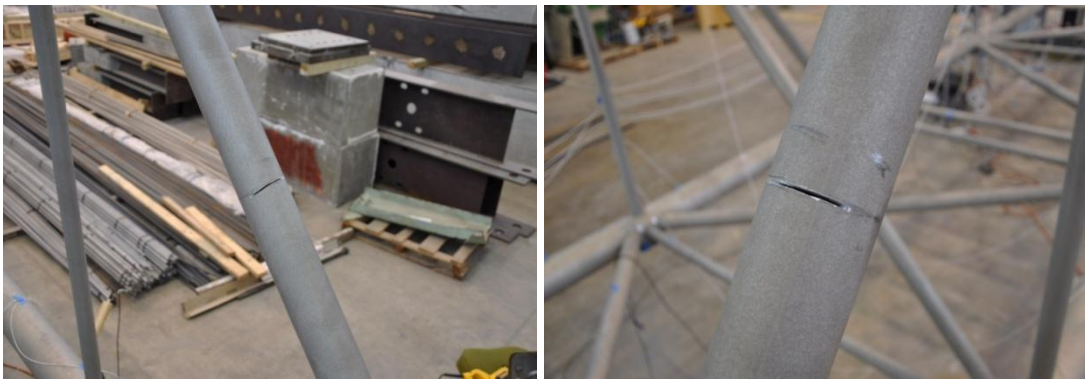

Figure 3.15: A third cut at back panel diagonal at bay 9 (damage case 1).

Figure 3.16: 90% cut at back panel diagonal at bay 9 (damage case 2).

Figure 3.17: Multiple damage case: 90% cut at back panel diagonal at bay 9 and 90% cut at bottom panel diagonal at bay 5 (damage case 3).

3.2 System Identification Methods

Numerous techniques are available for identifying the modal parameters from the free response data. Three method are used to evaluate the modal properties of the structure: The Complex Mode Indicator Function (CMIF) with peak-picking, The Frequency domain decomposition (FDD) with peak-picking and Eigen-system Realization Algorithm (ERA).

3.2.1 Method 1: Eigen-System Realization Algorithm

As this is a multi-input/output data time domain algorithm for minimum order realization of the modes shapes and natural frequencies of the system[32]. It is an extension of the Ho-kalman Algorithm[33] for a minimum order realization of the system. To implement this method, impulse response functions for one or more sets of initial conditions are used. The impulse response functions are obtained from inverse Fourier transform of the frequency response function. The eigen-system realization algorithm (ERA) is applied by first forming the Hankel matrix using the evaluated time domain impulse response functions as shown in

$$H(k-1)=\begin{bmatrix} Y(k) & Y(k+1) & \cdots & Y(k+p) \\ Y(k+1) & \ddots & & \vdots \\ \vdots & & \ddots & \vdots \\ Y(k+r) & & & Y(k+p+r) \end{bmatrix} \tag{3.1}$$

where, Y(k) = $m \times n$ pulse response matrix at the *jth* time step; i.e., *Yij(k) = ith* output at time *k* due to a pulse on input *j*. The parameters *r* and *s* correspond to the number of rows and columns of the Hankel matrix. In general practice, the number of rows is set to two-three times the number of models to be estimated and the number of columns is set to five times the number of rows. This matrix is evaluated for *H(0)* and the singular value decomposition (SVD) is performed. The SVD process gives the decomposition of the Hankel matrix into two unitary matrices and diagonal matrix. Relatively small singular values and the corresponding columns and rows are removed to condense the decomposition. The State Space representation for the discrete time system is found using

$$\begin{aligned} \hat{A} &= D_n^{\frac{-1}{2}} P_n^T H(1) Q_n D_n^{\frac{-1}{2}} \\ \hat{B} &= D_n^{\frac{-1}{2}} Q_n^T E_n \\ \hat{C} &= E_n^T P_n D_n^{\frac{-1}{2}} \\ E_n^T &= [I \quad 0]. \end{aligned} \tag{3.2}$$

The discrete time representation is converted to the continuous representation. The natural frequencies are evaluated by determining the eigenvalues of the continuous time state matrix, and the eigen-vectors are found using

$$\begin{aligned} Z &= \psi^{-1} A \psi \\ \Phi &= \psi^{-1} C. \end{aligned} \tag{3.3}$$

In conjugation with these parameter estimates, several accuracy indicators are developed by Pappa et. al[32] for use in assessing the results.

For the implementation of the ERA method to estimate the natural frequencies the data is passed through a low pass filter in the range 0 -45Hz and resampled from 512Hz to 128Hz. The impulse response functions for all the DOFs are evaluated by taking the inverse Fourier transform of the transfer functions. The ERA method requires some engineering judgment to evaluate the best possible combination of rows, columns singular value cut-off, experimental MAC estimate and modal damping estimate to determine the best modal parameters. A large number of combinations of row, column size are used for the Hankel matrix in the estimation process.

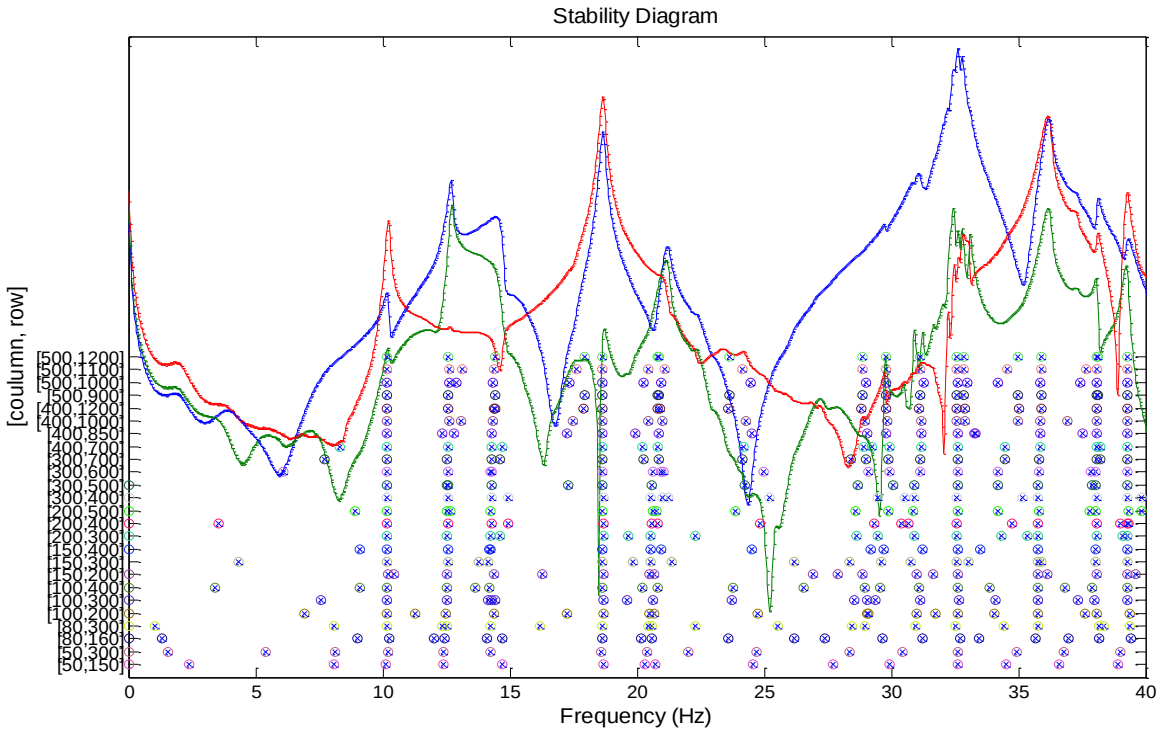

Figure 3.18: Stability diagram for 25 model realizations using ERA.

Figure 3.18: Stability diagram for 25 model realizations using ERA shows the stability diagram for different block size for the rows and column of the Hankel matrix. Hankel matrices with increasing matrix sizes are evaluated to determine the modal properties. The stability diagram presents the frequencies estimated by the ERA method

for various model realizations. The frequency response functions in the range of 0-40 Hz is also shown for reference. The case with the Hankel matrix of size (400, 1000) gave the best set of modal estimates using the EMAC and damping ratios as the accuracy indicators. Table 3.2: Frequencies estimated using the ERA method shows the frequencies estimated from the 6 sets in the *X*, *Y* and *Z* direction for the Phase 2 intact case data for the *Y* direction hammer excitation at node 10.

Table 3.2: Frequencies estimated using the ERA method

	X1 (Hz)	X2 (Hz)	Y1 (Hz)	Y2 (Hz)	Z1 (Hz)	Z2 (Hz)
1	10.157	10.219	10.231	10.229	10.250	10.157
2	12.596	12.646	12.630	12.515	12.663	12.596
3	14.328	14.626	14.641	14.574	14.751	14.328
4	18.653	18.677	18.635	18.671	18.627	18.653
5	20.998	21.077	21.222	20.911	20.9579	20.998
6	31.188	31.572	31.526	31.286	31.275	31.188
7	32.588	32.673	32.954	32.364	32.553	32.588
8	36.926	36.150	36.191	36.088	36.321	36.926
9	38.069	38.078	38.097	38.063	38.059	38.069
10	39.288	39.278	39.279	39.292	39.262	39.288

It is observed that, there is considerable variation in frequencies estimated for the various sets.

3.2.2 Method 2: FDD with Peak Picking

This method is an output only frequency domain modal identification technique to evaluate the modal properties[34,35,36]. Data acquired from each of the sensors is transformed into frequency domain by performing an FFT. The cross spectral density (CSD) functions between every node with each of the other node are obtained by averaging the output CSD over a number of frames. A CSD matrix is constructed at each of the discrete frequencies by assembling the CSD (S_{ij}). A Singular Value Decomposition (SVD) is performed on the CSD matrix at each of the discrete frequencies. The singular

value in each matrix evaluated at a discrete frequency is collected to form a vector. The vector corresponding to the natural frequencies can be estimated from the first column of its left SVD matrix.

Since the SVD is computationally expensive and only a small amount of data (CSD at the natural frequencies) contributes towards the modal identification, a new peak picking stage is added to the FDD. To optimize the data processing the averaging of CSD is discussed by Krishnan et. al[37] and the method is used here.

The acceleration responses for 144 DOFs are collected in 6 sets and modal estimation is performed on these sets individually. The modeshapes and natural frequencies are estimated from the acceleration responses using this method are shown in Table 3.3.

Table 3.3: Frequencies estimated using the FDD-PP method

	X1 (Hz)	X2 (Hz)	Y1 (Hz)	Y2 (Hz)	Z1 (Hz)	Z2 (Hz)
1	10.296	10.296	10.296	10.390	10.296	10.296
2	12.726	12.734	12.726	12.703	12.750	12.750
3	14.320	14.320	14.414	14.390	14.414	14.321
4	18.578	18.578	18.578	18.484	18.578	18.484
5	21.304	21.304	21.304	21.304	21.304	21.312
6	31.078	31.078	31.078	31.078	31.078	31.078
7	32.632	32.617	32.625	32.609	32.625	32.617
8	36.046	36.140	36.140	36.140	36.140	36.046
9	38.101	38.093	38.125	38.101	38.117	38.093
10	39.281	39.265	39.296	39.210	39.296	39.210

3.2.3 Method 3: Complex Mode Indicator Function

A system identification algorithm based on singular value decomposition is developed for traditional FRF data to identify the modeshapes and frequencies which works well for

closely spaced modes[34,38] The CMIF method indicates the existence of complex modes and their relative magnitude of each mode.

$$[N(\omega)] = [H(\omega)]^H[H(\omega)] = [V(\omega)]\,[\Lambda(\omega)]\,[V(\omega)]^H \qquad \text{Equation 3.4}$$

where, $[N(\omega)]$is the normal matrix and $[H(\omega)]$ is the FRF matrix $[V(\omega)]$is the left singular matrix and $[\Lambda(\omega)]$is the singular matrix.

CMIF is a frequency domain method that evaluates the eigenvalues from the normal matrix formed from the FRF matrix, at each spectral line. The normal matrix is defined as the shown in equation below from the FRF matrix. It is obtained by pre-multiplying the Hermitian matrix of the FRF matrix to itself. The singular value decomposition is performed on the normal matrix to obtain the singular value and the corresponding modeshapes. The peaks detected in the CMIF plot; Figure 3.19: Plot of the singular values evaluated from 0-40Hz indicates the existence of modes and the corresponding frequencies of these peaks give the damped natural frequencies for these modes. Peak-picking is introduced into the process to reduce the SVD calculations at each spectral line. The approximate peaks are estimated and picked by the user from visual inspection of the FRF plots. A smaller window is created at each of the peaks to evaluate the maximum singular value in this frequency range and determine the best modal estimate. Figure 3.19 shows the CMIF singular values plot for the full frequency range on 0 -40Hz.

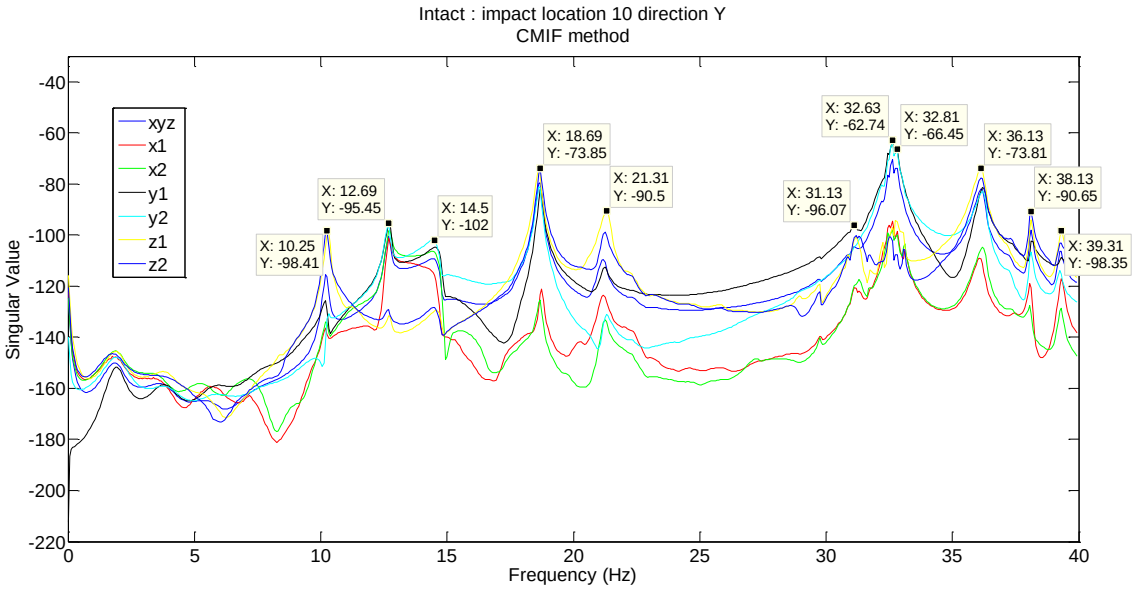

Figure 3.19: Plot of the singular values evaluated from 0-40Hz.

Table 3.4: Frequencies estimated using the CMIF method.

Mode	X1 (Hz)	X2 (Hz)	Y1 (Hz)	Y2 (Hz)	Z1 (Hz)	Z2 (Hz)	Tri-axial (Hz)
1	10.268	10.262	10.237	10.375	10.500	10.243	10.468
2	12.625	12.625	12.593	12.692	12.625	12.625	12.625
3	14.531	14.437	14.437	14.500	14.531	14.531	14.531
4	18.718	18.750	18.698	18.718	18.718	18.750	18.718
5	21.581	21.687	21.687	21.688	21.781	21.787	21.781
6	31.587	31.531	31.568	31.587	31.507	31.525	31.562
7	32.675	32.587	32.652	.32.650	32.637	32.752	32.635
7	36.343	36.312	36.187	36.312	36.250	36.312	36.343
8	38.031	38.000	38.000	38.062	38.031	38.0312	38.031
9	39.093	39.125	39.125	39.062	39.000	39.125	39.062

3.3 Implementation of ASH and AS Flexibility Method

The general methodology for the ASH flexibility and AS flexibility was detailed in the previous chapter for a structure. The experimental implementation of these algorithms to data evaluated from the structure is discussed below.

3.3.1 ASH Flexibility Method

The ASH flexibility method is applicable to structure which display beam type behavior when subjected to loads. The present three dimensional space truss displays beam like behavior since the structure has welded joints and transfers shear stresses when subjected to loads. Hence, the ASH flexibility method can be implemented to each of the main chords assuming that all the main chords depict beam like behavior individually. As shown from the numerical analysis, damage to dissociate elements from that of the nodes at which the ASH flexibility is evaluate, is not very easy to detect. The *Y* direction and *Z* direction modeshapes (transverse to the orientation of the element) are needed to evaluate the ASH flexibility matrices.

The idea is that damage to the structure in the front and back plane diagonals will cause change in the stiffness of the structure in the *Y* direction and this change can be detectable in the *Y* direction modeshapes. Similarly, with the *Z* direction modes, the data is expected to track *Z* direction stiffness change due to damage to bottom or top panel diagonals[39].

To evaluate the damage indices from the ASH flexibility difference we use the diagonal terms of the flexibility matrix to represent the damage index for the corresponding bays. The damage index can be conceptualized as change in bending angle per unit length at an element when a unit moment is applied at that element as

$$F_{\theta\,k,i} = \frac{1}{l_k}\frac{\left[\left(F_{k+1,i+1} - F_{k+1,i}\right) - \left(F_{k,i+1} - F_{k,i}\right)\right]}{l_i} \qquad (3.5)$$

where, $F_{k+1,i+1}$is the dynamically measured classical flexibility matrix, $F_{\theta\,k,i}$is the ASH flexibility matrix. The dynamically measured truncated classical flexibility matrix is evaluated from only the first 10 lower modes of the structure as

$$F = \Phi\Omega^{-1}\Phi^{T} = \sum_{r=1}^{n} \frac{1}{\omega_r^2}\varphi_r \cdot \varphi_r^{T} \qquad (3.6)$$

In (3.6, the modal matrix and modeshapes used are mass normalized modal properties. There are two ways to obtain mass normalized matrices: from driving point measurement method or using an accurate model of the structure and extracting the modal mass for each of the modes. Since, both these are not available; the modeshapes are normalized to have a magnitude of unity. The same realization is used for the entire analysis of the intact and damaged measured flexibility matrix and is a pseudo dynamically measured flexibility matrix.

From (3.5, it is shown that that damage index is inversely proportional to the length of the element. For the structure in question, the dimension bay 7 is smaller than the other bays and has higher flexibility between the nodes because of the bolted joints. Hence, the damage index for bay 7 is much higher than that of the rest of the bays and not included in the comparison with the other bays. The modeshapes at the boundaries are not measured and are assumed to be identically 0. This results in a different calculation at the boundaries as some of the terms go to zero as shown in eqn. Hence, these bays are also not considered in the comparison of the damage indices to evaluate the damage indices.

3.3.2 AS Flexibility Method

The damage indices for the AS flexibility method is defined as the change in axial strain from healthy to damaged structure when unit opposing forces are applied to an element. This method is designed to work effectively for structures that react to load primarily by axial deformation. For the structure under consideration, the vertical elements connecting the bottom panel and top panel are chosen to evaluate the AS flexibility method. It is assumed that the damage to the diagonal at a bay will reduce the stiffness between the horizontal panels and this can be measured by the change in AS flexibility of the adjacent vertical members as

$$ASF_{ji} = \frac{\delta l_j}{l_j} = \frac{c_j \delta X_j - s_j \delta Y_j}{l_j} \tag{3.7}$$

where, δX_j is the axial strain flexibility in the *X* direction, δY_j is the axial strain flexibility in the *Y* direction and c_j and s_j are cosine and sine of the orientation of the element. The implementation of the AS flexibility method to the vertical elements reduce the formula to a simpler form requiring the use of only *Y* direction modeshapes are required. (3.8 shows the simplification to the full equation when applied to the specific elements. The angle θ for these elements are 90°. Hence, $cos\theta = 0$ and $sin\theta = 1$, simplifying the equation to

$$ASF_{ji} = \frac{\delta l_j}{l_j} = \frac{-\delta Y_j}{l_j} \tag{3.8}$$

Where, δY_j also reduces to

$$\delta Y_j = \cancel{\frac{c_i}{l_i}\left[\left(F_{2p,2d-1} - F_{2p,2g-1}\right) - \left(F_{2o,2d-1} - F_{2o,2g-1}\right)\right]} + \frac{s_i}{l_i}\left[\left(F_{2p,2d} - F_{2p,2g}\right) - \left(F_{2o,2d} - F_{2o,2g}\right)\right] \tag{3.9}$$

A note of consideration is that only *Y* direction modeshapes are used, as observed from the indices of the remainder of the equation. This AS flexibility is determined only for these elements because this will not require any "stitching of modeshapes" between different sets of data, which can cause additional noise due to user input.

3.4 Damage Detection Experimental Results

In this chapter, the modeshapes and natural frequencies determined from intact and damaged cases are used to experimentally validate the ASH and AS flexibility damage detection method. The AS and ASH flexibility damage detection method is also used to demonstrate the baseline damage index proposed to improve robustness of damage detection methods.

It is first important to establish that the estimated modeshapes and natural frequencies from the various methods and other parameters used at the modal identification stage do not falsely detect damage in the structure. Also, by comparing the various modal parameters identified from the healthy state using the damage detection algorithm determines the baseline damage index above which, damage can be reliably ascertained in the structure.

Since the data in all 3 directions are measure at all degrees of freedom, the modal properties in the *Y* and *Z* direction can be determined for all the nodes of the structure. To demonstrate the applicability of this method, the modal properties of the whole structure needs to be divided into separate modeshapes for each of the main chords.

During testing of the various healthy and damage cases, it is ensured that the same protocols are used to record data from the structure to maintain consistency in the recorded data and to ensure the best possible vibration measurements are taken. This

ensures that similar levels of random noise from various sources are present in all sets of data. The same modal analysis method is performed to all the data used in the analysis to ensure similar levels of noise are carried though the identification process. Hence, the modal analysis process is required to be automated consistent process. The ERA method requires user judgment at various stages to determine the Hankel matrix size, the cut-off singular value etc. that cannot be automated. Every set of data needs a stability analysis performed and the user to retain the modes that are acceptable. Damping ratios, experimental MAC are used as guides to select the best possible modes. The ERA method does not have consistency in the modal properties evaluated to be successful with the method presented and is not presented.

The use of a common modal analysis with same number of averages per set, zero padding to the same length, using same window size in the peak picking process for the CMIF method ensures that the noise reduction due to averaging is maintained and similar levels of noise are present in all the damage cases. In the analysis, This is paramount to successful application of the baseline method because when determining the baseline from experimental data, the baseline limits are set for a particular amount of noise. As discussed previously, two modal identification methods are used to evaluate the modal properties of the structure: the ERA and CMIF with peak-picking. These two methods reduce the same data into the modal parameters with different amount of noise in the results.

In general methods are developed assuming that the structural behavior can be characterized by a linear equations of motion and experimental data is assumed to contain random ambient noise over this exact linear vibration signal. But, in general, other factors

like nonlinearities from environmental factors and material nonlinearities cause added discrepancies to the assumed linear vibration behavior. This in general cannot be quantified accurately because if it not possible to obtain exact modal properties from the structure, and hence it is not possible to predict the amount of noise simply from the vibration data of an unexcited system. Hence, the baseline damage index established a level of noise from the actual data in terms of the damage detection method in question rather than assign a threshold in the damage detection indices from user intuition or experience.

3.4.1 Establishing the Baseline Damage Index

The data for any of the cases consists of approximately 15 hits. This data for the hammer hit at node 10 (as close as possible to the node) in the *Y* direction is used in the analysis. The data is processed using CMIF with six averages each in three sets with one hit overlapping between the repetitions. Each hit is zero padded with 7*N (N = 8192) points when evaluating the frequency response functions. To reduce the computational cost the frequency domain CMIF method is applied only at some discrete windows of the full frequency domain using the peak-picking process. These bands are provided by the user with information from full CMIF and its singular value diagram or frequencies estimated by the time domain ERA method. This process only ensures that the computational cost and the user input does not govern the actual process of data and noise reduction.

The three modal estimates for the intact case are input into the ASH flexibility method to determine the baseline damage index. As we know that the data is for the same case, the peaks in the damage indices are due to the noise. The maximum damage index for the all the damage indices is determined to be the baseline damage index. Figure 3.20

shows damage indices for the 11 bays for the four main chords using *Y* direction modeshapes. The damage indices were obtained from evaluating the ASH flexibility based damage detection method with the three modal estimates, taking two at a time in all permutations. The damage indices for the ends (bay 1 and 11) are ignored when setting the baseline limit. Also, the bay 7 value is omitted in the baseline damage index and is set as a bounding line that is greater than all the damage indices for the bays.

This assumption is valid as the structure is uniform and from the numerical simulation we note that the damage indices are of approximately the same magnitude for all bays for the same damage. In the case of non-uniform structure, where the elements are of different length and/or varying properties each of the sub-structure or element could have a baseline damage index defined.

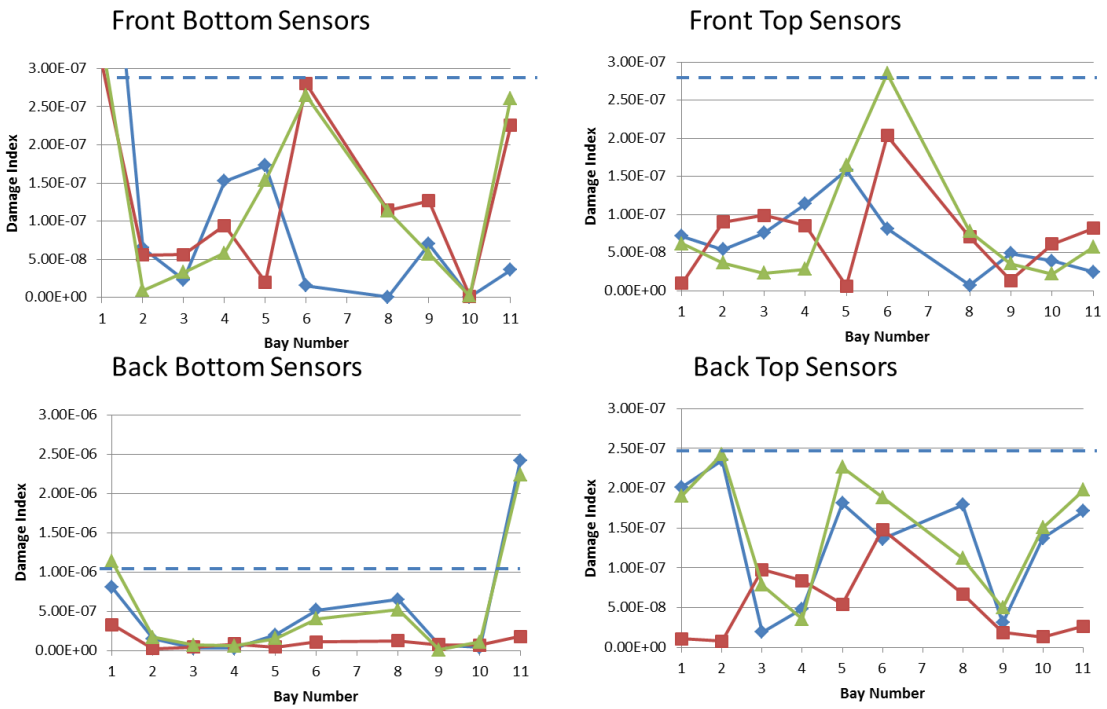

Figure 3.20: ASH *Y* direction flexibility damage indices to determine the baseline damage indices.

The analysis was repeated using the *Z* direction modeshapes for all the main chords as shown in Figure 3.21.

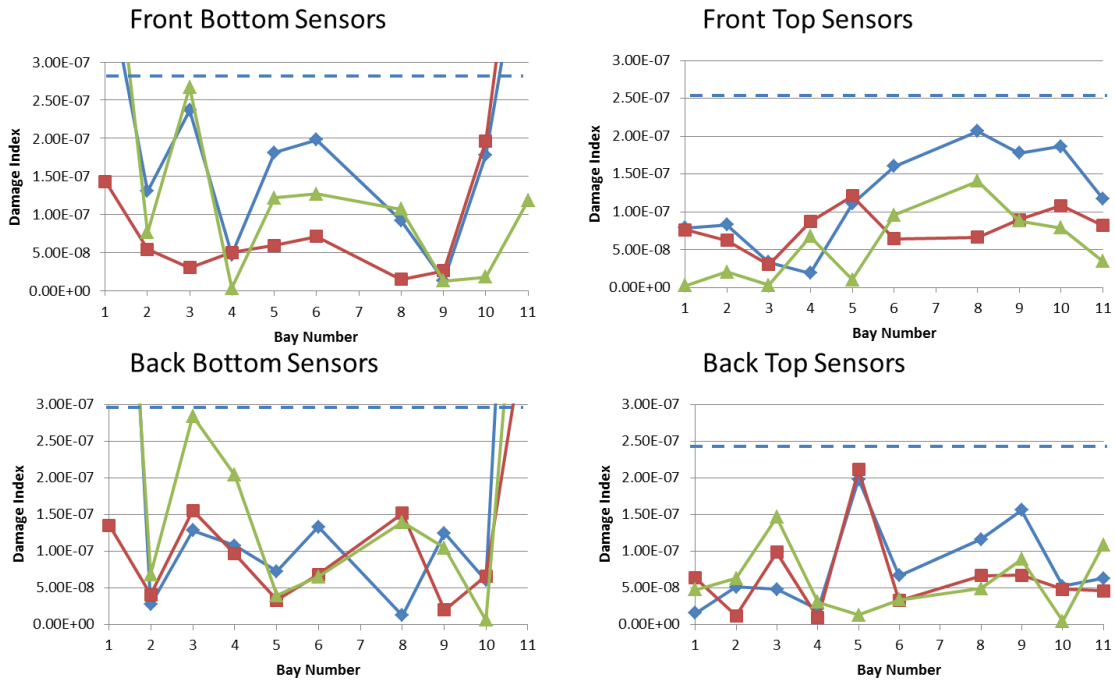

Figure 3.21: ASH *Z* direction flexibility damage indices to determine the baseline damage indices.

Figure 3.22 shows damage indices for the 12 vertical elements for the front and back panel using *Y* direction modeshapes to evaluate the change in AS flexibility due to variation in modal estimate in the same healthy case. The damage indices were obtained from evaluating the AS flexibility based damage detection method with the three modal estimates, taking two at a time in all permutations.

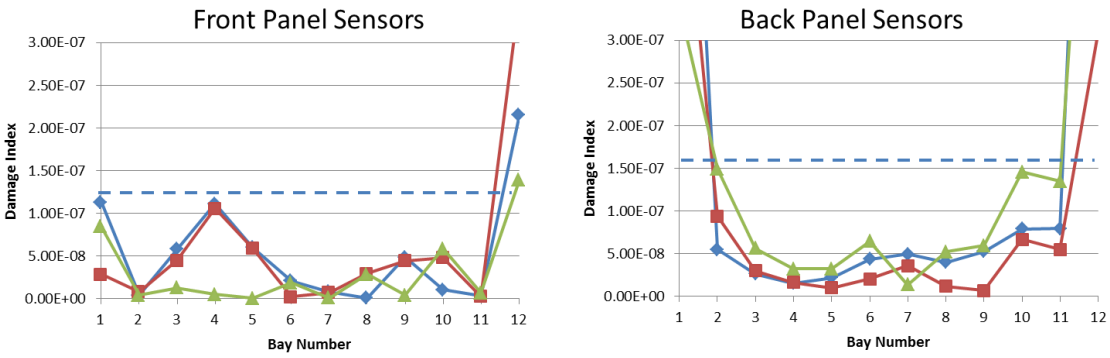

Figure 3.22: AS *Y* direction flexibility damage indices to determine the baseline damage indices.

Table 3.5 shows the baseline damage indices used for the cases of damage1, damage2 and damage3.

Table 3.5: Baseline value for the ASH and AS flexibility indicies.

	ASH [Y Direction Flexibility]				**ASH [Z Direction Flexibility]**				**AS [Y Flexibility]**	
	Front Bottom	Front Top	Back Bottom	Back Top	Front Bottom	Front Top	Back Bottom	Back Top	Front Panel	Back Panel
Baseline Value	3.0E-7	3.0E-7	7.0E-7	2.5E-7	3.0E-7	2.5E-7	3.0E-7	2.5E-7	1.5E-7	1.5E-7

3.4.2 Damage Detection for Phase 2 Damages

In this study, to validate the damage detection method 3 damage scenarios are induced on the structure. The sensors from each major chord are used separately to evaluate the ASH flexibility damage index and the front and back panel sensors are used to evaluate the AS flexibility damage index.

For damage indices to be accepted the value of the peak when comparing pre and post damage configurations must be higher than the baseline value. This damage index value and location of peak are accepted if it is above the baseline limit. For situations

where there are peaks in the damage indices but are below the baseline, the peaks are not considered to be valid damage localization.

Three modal estimates are obtained for all the damage cases per the same guidelines used for the healthy case. These are input into the ASH flexibility method against the healthy case to determine the damage indices. Figure shows damage indices for the 11 bays for the four main chords using Y direction modeshapes. The damage indices were obtained from evaluating the ASH flexibility based damage detection method with the three modal estimates each from damaged case and the healthy case, taking two at a time.

It is observed from the numerical simulation that for a noise level the damage is easiest detected at the sensors adjacent to the damage. The MAC of the sensors that coincide with the damage location showed the lowest MAC correlation. Hence, the modeshapes and frequencies for the nodes next to the damage location is the most sensitive to changes in the properties of the structure. This can be attributed to the fact that damage to an element of the structure has the largest projection on the sensors closest to the damage location. Damage to disjoint locations from the sensor domain are difficult to estimate because the change is modal properties at the sensor location change only by a small amount for the same extent of damage.

3.4.2.1 Damage1 vs Intact

In this case the damage is one third cut in the middle of the back panel diagonal at Bay 9.The damage indices for the ASH flexibility method for the *Y* direction modes are shown in

Figure 3.23 for the main chords. The value of the peaks for the front-bottom, front-top and back-bottom are lower than the baseline and no damage is localized using the three chord information. In the last plot for the back-top chord the damage indices are larger than the baseline damage index at bay 5 and 6. According to the definition of the method, this is a damage location detected by the ASH *Y* direction flexibility method. From the information, known about the actual location, this result obtained is a false positive.

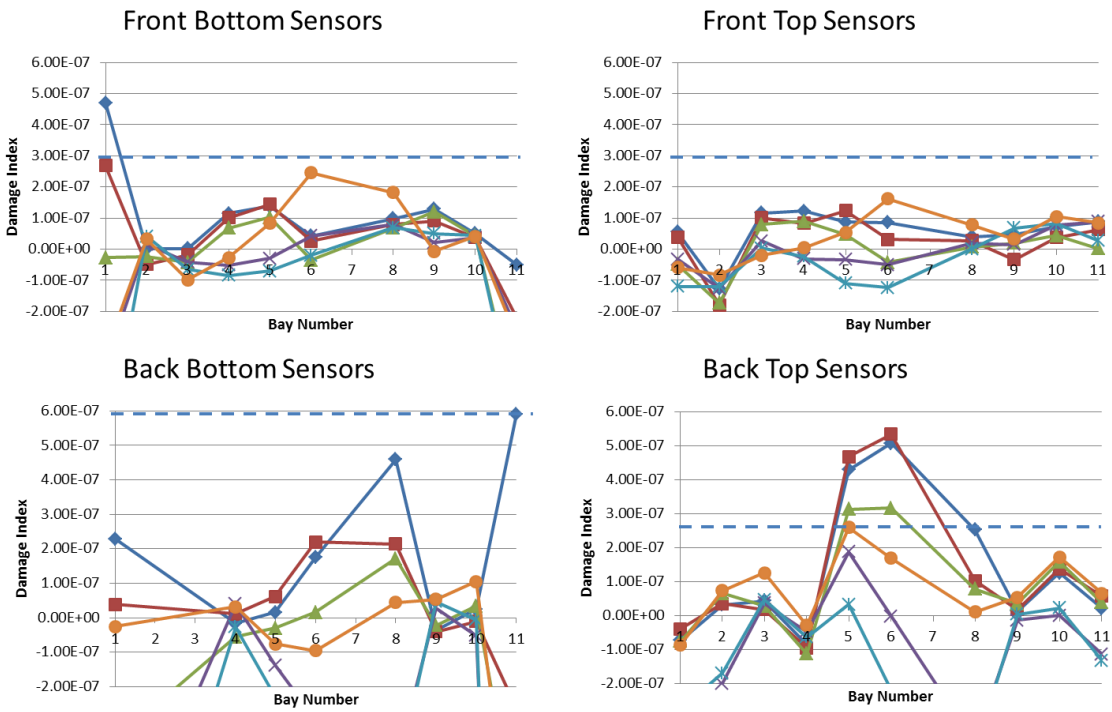

Figure 3.23: ASH *Y* direction flexibility based damage index for the 4 main chord for 1/3 damage at back panel diagonal element at Bay 9.

The damage indices for the ASH flexibility method for the *Z* direction modes are shown in Figure 3.24 for all four main chords. The values of the peaks for the chords are lower than the baseline and no damage is localized. Using the change in *Z* direction modes from healthy to damage 1 case, no information can be deduced about the damage location. The damage induced in this case does not cause a significant change in the *Z* direction modes to the extent that the change in the structure can be detectable using the ASH flexibility method.

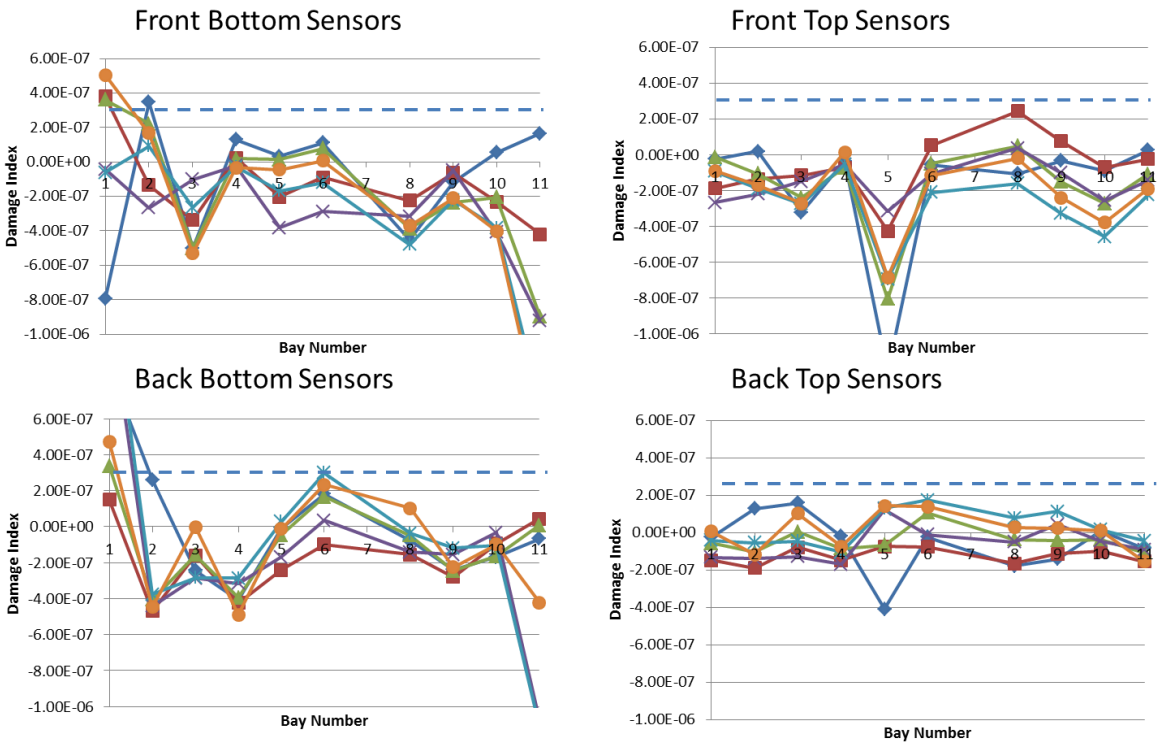

Figure 3.24: ASH *Z* direction flexibility based damage index for the 4 main chord for 1/3 damage at back panel diagonal element at Bay 9.

Figure 3.25 shows the damage indices for the AS flexibility method for the *Y* direction modes for the 12 vertical members for the front and back panel. For the back panel, the damage indices for 2 bays are above the baseline damage index determined. The vertical members at 6 and 8 have damage indices higher than the baseline index. Location 8 is accurate damage localization, as this vertical member is adjacent to the damaged diagonal and a false positive is detected at vertical element 5.

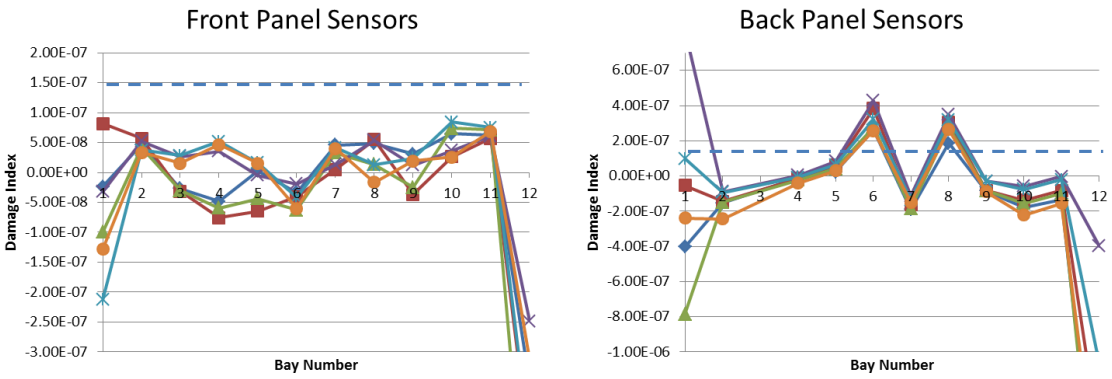

Figure 3.25: AS *Y* direction flexibility based damage index for the vertical members for 1/3 damage at back panel diagonal element at Bay 9.

The information from all the plots are condensed into the Table 3.6, using color coded numbers. Green is used to represent that the damage index is higher than the base line and damage is detected to the correct location. Red is used to represent that the damage index is higher than the baseline and damage is not detected by any of the peaks to the correct location. Yellow is used to represent that the damage index is higher than the baseline and correct location but there is another peak that locates damage incorrectly.

Table 3.6: Damage detection results for damage case 1.

	ASH [Y Direction Flexibility]								**ASH [Z Direction Flexibility]**								**AS [Y Flexibility]**			
	Front Bottom		Front Top		Back Bottom		Back Top		Front Bottom		Front Top		Back Bottom		Back Top		Front Panel		Back Panel	
Baseline value	**3.0E-7**		**3.0E-7**		**7.0E-7**		**2.5E-7**		**3.0E-7**		**2.5E-7**		**3.0E-7**		**2.5E-7**		**1.5E-7**		**1.5E-7**	
Damage 1	**1.0 E-7**	**5**	**1.0 E-7**	**4**	**3.0 E-7**	**8**	**5.2 E-7**	**6**	**3.7 E-7**	**2**	**2.0 E-7**	**8**	**2.0 E-7**	**6**	**1.8 E-7**	**3**	**0.7 E-7**	**10**	**3e -7**	**6**
	2.4 E-7	**6**	**1.5 E-7**	**6**	**2.0 E-7**	**6**	**4.5 E-7**	**5**							**1.8 E-7**	**6**	**0.5 E-7**	**8**	**3e -7**	**8**

3.4.2.2 Damage2 vs Intact

In this case the damage is from the previous case is enlarged to about 80% cross-section cut at the back panel diagonal at bay 9. The damage indices for the ASH flexibility method for the *Y* direction modes are shown in Figure 3.26 for all four main chords. The value of the peaks for the front-bottom, front-top and back-bottom are lower than the baseline and no damage is localized using the three chord information. In the last plot for the Back-top chord the damage indices are larger than the baseline for bay 9.This is accurate damage localization for the structure.

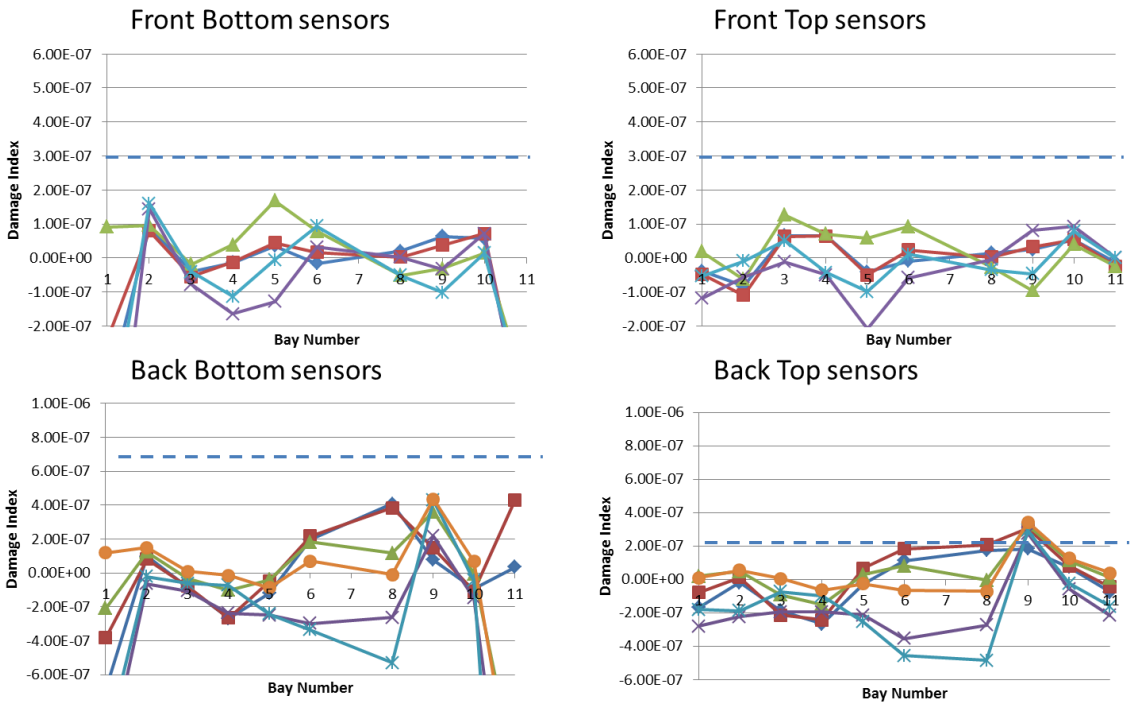

Figure 3.26: ASH *Y* direction flexibility based damage index for the 4 main chord for 3/4 damage at back panel diagonal element at Bay 9.

The damage indices for the ASH flexibility method for the *Z* direction modes are shown in Figure 3.27 for all four main chords. The values of the peaks for the chords are higher than the baseline at numerous locations. From the results, a number of false

damage localization is observed from the ASH Z direction flexibility plots. This has to be accepted as false positive for the validation of the ASH flexibility method. The maximum damage index in the back-bottm chord at bay 10 is due to disconnected sensor and not due to damage and is not considered as an accurate localization of damage at bay 9.

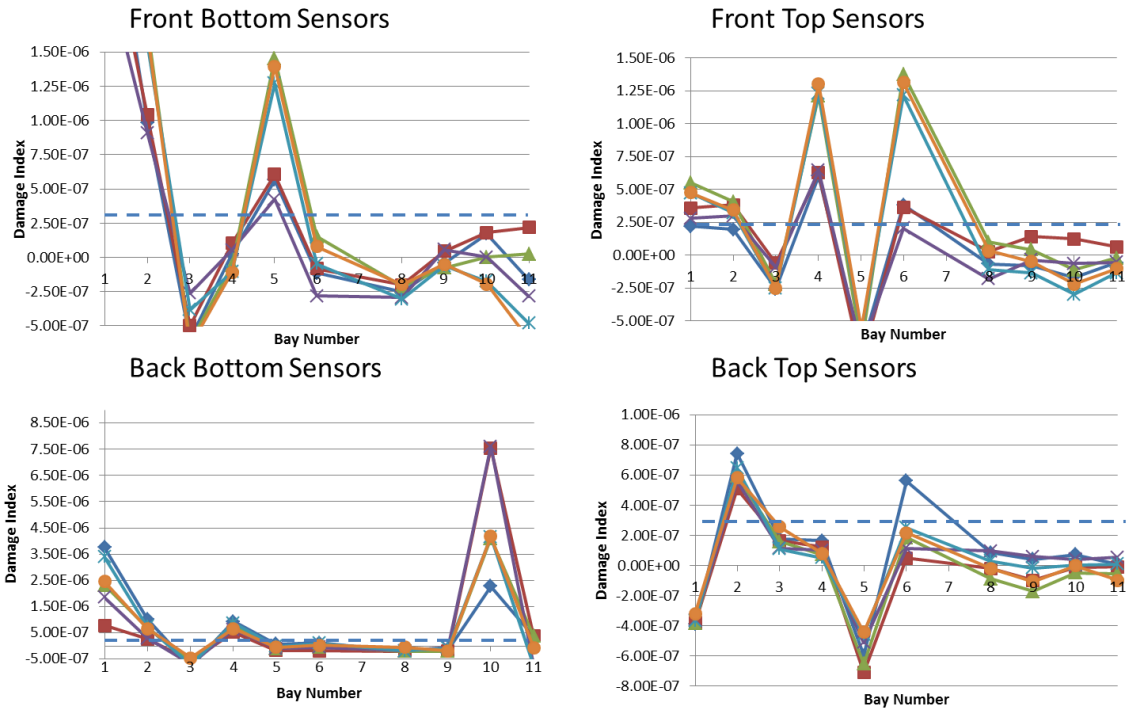

Figure 3.27: ASH *Z* direction flexibility based damage index for the 4 main chord for 3/4 damage at back panel diagonal element at Bay 9.

Figure 3.28 shows the damage indices for the AS flexibility method for the *Y* direction modes for the 12 vertical members for the front and back panel. The damage indices are all below the baseline and no damage can be localized using the data.

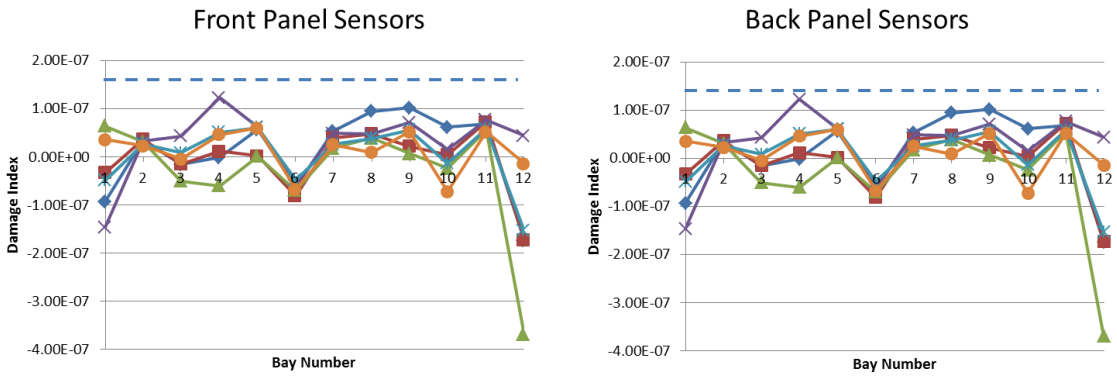

Figure 3.28: AS *Y* direction flexibility based damage index for the vertical members for 3/4 damage at back panel diagonal element at Bay 9.

The information from all the plots are condensed into the Table 3.7, using color coded numbers as described in the previous section.

Table 3.7: Damage indices for damage case 2.

	ASH [Y Direction Flexibility]								**ASH [Z Direction Flexibility]**								**AS [Y Flexibility]**			
	Front Bottom		**Front Top**		**Back Bottom**		**Back Top**		**Front Bottom**		**Front Top**		**Back Bottom**		**Back Top**		**Front Panel**		**Back Panel**	
Baseline value	**3.0E-7**		**3.0E-7**		**7.0E-7**		**2.5E-7**		**3.0E-7**		**2.5E-7**		**3.0E-7**		**2.5E-7**		**1.5E-7**		**1.5E-7**	
Damage 2	**1.5 E-7**	**2**	**1.2 E-7**	**3**	**4.0 E-7**	**8**	**3.0 E-7**	**9**	**12.0 E-7**	**5**	**8.0E -7**	**4**	**10.0 E-7**	**4**	**6.0 E-7**	**2**	**0.5 E-7**	**4**	**0.8 E-7**	**9**
	1.8 E-7	**5**			**4.4 E-7**	**9**	**2.6 E-7**	**8**			**11.0 E-7**	**6**			**3.0 E-7**	**6**	**0.8 E-7**	**9**	**0.8 E-7**	**4**

3.4.2.3 Damage 3 (Multiple Damage Case) vs Intact

In this case damage of about 80% cross-section cut at the bottom panel diagonal at bay 5 is added to the preexisting damaged structure at back panel diagonal at bay 9. The damage indices for the ASH flexibility method for the *Y* direction modes are shown in Figure 3.29 for all four main chords. The value of the peaks for the front-bottom and back-top detect damage at the bay 9 and bay 5 and 9 respectively.

The damage indices for the ASH flexibility method for the *Z* direction modes are shown in Figure 3.30. The values of the peaks for the four chords are higher than the baseline at numerous locations. The front bottom sensors detect damage at both bays accurately. The back-bottom sensors also show accurate detection of bay 5 damage in the structure.

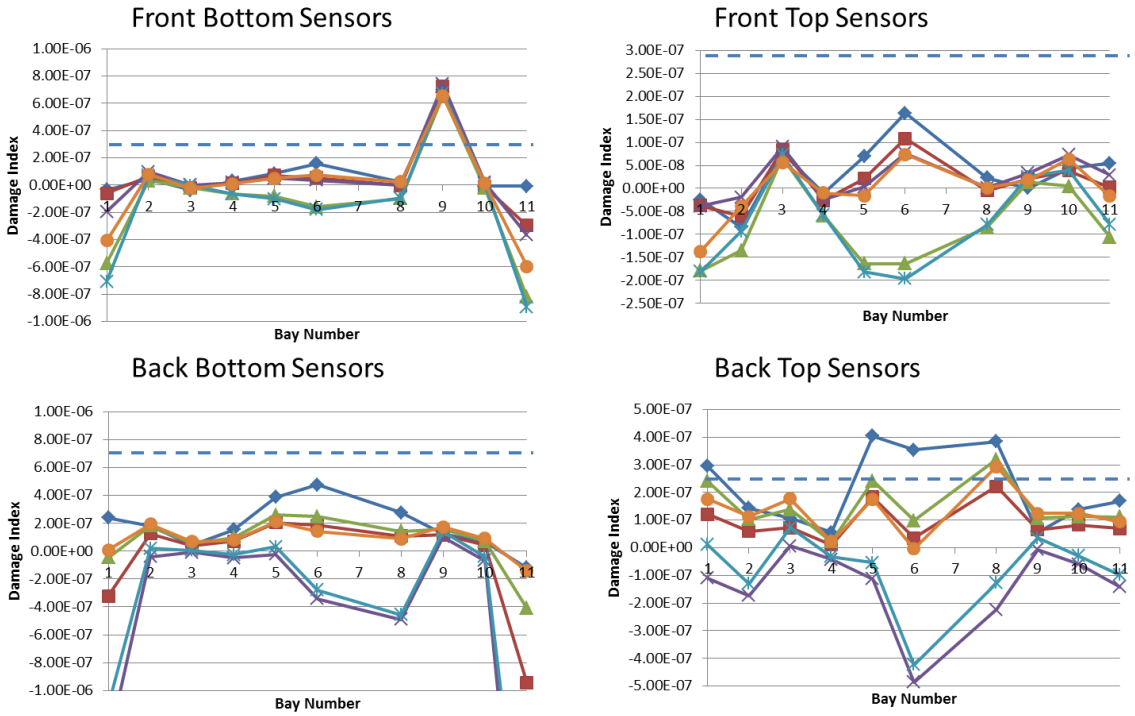

Figure 3.29: ASH *Y* direction Flexibility based damage index for the 4 main chords for 3/4 damage induced at back panel diagonal element at Bay 9 and 3/4 damaged induced at the bottom panel diagonal element at Bay 5.

The back-top sensors detect damage in bay 2 and bay 6; this corresponds to false positive and adjacent damage location to bay 5. All other cases have the damage indices below the baseline and damage is not localized to any bay.

Figure 3.31 shows the damage indices for the AS flexibility method for the *Y* direction modes for the 12 vertical members for the front and back panel. The damage indices for the front panel detect a change in larger change in axial strain than the

baseline strains for locations 8 and 9 which are adjacent to the actual diagonal member where damage was caused. Form the back bottom case, no damage is localized to any bay.

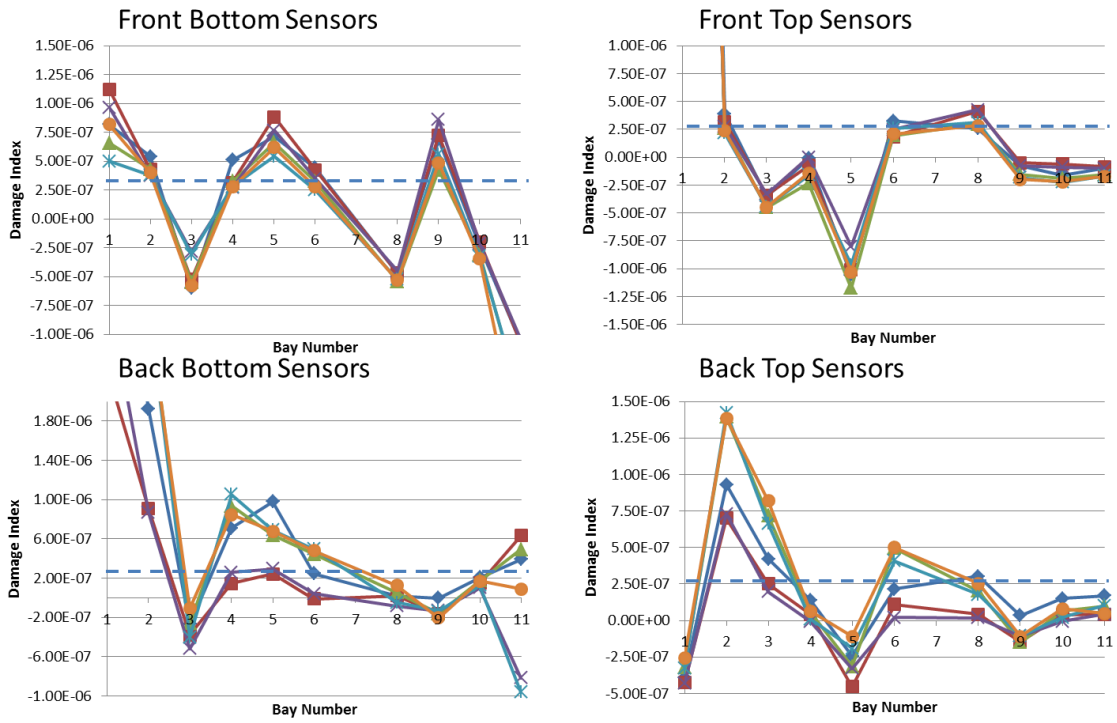

Figure 3.30: ASH *Z* direction Flexibility based damage index for the 4 main chords for 3/4 damage induced at back panel diagonal element at Bay 9 and 3/4 damaged induced at the bottom panel diagonal element at Bay 5.

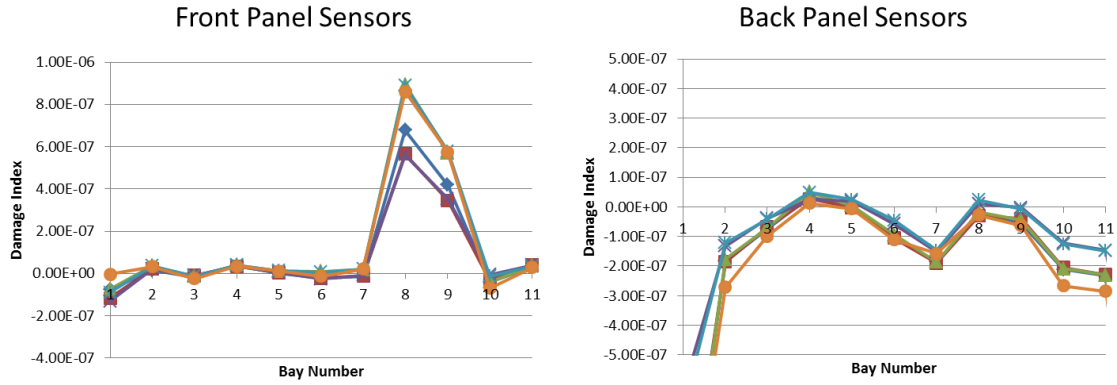

Figure 3.31: AS *Y* direction flexibility based damage index for the vertical members for 3/4 damage induced at back panel diagonal element at Bay 9 and 3/4 damaged induced at the bottom panel diagonal element at Bay 5.

Table 3.8: Damage indices for damage case 3.

	ASH [Y Direction Flexibility]								ASH [Z Direction Flexibility]								AS [Y Flexibility]			
	Front Bottom		Front Top		Back Bottom		Back Top		Front Bottom		Front Top		Back Bottom		Back Top		Front Panel		Back Panel	
Baseline value	3.0E-7		3.0E-7		7.0E-7		2.5E-7		3.0E-7		2.5E-7		3.0E-7		2.5E-7		1.5E-7		1.5E-7	
Damage5	7.0 E-7	9	1.0 E-7	3	3.0 E-7	5	2.5 E-7	5	6.0 E-7	5	2.0 E-7	6	10.0 E-7	4	2.5 E-7	6	8.0 E-7	8	-	-
			1.5 E-7	6	3.5 E-7	6	3.0 E-7	8	5.0 E-7	9	2.5 E-7	8	8.0E-7	5	1.0 E-7	8	5.0 E-7	9		

The information from all the plots are condensed into the Table 3.8, using color coded numbers as described in previous section. It is observed that as the damage is increased more of the cases have higher peaks above the baseline damage index.

3.4.3 Damage Detection for Phase 1 Damages

A second baseline index is calculated for the same phase 1 intact case. In the phase 1 of testing, the sensors the sensor mounts were moved from the front to the back panel changing the mass distribution during testing.

Baseline damage index in defined, similar to the previous section, as the maximum value of the damage indices when damage detection algorithm is evaluated between multiple sets of the same structural configuration. Figure 3.29 - Figure 3.31 present the baseline for the 2 cases that will be analyzed in this section and Table 3.9 shows the baseline values for the 4 main chords using ASH *Y* and *Z* direction flexibility and AS *Y* direction flexibility damage detection method.

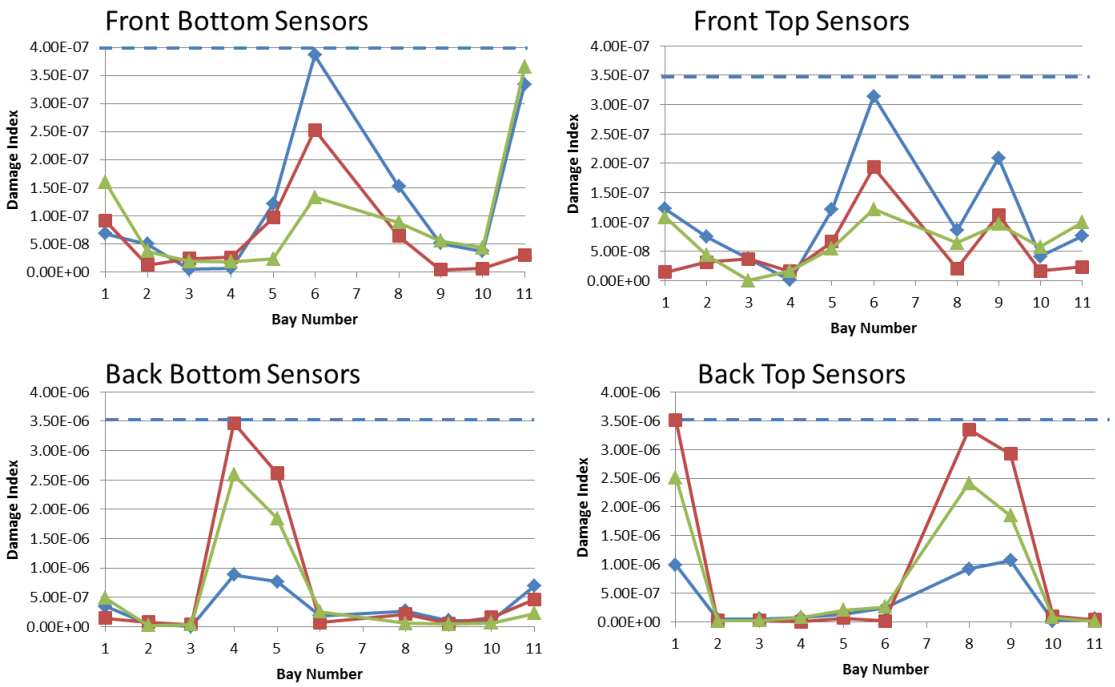

Figure 3.32: ASH *Y* direction flexibility damage indices to determine the baseline damage indices.

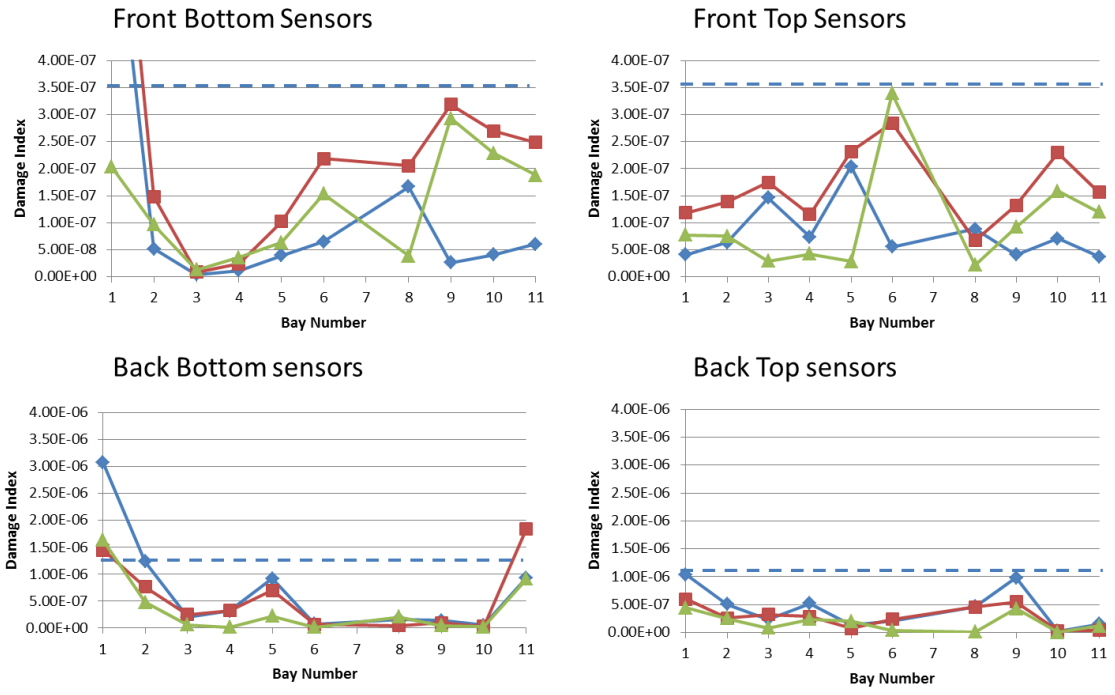

Figure 3.33: ASH *Z* direction flexibility damage indices to determine the baseline damage indices.

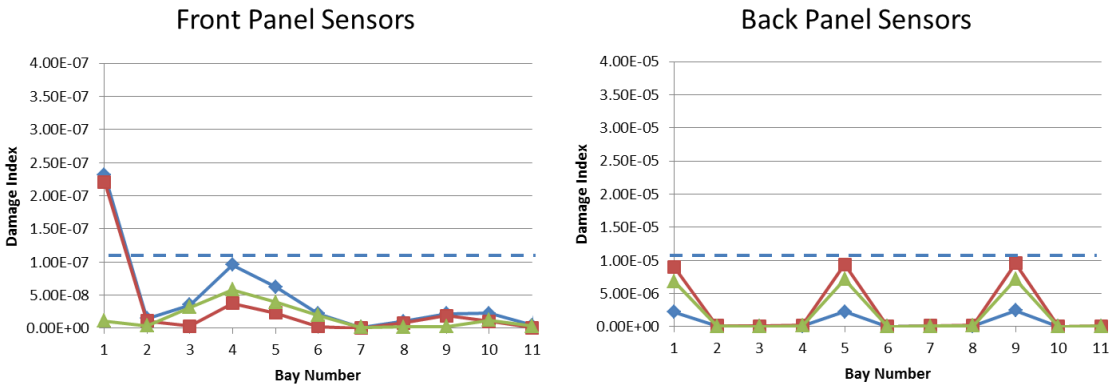

Figure 3.34: AS *Y* direction flexibility damage indices to determine the baseline damage indices for vertical elements of the front and back panel.

Table 3.9: Baseline damage indices for Phase 1 tests.

	ASH [Y Direction Flexibility]				**ASH [Z Direction Flexibility]**				**AS [Y Flexibility]**	
	Front Bottom	**Front Top**	**Back Bottom**	**Back Top**	**Front Bottom**	**Front Top**	**Back Bottom**	**Back Top**	**Front Panel**	**Back Panel**
Baseline value	**4.0E-7**	**3.5E-7**	**3.5E-6**	**3.5E-6**	**3.5E-7**	**3.5E-7**	**1.5E-6**	**1.0E-6**	**1.0E-7**	**1.0E-5**

3.4.3.1 Damage 4 vs Intact 2

In this case, damage is located at front panel diagonal at bay 5. The damage indices for the ASH flexibility method for the *Y* direction modes are shown in Figure 3.35 for all four main chords. The value of the damage indices for only one combination of the cases from the healthy and damaged state have damage peak greater than the baseline denoting accurate damage detection at bay 5.

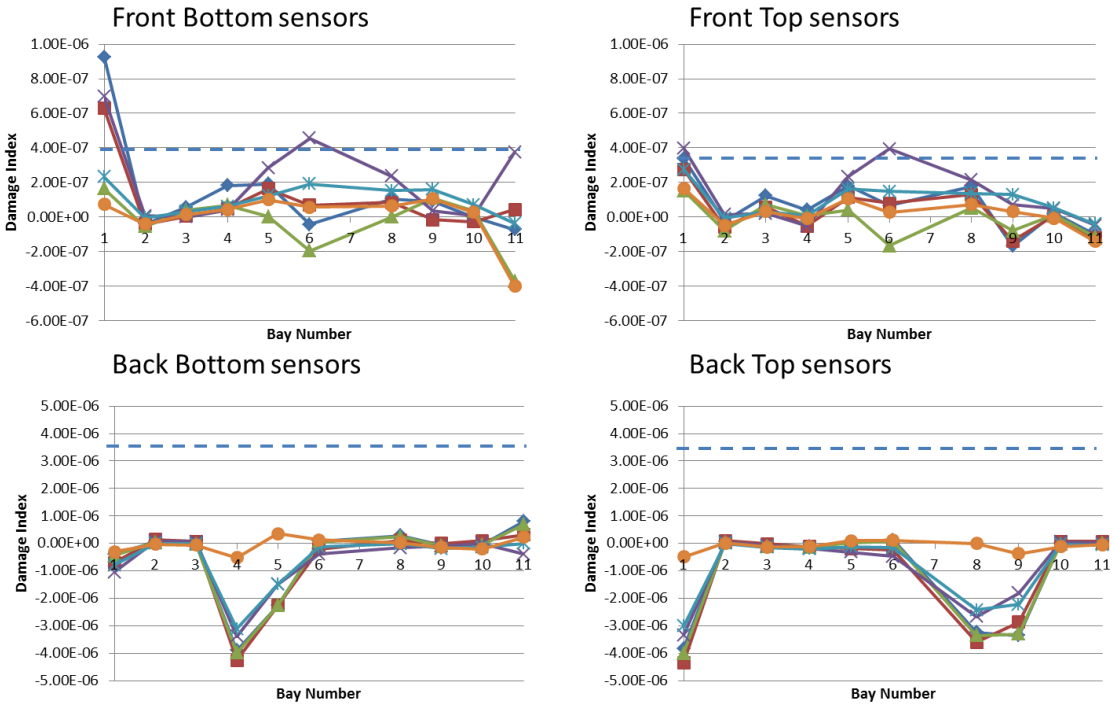

Figure 3.35: ASH *Y* direction flexibility based damage index for the 4 main chord for 1/2 damage at front panel diagonal element at Bay 5.

The damage indices for the ASH flexibility method for the *Z* direction modes are shown in Figure 3.36 for all four main chords. The value of the peak for the front panel chords is higher than the baseline at bay 5 and 8 respectively. The front-bottom sensors detect damage at both bays accurately. The front-top sensors detect the location to bay 8,

which is a false positive. All other cases have the damage indices below the baseline and damage is not localized to any bay.

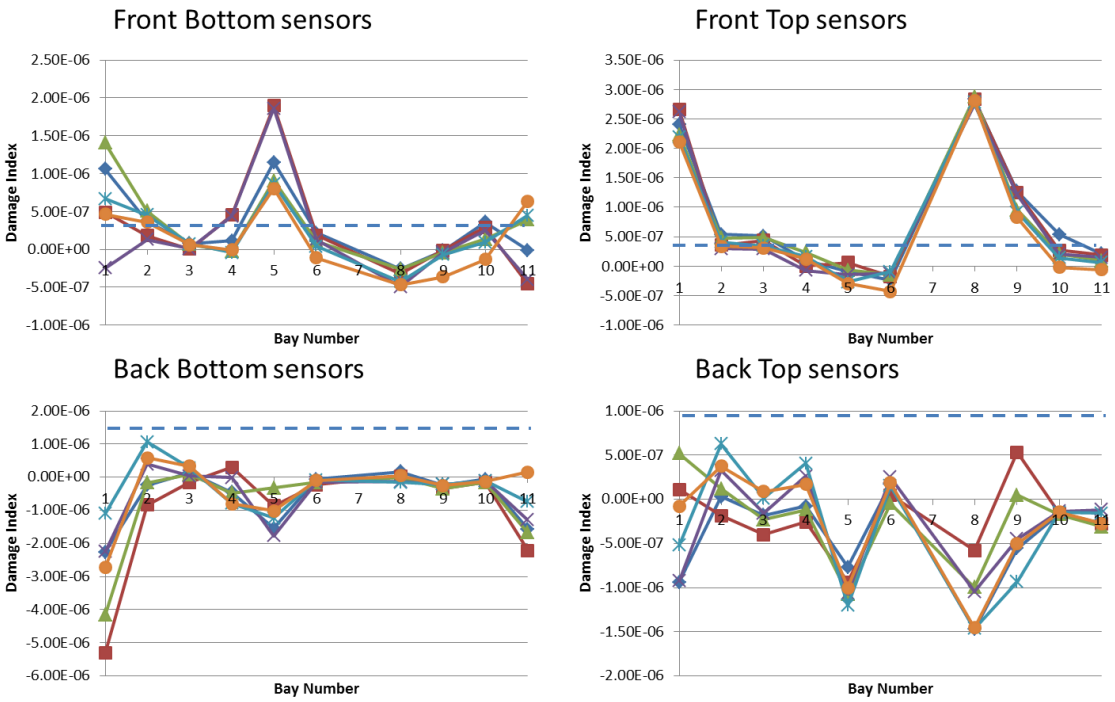

Figure 3.36: ASH *Z* direction flexibility based damage index for the 4 main chord for 1/2 damage at front panel diagonal element at Bay 5.

Figure 3.37 shows the damage indices for the AS flexibility method for the *Y* direction modes for the 12 vertical members for the front and back panel. The damage indices for the front panel detect a larger damage index than the baseline for 5th and 9th vertical elements which are adjacent to the actual diagonal member where damages were created.

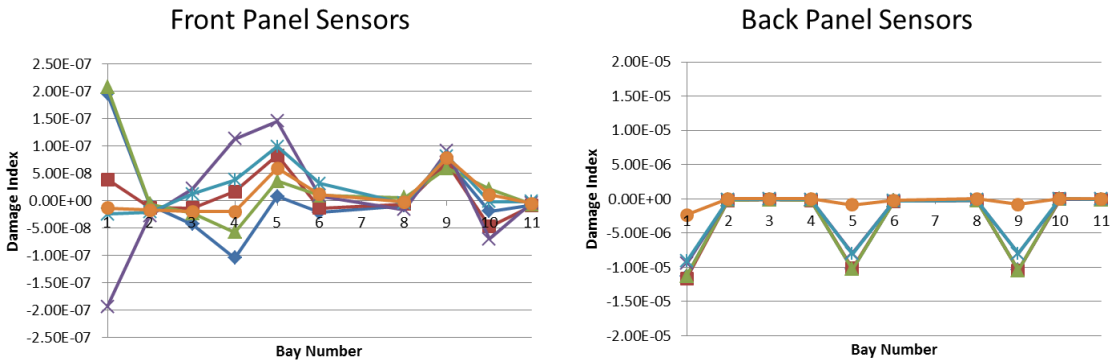

Figure 3.37: AS *Y* direction flexibility based damage index for vertical elements for 1/2 damage at front panel diagonal element at Bay 5.

Table 3.10: Damage indices for damge case 4.

	ASH [Y Direction Flexibility]								ASH [Z Direction Flexibility]								AS [Y Flexibility]			
	Front Bottom		Front Top		Back Bottom		Back Top		Front Bottom		Front Top		Back Bottom		Back Top		Front Panel		Back Panel	
Baseline value	4.0E-7		3.5E-7		3.5E-6		3.5E-6		3.5E-7		3.5E-7		1.5E-6		1.0E-6		1.0E-7		1.0E-5	
Damage 5	4E-7	5	4E-7	5	.5E-6	2	.2E-6	6	18E-7	5	25E-7	8	1E-6	3	.5E-6	2	1.2E-7	5	.01E-5	8
									4E-7	8					.4E-6	4	0.8E-7	9		
															.5E-6	9				

The information from all the plots are condensed into the Table 3.10, using color coded numbers.

3.4.3.2 Damage 5 vs Intact 2

In this case damage of 100% cross-section cut at the front-panel diagonal at bay 5 is created by extending the previous damage. The damage indices for the ASH flexibility method for the *Y* direction modes are shown in Figure 3.38 for all four main chords. The value of the peaks for the front-bottom and front-top have damage indices above the baseline at bays 4,5 and 5,9 respectively.

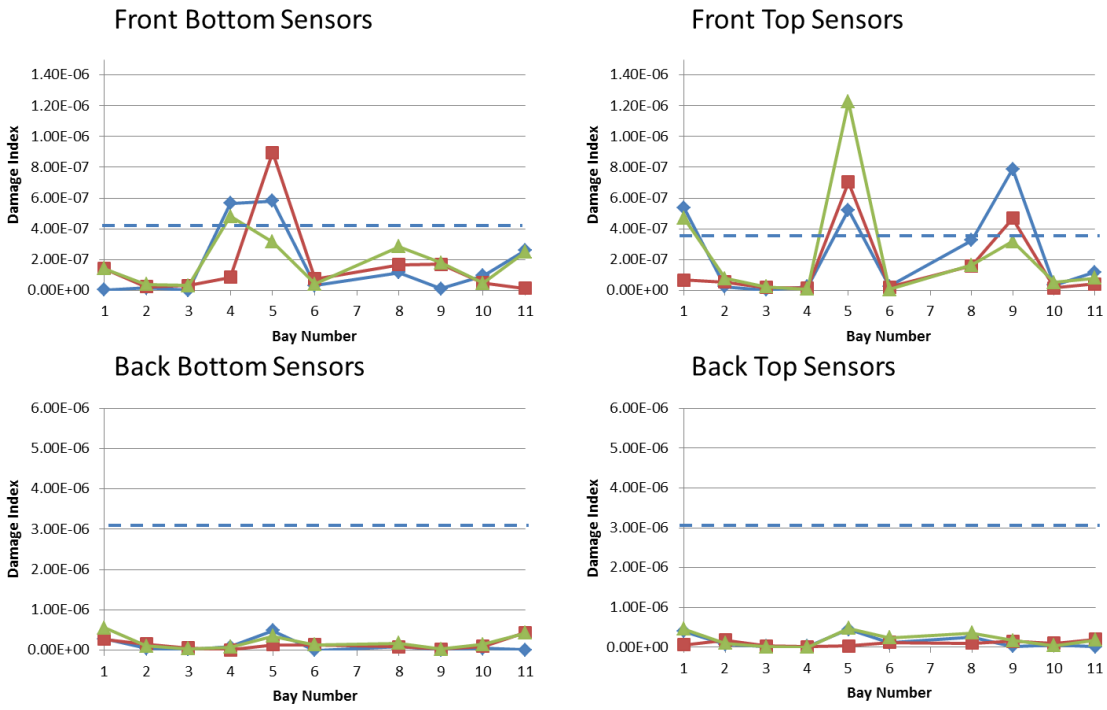

Figure 3.38: ASH *Y* direction flexibility based damage index for the 4 main chord for full cut at front panel diagonal element at Bay 5.

The damage indices for the ASH flexibility method for the *Z* direction modes are shown in Figure 3.39 for all four chords. The front-bottom sensors detect damage at bay 4, which is adjacent to the damaged bay. The front-top sensors show accurate detection of damage at bay 5, but also detect damage at bay 3 and 8. All other cases have the damage indices below the baseline and damage is not localized to any bay.

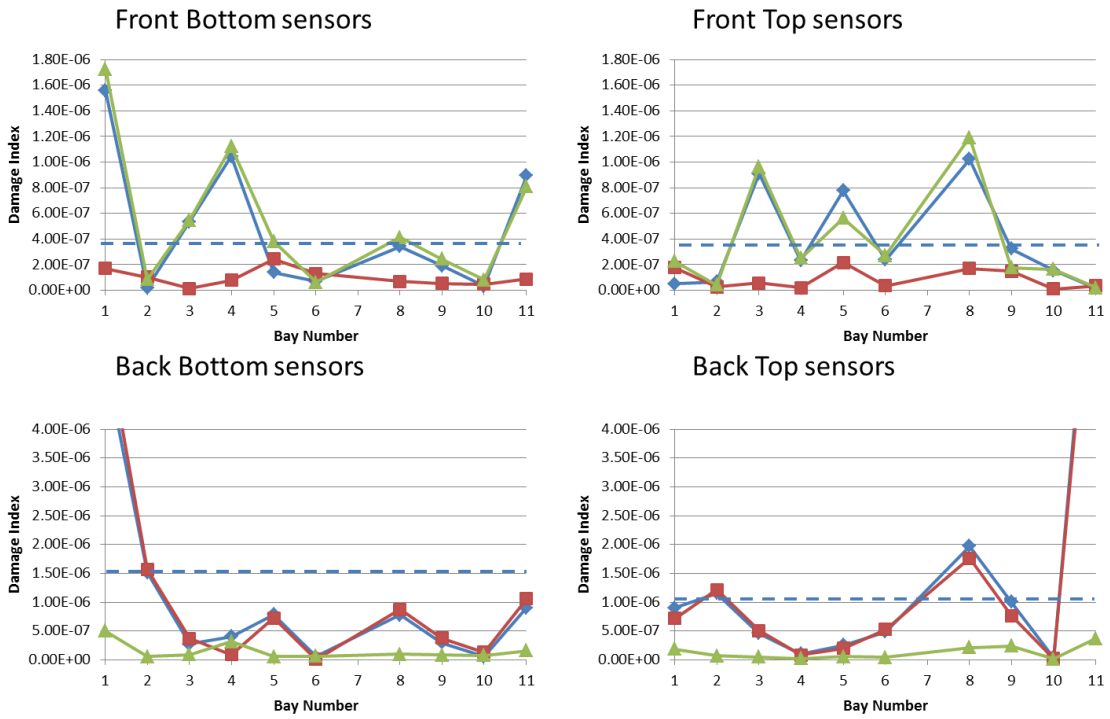

Figure 3.39: ASH Z direction flexibility based damage index for the 4 main chord for full cut at front panel diagonal element at Bay 5.

Figure 3.40 shows the damage indices for the AS flexibility method for the *Y* direction modes for the 12 vertical members for the front and back panel. The damage indices for the front panel detect a change in larger change in axial strain than the baseline strains for locations 5 and 8 which are adjacent to the actual diagonal member where damage was caused. Form the back bottom case, no damage is localized to any bay.

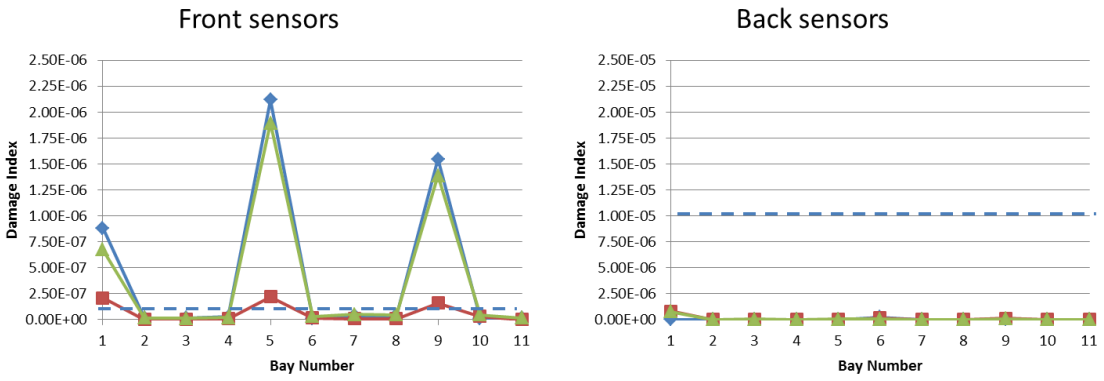

Figure 3.40: AS *Y* direction flexibility based damage index for the vertical elements for full cut at front panel diagonal element at Bay 5.

Table 3.11: Damage indices for a damage case 5.

	ASH [Y Direction Flexibility]								ASH [Z Direction Flexibility]								AS [Y Flexibility]			
	Front Bottom		Front Top		Back Bottom		Back Top		Front Bottom		Front Top		Back Bottom		Back Top		Front Panel		Back Panel	
Baseline value	4.0E-7		3.5E-7		3.5E-6		3.5E-6		3.5E-7		3.5E-7		1.5E-6		1.0E-6		1.0E-7		1.0E-5	
Damage5	9E-7	5	12 E-7	5	0.5 E-6	5	0.6 E-6	5	10 E-7	4	8E-7	5	.7E-6	5	1.2 E-6	2	20 E-7	5	.02 E-5	6
			8E-7	9	0.3 E-6	8			4E-7	8	9E-7	3	.9E-6	8	1.8 E-6	8	15 E-7	9	.01 E-5	9
											12 E-7	8								

The information from all the plots are condensed into the Table 3.11, using color coded numbers.

3.4.4 Discussions

The data used in this analysis is from the experiment case where the structure was impacted with modal sledge hammer at node 10 in the Y direction. The implications of the impact direction are that the *Y* direction modes are excited to higher extent as compared to the *Z* direction modes. Hence, the Y direction modal estimates have less noise as compared to the *Z* direction.

The study reaffirms that there is a requirement to evaluate the baseline damage index to prove the reliability of the damage detected. Damage detection of the five cases

are performed using the same method and fairly successful results are obtained using the representative damage detection method. Better data reduction to evaluate the modal properties and a better damage detection algorithm which is sensitive to damage in the structure but insensitive to noise might yield better results and also detect damage in damage case; Damage1 with the smallest level of damage induced on the structure.

In all cases, that chord closest to the damage location and the panel where the damage was created, detected damage most easily.

CHAPTER 4. CONCLUSIONS

In this study, a baseline damage index for reliable damage detection is established. The method is also demonstrated on a full scale highway sign support truss with relative success in determining the damage location.

One of the drawbacks of damage detection methods is that when two sets of appropriate data corresponding to intact and damage structure is provided to a damage detection method, a damage index is provided by the algorithm. The next step in the process is to evaluate the acceptability and accuracy of the damage indices provided by the method. The baseline damage index developed in this thesis shows that this judgment process can be quantified and damage detection can be made objective without user defined thresholds from user experience and intuition.

The gist of the method is that, it is shown that the for a certain noise level, when the maximum (peak) damage index is above the baseline damage index determined for that noise level, the damage localization provided is accurate. This baseline damage index is then extended to numerically establish a benchmarking scheme for damage detection methods.

Two damage detection methods are used to demonstrate the baseline damage detection method. The ASH flexibility and AS flexibility methods for damage detection are validated on two structures: A one dimensional beam model and three dimensional space truss. The results of the baseline damage index showed that the method is robust when applied to various structures. The baseline damage index results show a similar trend for the damage to the elements of the one dimensional structure and the various cases of the three dimensional structure. Only results for 1% noise levels are used to compare the quality of the damage detection capabilities.

- For the 1D model with 1% noise added to the mode shapes, damage greater than 10% reduction of stiffness property is required to reliability predict the correct damage location.
- For the 3D model with 1% noise added to the mode shapes, damage to the front-bottom chord needs to be greater than 50% reduction of stiffness property to reliability predict the correct damage location.
- For the 3D model with 1% noise added to the mode shapes, damage to the front-chord needs to be greater than 70% reduction of stiffness property to reliability predict the correct damage location.
- For the 3D model with 1% noise added to the mode shapes, damage to the front-panel needs to be greater than 10% reduction of stiffness property to reliability predict the correct damage location.
- For the 3D model with 1% noise added to the mode shapes, damage to the back-panel needs to be greater than 70% reduction of stiffness property to reliability predict the correct damage location.

The structure studied here are quite different with respect to the overall stiffness, the complexity and type of damage. Two indicators were used to compare the results from the structure quantitatively. The indicators were required to measure the extent of total damage to the structure and the observability of the structural damage using the measurement sensors.

The Global Stiffness change is derived from the change in natural frequencies between intact and damaged models. It provided an indicator for the overall stiffness reduction to the model due to damage. The MAC correlation between the damaged and intact mode shapes at the measured DOFs is another parameter used to rate the structure.

- The damage to the one dimensional beam model from 10% to 90% reduction in stiffness decreased the average global stiffness by 0.24 with a minimum of 0.05 and maximum of 0.4.
- The damage to the main chord elements of the three dimensional space frame from 10% to 90% reduction in stiffness decreased the average global stiffness by 0.05 with a minimum of 0 and maximum of 0.21.
- The damage to the secondary diagonal elements of the three dimensional space frame from 10% to 90% reduction in stiffness decreased the average global stiffness by 0.07 with a minimum of 0 and maximum of 0.22.
- Hence, equivalent damage to the 1D model for same change in global stiffness is only about 40% reduction in modulus of the 1D elements.

It was shown that the indicators can be used to compare similar extent of damage on different structures. The indicators provide a framework to compare structures and the

damage detection capability on different structures. The conclusions from the two damage detection results and the indicators are described below.

- The baseline damage index is consistent method to judge the damage detection results in an objective manner for both structures studied.
- For the three dimensional highway sign truss model, it was shown that damage can be reliably detected to the smallest level when the damaged element is collocated with the measurement location.
- For the 3D truss structure the damage to the secondary diagonals are easiest to detect due to low MAC correlation despite the small reduction in global stiffness.

There is a need to develop effective, fast, automatic and cost-effective structural health monitoring system in the near future to assist in managing our aging infrastructure. To achieve the goal of automated health monitoring, we need to remove the need for user involvement in the process. Also two other factors that are coupled are important in development of the baseline damage index; noise in the structure is not quantifiable and location and extent are of damage in structures are unknown. The baseline damage index achieves to translate the noise in the system at the sensor measurements to the next step of the damage detection method. I believe this is crucial and fundamental to proving the reliability of a damage detection result in real world applications.

The general threshold used to predict damage is numerically demonstrated to be dependent on the noise level in the simulation. Hence, the best way to estimate the baseline damage index must be based on the data-centric baseline method developed here. This ensures that the correct baseline or threshold is chosen instead of an ad-hoc limit based on user judgment or experience.

An experiment to demonstrate the proposed approaches is performed on a full-scale highway sign support truss to fully estimate the 3D modal properties of the structure. The structure was instrumented with accelerometers at 144 DOFs (including X, Y and Z) to measure the response of the structure to impact excitation in Y and Z direction at 4 nodes of the structure at the frequency of 512 Hz. This test was repeated for 2 sets of the intact structure and 5 sets of different damage cases including a 3D multiple damage case. A rich data set is developed for the modal properties of the structure using 3 modal estimation methods: Eigen-system Realization Algorithm, output-only Frequency Domain Decomposition with Peak-Picking and Complex Mode Indicator Function.

The complexity of the structure can be judged from the mode shapes identified. The structural behavior is very complex with fixed-fixed behavior for the bottom panel nodes and free-free behavior of the top panel nodes. Also, the Y and Z direction stiffness of the structure are very similar and results in coupled mode shapes and complex interactions as shown in the mode shapes identified.

The ASH and AS flexibility damage detection method are experimentally validated using the data from the intact and 5 damage cases. The modal properties for all the damage cases are evaluated from only the Y direction impact test at node 10 for the analysis. The baseline damage index is demonstrated to be an acceptable approach to defining the threshold for damage detection. The baseline damage index effectiveness is acceptable for most cases shown but do not detect damage accurately in a few cases and results in false positives.

4.1 Future Work

The method can be extended to benchmark other damage detection method and compare the effectiveness of different methods based on the framework developed in this thesis. The baseline damage index with the indicators to rate a structure can be used to evaluate damage detection methods on other structure.

The baseline damage index evaluated for non-uniform structure with each bay having a different baseline is an important study that can be performed. Most structure in the real world are non-uniform and this analysis will enhance the applicability of defining a more robust baseline damage index for complex structure.

Experimental validation was performed using only vibration data from all the node for the all the damage cases for the impact excitation at node 10 in the Y direction. Data for impact excitation in Z direction at node 10, Y and Z direction impact at node 33 and white noise shaker excitation at node 4 for all the intact and damage cases need to be processed and analyzed using the baseline method.

Wireless data for impact and shaker excitation is also available for all the damage cases as well and will make a good study to compare the “noise” levels of the wired and wireless data using the baseline damage index.

LIST OF REFERENCES

LIST OF REFERENCES

1. Lynch, J. P., Loh, K.; “A summary review of wireless sensors and sensor networks for structural health monitoring.” Shock and Vibration Digest, 2006

2. Rytter, A.; “Vibration based inspection of civil engineering structures,” Ph. D. Dissertation, Department of Building Technology and Structural Engineering, Aalborg University, Denmark., 1993

3. Moore, M., Phares, B., Graybeal, B., Rolander, D., & Washer, G.; “Reliability of visual inspection of highway bridges.” FHWA Report No. FHWA-RD-01-020, FHWA, U.S. Dept. of Transportation, Washington, DC., 2001

4. ASCE, “Report Card for America's Infrastructure”, American Society of Civil Engineers, Reston, VA:, 2005

5. ASCE, “Report Card for America's Infrastructure”, American Society of Civil Engineers (ASCE), Reston, Virginia, March 25, 2009.

6. Kiremidjian, A.S., Straser, E.G., Meng, T.H., Law, K. and Soon, H.; “Structural damage monitoring for civil structures”. Proc., Int. Workshop on Structural Health Monitoring, Stanford, CA, 371-382, 2007

7. Lynch, J.P., Kiremidjian, A.S., Law, K.H., Kenny, T. and Carryer, E.; “Issues in wireless structural damage monitoring technologies”, Proc., the Third World Conference on Structural Control, Vol.2: 667-672, 2002

8. Spencer, Jr., B.F. and Nagayama, T.; “Smart sensor technology: a new paradigm for structural health monitoring”. Proc., Asia-Pacific Workshop on Structural health Monitoring, Yokohama, Japan, 2004.

9. Farrar, C. R., and Jauregui, D. V.; "Damage Detection Algorithms Applied To Experimental And Numerical Modal Data From The I-40 Bridge," Los Alamos National Lab report LA-13074-MS, 1996

10. Farrar, C. R., Doebling, S. W., Cornwell, P. J., and Straser, E. G.; “Variability of Modal Parameters Measured on the Alamosa Canyon Bridge,” Proc. 15th International Modal Analysis Conf., Orlando, FL, pp. 257-263, 1998

11. Sun L.M., Min Z.H. and Dan D.H., “Correlation analysis on long term monitoring data of Donghai Bridge., Fourth International Conference on Bridge Maintenance, Safety and Management, IABMAS'08, Seoul, Korea, 2007

12. Sun L. M., Sun Z. Dan D.H. and Zhang. Q. W.; “Large-span bridge and their health monitoring systems in China”, International Symposium on Integrated Life-Cycle Design and Management of Infrastructure, p.79-95, 2001

13. Min Z., Sun L., Dan D., Sun Z.; **"**Effect Analysis of Environmental Factors on Structural Modal Parameters of Cable-stayed Bridge**",** Journal of Vibration and Shock ,28(10) : 99-105, 2009

14. Peeters B. and De Roeck G.; "One-year monitoring of the Z24-Bridge: environmental effects versus damage events", Earthquake Eng Struct. Dyn.,30:149-171, 2001

15. He, J. and Ewins, D. J.; "Analytical Stiffness Matrix Correction Using Measured Vibration Modes," Modal Analysis: The International Journal of Analytical and Experimental Modal Analysis, Vol. 1, No. 3, pp. 9–14, 2001

16. Doebling, S. W., Farrar, C. R., Prime, M. B., and Shevitz, D. W; "Damage Identification and Health Monitoring of Structural and Mechanical Systems from Changes in their Vibration Characteristics: A Literature Review", Los Alamos National Laboratory report LA-13070-MS, 1996

17. Pandey, A. K., Biswas, M., and Samman, M. M.; "Damage Detection From Changes In Curvature Mode Shapes", Journal of Sound and Vibration, Vol. 145, No. 2, pp. 321–332, 1991

18. Salawu, O. S. and Williams, C.; "Damage Location Using Vibration Mode Shapes," 12th International Modal Analysis Conference, pp. 933–939, 1994

19. Cawley P, Adams R.D.; "The Location of Defects in Structures from Measurements of Natural Frequencies", J. Strain Analysis,14(2):49–57, 1979

20. Pandey A.K., Biswas M.; "Damage Detection in Structures using Changes in Flexibility", Journal of Sound and Vibration Vol. 169(1), p. 3-17, 1994

21. Brock, J. E.; "Optimal Matrices Describing Linear Systems," AIAA Journal, Vol. 6, No. 7, pp. 1292–1296, 1968

22. Doebling, S. W.; "Minimum-Rank Optimal Update of Elemental Stiffness Parameters for Structural Damage Identification," AIAA Journal, Vol. 34, No. 12, pp. 2615-2621, 1996

23. Lam, H. F., Ko, J. M., and Wong, C. W.; "Detection of Damage Location Based on Sensitivity Analysis", 13th International Modal Analysis Conference, pp. 1499– 1505, 1995

24. Haug, E. F. and Choi, K. K.; "Structural Design Sensitivity Analysis with Generalized Global Stiffness and Mass Matrices," AIAA Journal, Vol. 22, No. 9, pp. 1299–1303, 1984

25. Cobb, R. G., and Liebst, B. S.; "Structural Damage Identification Using Assigned Partial Eigen-structure," AIAA Journal, Vol. 35, No. 1, pp. 152-158, 1997

26. Doebling S.W.,Farrar C.R.; “Prime: A summary review of vibration-based damage identification methods”, The Shock and Vibration Digest Vol. 30(2), pp. 91-105, 1998

27. Yan G., Duan Z., Ou J.; “Damage detection for beam structures using an angle-between-string-and-horizon flexibility matrix”, Structural Engineering and Mechanics 36(5), 2010.

28. Yan, G., Duan, Z., & Ou, J.; “Damage Detection for Truss or Frame Structures Using an Axial Strain Flexibility”, Smart Structures and Systems , 5 (3), 2009

29. Bernal, D., Dyke, S.J., Lam, H.-F. and Beck, J.L.; “Phase II of the ASCE Benchmark Study on SHM”, 15th ASCE Engineering Mechanics Conference, New York, New York, June 2–5, 2002

30. Makola M.A., Richardson A., Hanif J.; “Placement of sensors, actuators on civil structures using genetic algorithms”; Earthquake Eng. Struct. Dyn, 30:1167–1184, 2001

31. Garlich M.J. and Thorkildsen E.T.; “Guidelines for the Installation, Inspection, Maintenance and Repair of Structural Supports for Highway Signs, Luminaires, and Traffic Signals”, FHWA NHI 05-036, 2005

32. Juang, J. N., and Pappa, R. S.; “An eigensystem realization algo- rithm for modal parameter identification and model reduction.” J. Guid. Control Dyn., 8, 620–627, 1985

33. Ho B.L. and Kalman R.E.; “Effiective Construction of Linear state variable model from Input/Output data”, 3rd Allerton Conference on curcuits and System theory, p - 449-459, 1965

34. Allemang R.J. and Brown D.L. 1982. A correlation coefficient for modal vector analysis. Proceedings of the 1st International Modal Analysis Conference. Orlando, FL.

35. Brincker, R., Zhang, L., Andersen, P.; "Modal Identification from Ambient Responses using Frequency Domain Decomposition”, 18th Int. Modal Analysis Conference, Kissimmee, 2001

36. Zimmerman, A., T., Shiraishi, M., Swartz, R., A., and Lynch, J., P.; "Automated modal parameter estimation by parallel processing within wireless monitoring systems", J. of Infrastruct. Sys., 14(1), 102-113, 2008

37. Krishnan S.S., Sun Z., Irfanoglu A., Dyke S.J. and Yan G.; “Evaluating the performance of distributed approaches for modal identification”, SPIE XIVI (2), 2010

38. Shih C. Y., Tsuei Y. G., Allemang R. J., Brown D. L.; “Complex Mode Indication Function and its Applications to Spatial Domain Parameter Estimation”, IMAC VII, 1989

39. Yan, G., Dyke, S., & Irfanoglu, A.; “Experimental Validation of a Damage detection Approach on a Full-Scale Highway Sign Support”, Mechanical Systems and Signal Processing, 2010, (Inpress)

APPENDICES

Appendix A Description of the Mode Shapes

The mode shapes and natural frequencies evaluated using the CMIF method is presented. The data analysed is from the hammer input excitation at node 10 in the Y direction. The acceleration response from all the 6 data sets is used to evaluate the three dimensional modeshape. Table shows the frequencies at which the modes are evaluated. The different cases have slight variation in frequencies in the various cases. The mode shapes in the Y and Z direction are scaled proportionally using the 7th set with collocated tri-axial measurement.

Table A.1: First nine natural frequencies for the six sets of data.

Mode	x1 (Hz)	x2 (Hz)	y1 (Hz)	y2 (Hz)	z1 (Hz)	z2 (Hz)	Tri-axial (Hz)
1	10.468	10.625	10.375	10.375	10.500	10.437	10.468
2	12.625	12.625	12.593	12.625	12.625	12.625	12.625
3	14.531	14.437	14.437	14.500	14.531	14.531	14.531
4	18.718	18.750	18.718	18.7185	18.718	18.750	18.718
5	21.781	21.687	21.687	21.687	21.781	21.687	21.781
6	31.687	31.531	31.468	31.687	31.687	31.562	31.562
7	36.343	36.312	36.187	36.312	36.250	36.312	36.343
8	38.031	38.000	38.000	38.062	38.031	38.031	38.031
9	39.093	39.125	39.125	39.062	39.000	39.125	39.062

It is a very complicated structure with complex three dimensional modes. The behavior of the bottom panel nodes is that of fixed –fixed structure and top panel is that of a free-free structure. Also, the stiffness of both Z and Y direction are similar. The mode shapes are presented and a brief description of the mode is presented.

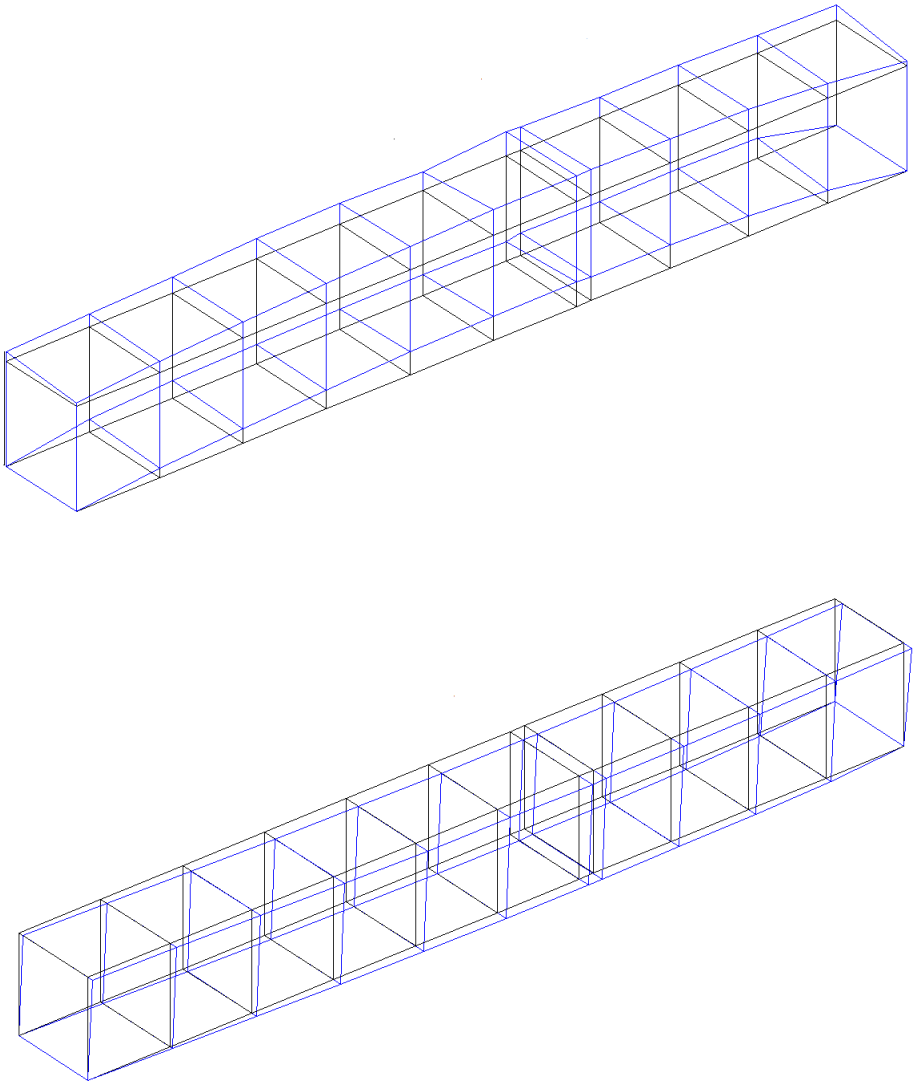

Figure A.1: First mode shape identified at 10.43 Hz (a) Y direction mode, (b) Z direction mode.

The first mode evaluated is at 10.46 Hz. The nodes at the bottom panel exhibit first bending in the Y direction, because of the fixed boundary conditions at the ends, but the top nodes show approximately rigid body motion, with all the nodes moving vertically to the same extent. The Z direction mode shape is also of similar magnitudes

and all node are moving in sync out of plane. This results in a the first mode being not purely in one direction but both in Y and Z direction.

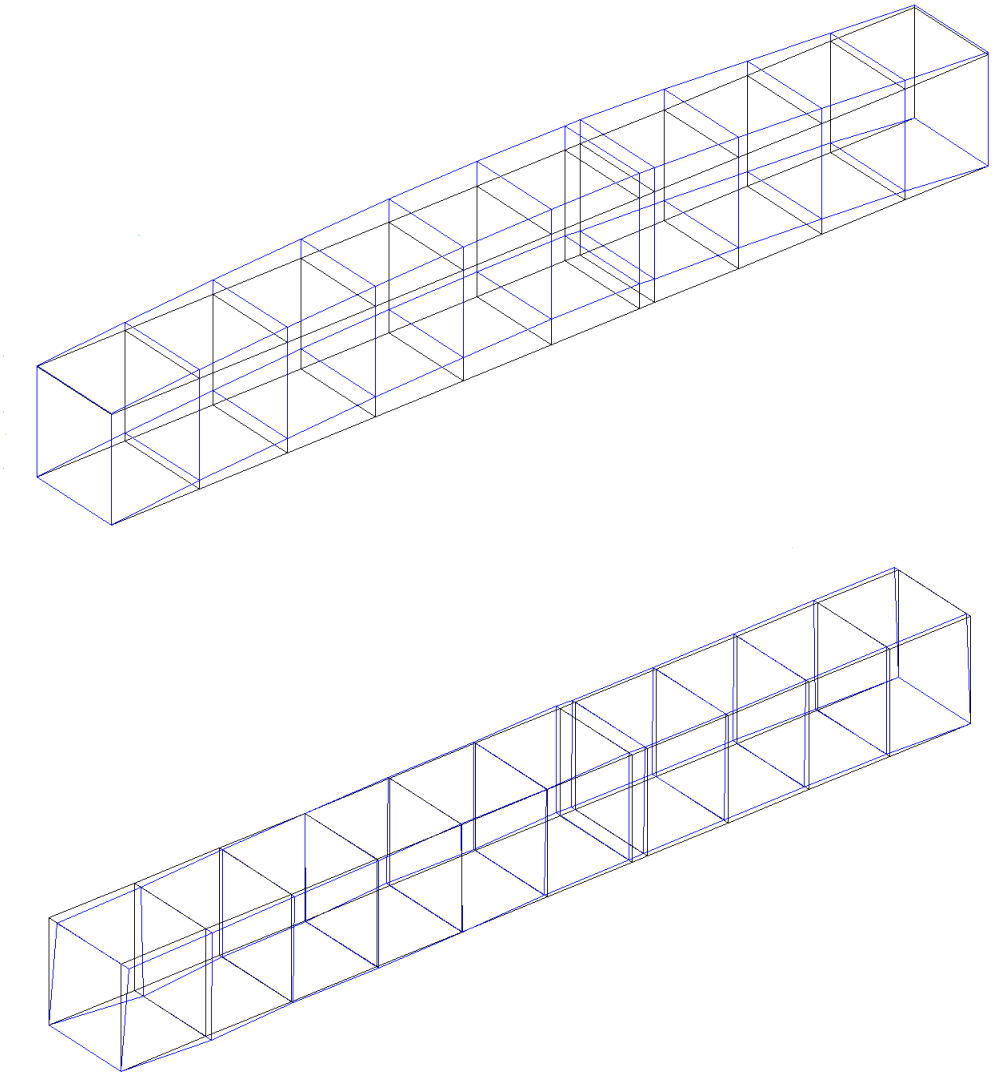

Figure A.2: Second mode shape identified at 12.61 Hz (a) Y direction mode, (b) Z direction mode.

All the nodes in the second mode depict first bending behavior in the Y direction. The magnitude of the Z direction mode is quite small in comparison to the Y-direction.

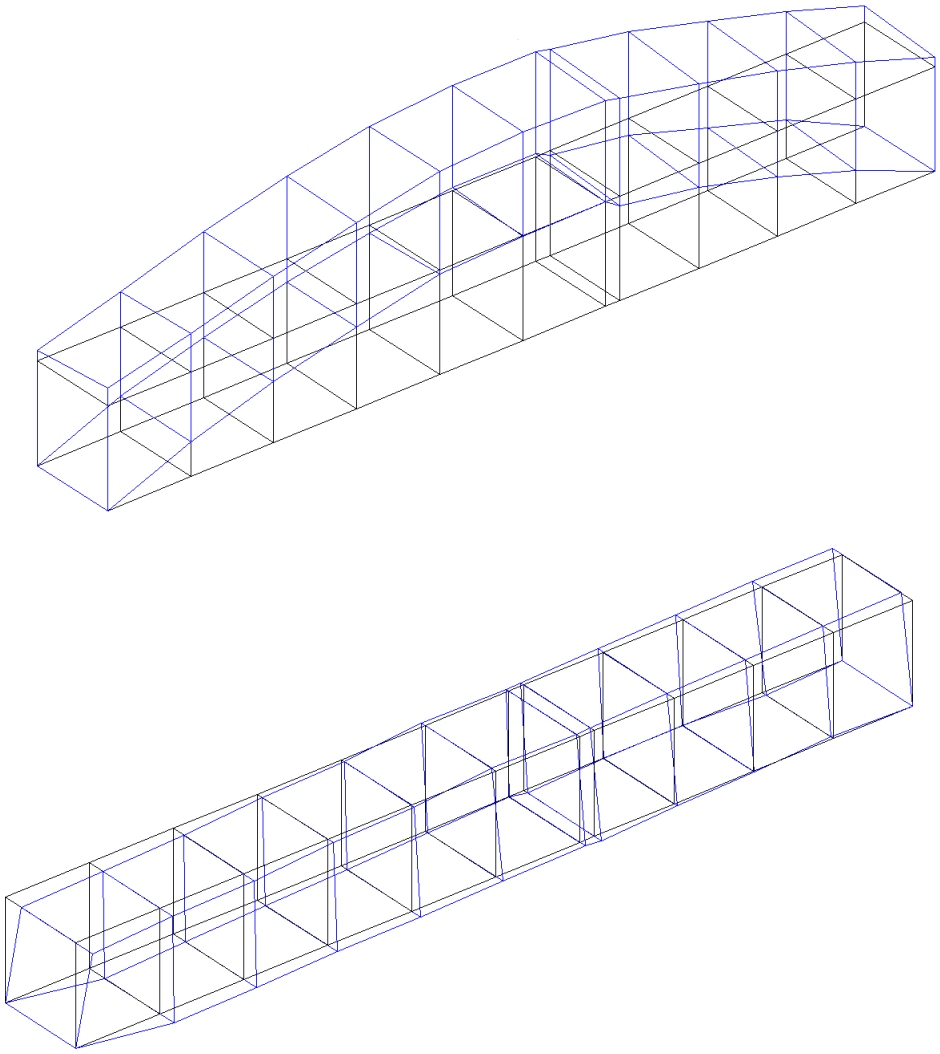

Figure A.3: Third mode shape identified at 14.51 Hz (a) Y direction mode, (b) Z direction mode.

The second mode at 12.61 and third mode at 14.51 show the same behavior in the Y-direction. But on closer examination of the small magnitude Z-direction behavior shows distinctly orthogonal behavior.

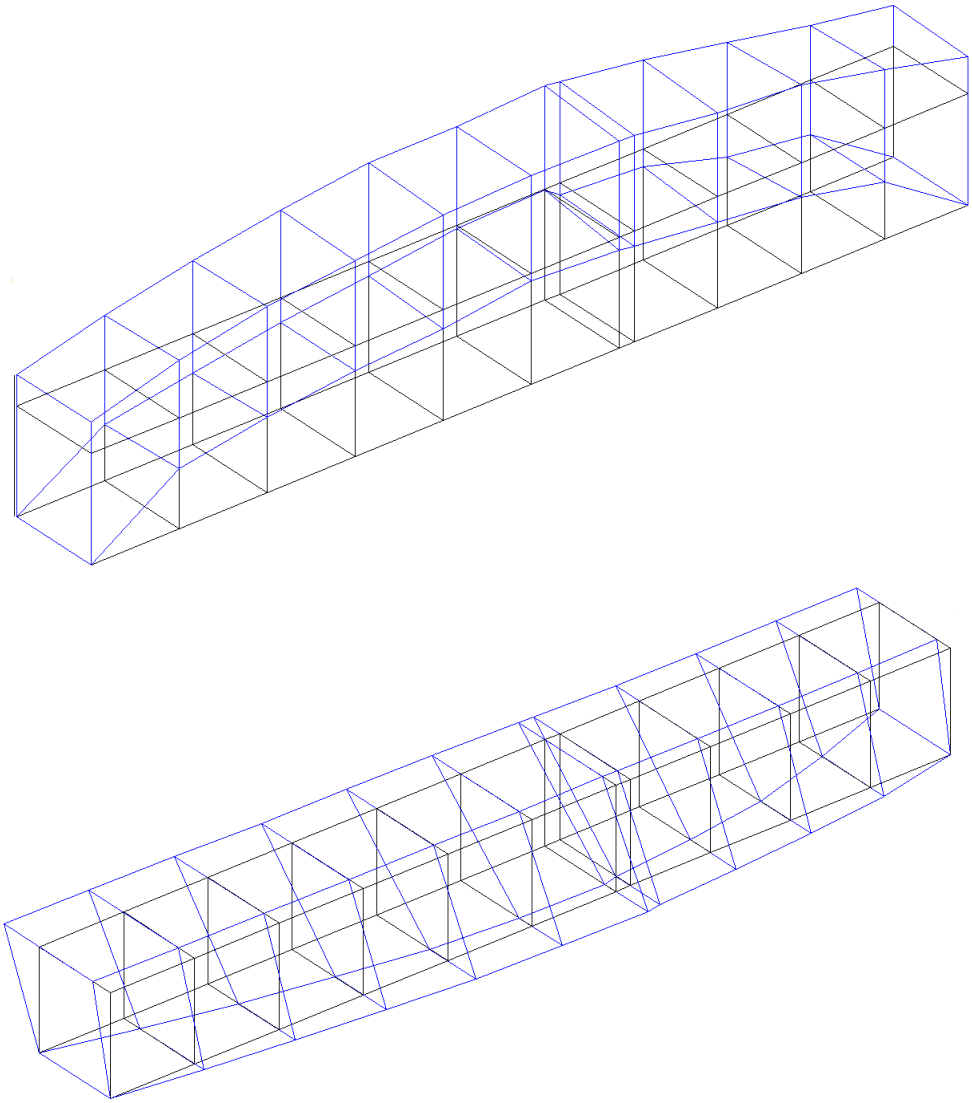

Figure A.4: Fourth mode shape identified at 18.93 Hz (a) Y direction mode, (b) Z direction mode.

The fourth mode is evaluated at 18.93 Hz. The Y direction behavior is still first bending, but the Z-direction mode is showing a shearing behavior. The structure responds in the shape shown in figure, where the bottom panel is showing first bending while the top panel is showing rigid body motion in the opposite direction.

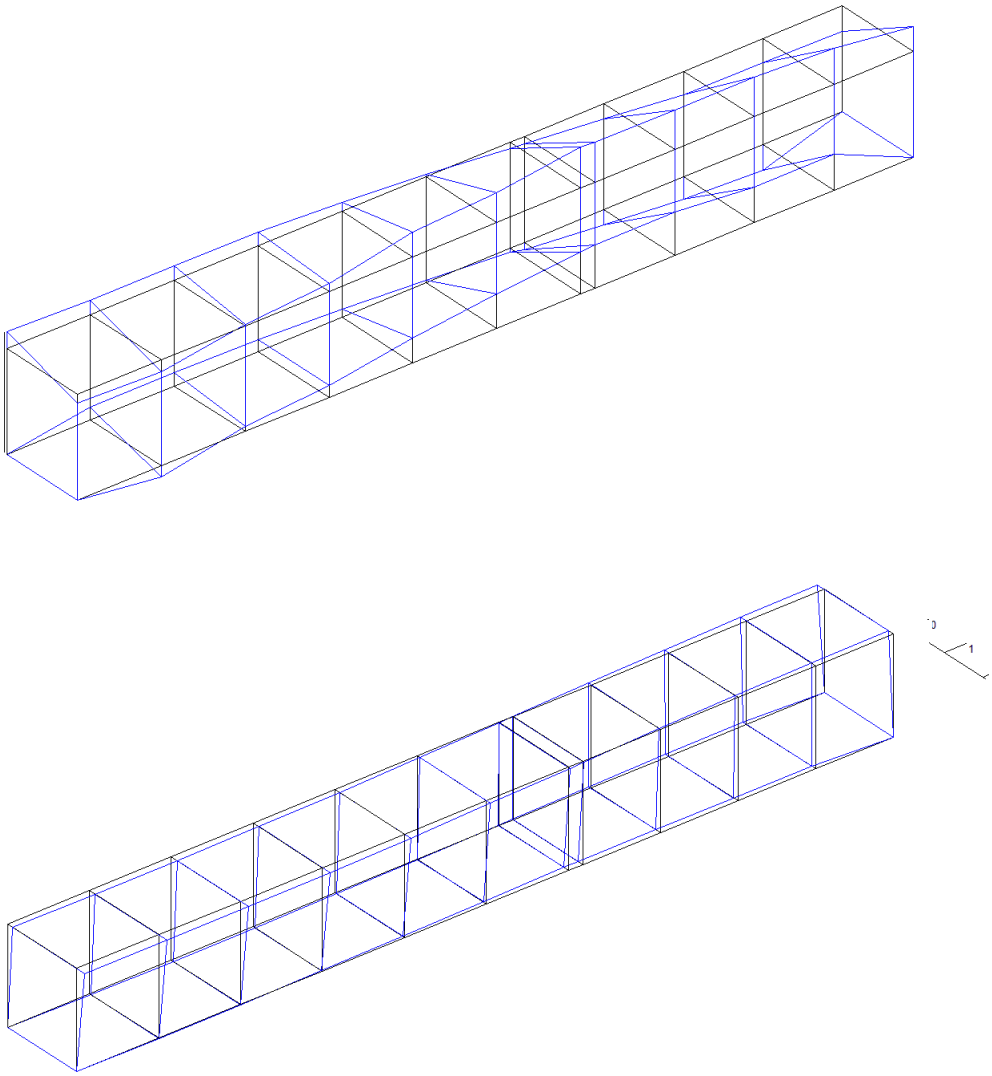

Figure A.5: Fifth mode shape identified at 21.72 Hz (a) Y direction mode, (b) Z direction mode.

The mode shape at 21.72 Hz is an asymmetric 2nd bending in the Y direction. The front panel is oscillating in Y direction in the 2nd bending mode and the back panel is oscillating also in 2nd bending but out of phase with respect to the front panel. The Z direction also shows 2nd bending behavior but all the chords are in phase with each other.

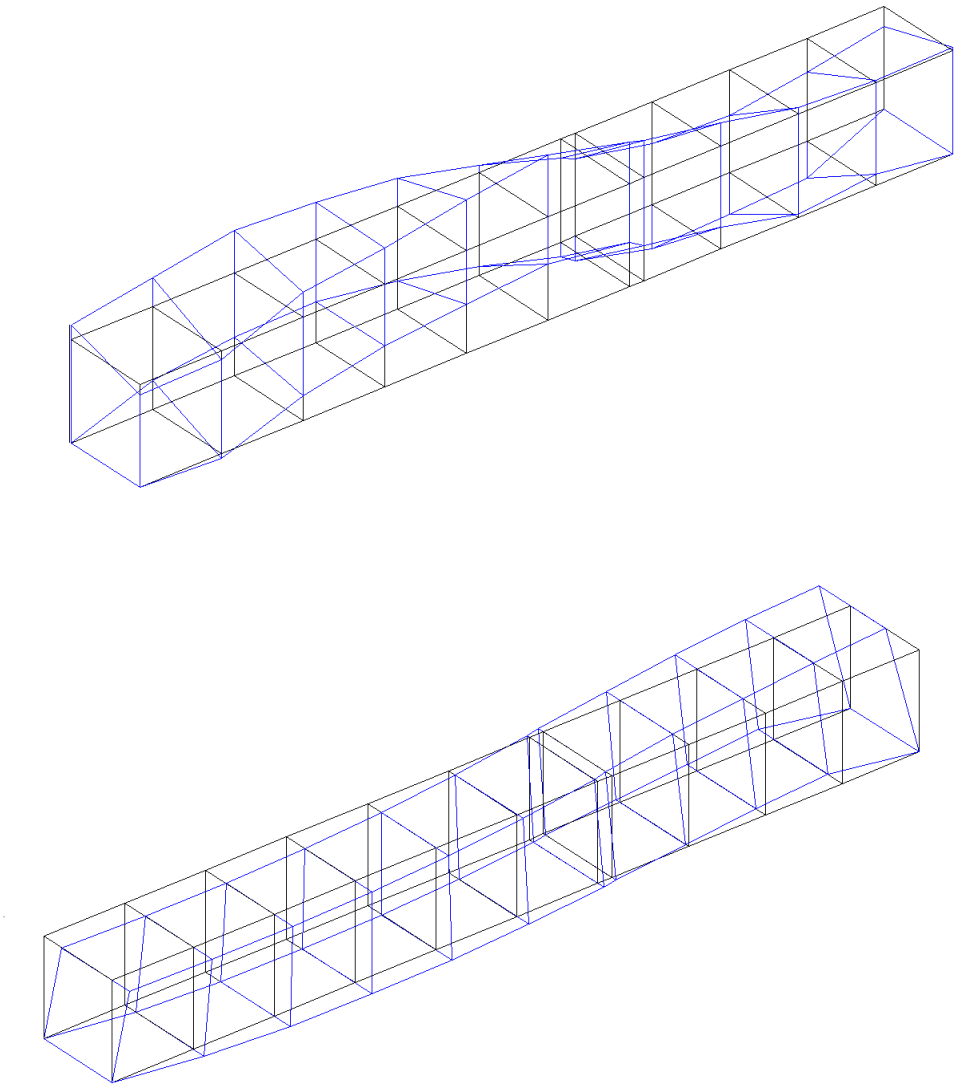

Figure A.6: Sixth mode shape identified at 31.68 Hz (a) Y direction mode, (b) Z direction mode.

The behavior of the Y direction mode shape of the sixth mode is very similar to that of the fifth mode. The Y direction mode shows a 2nd twisting behavior. The Z direction mode also shows distinct 2nd bending behavior for the bottom panel. Since, the top panel does not have any restrictions, it shows 2nd bending of a free-free structure.

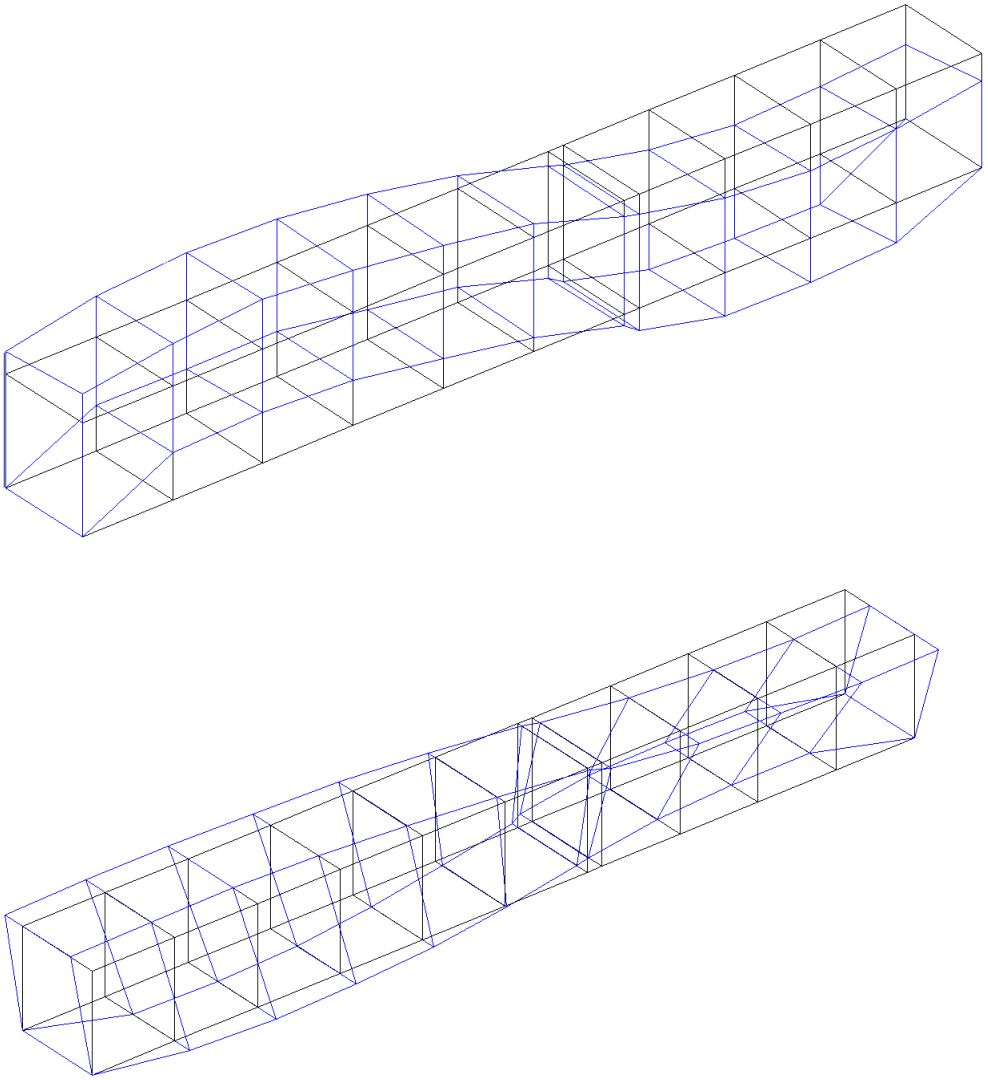

Figure A.7: Seventh mode shape identified at 36.31 Hz (a) Y direction mode, (b) Z direction mode.

The seventh mode at 36.31 Hz shows pure second bending in the Y direction. In the Z direction the mode behavior is similar to the sixth mode but here the bottom panel and top panel oscillations are out of phase.

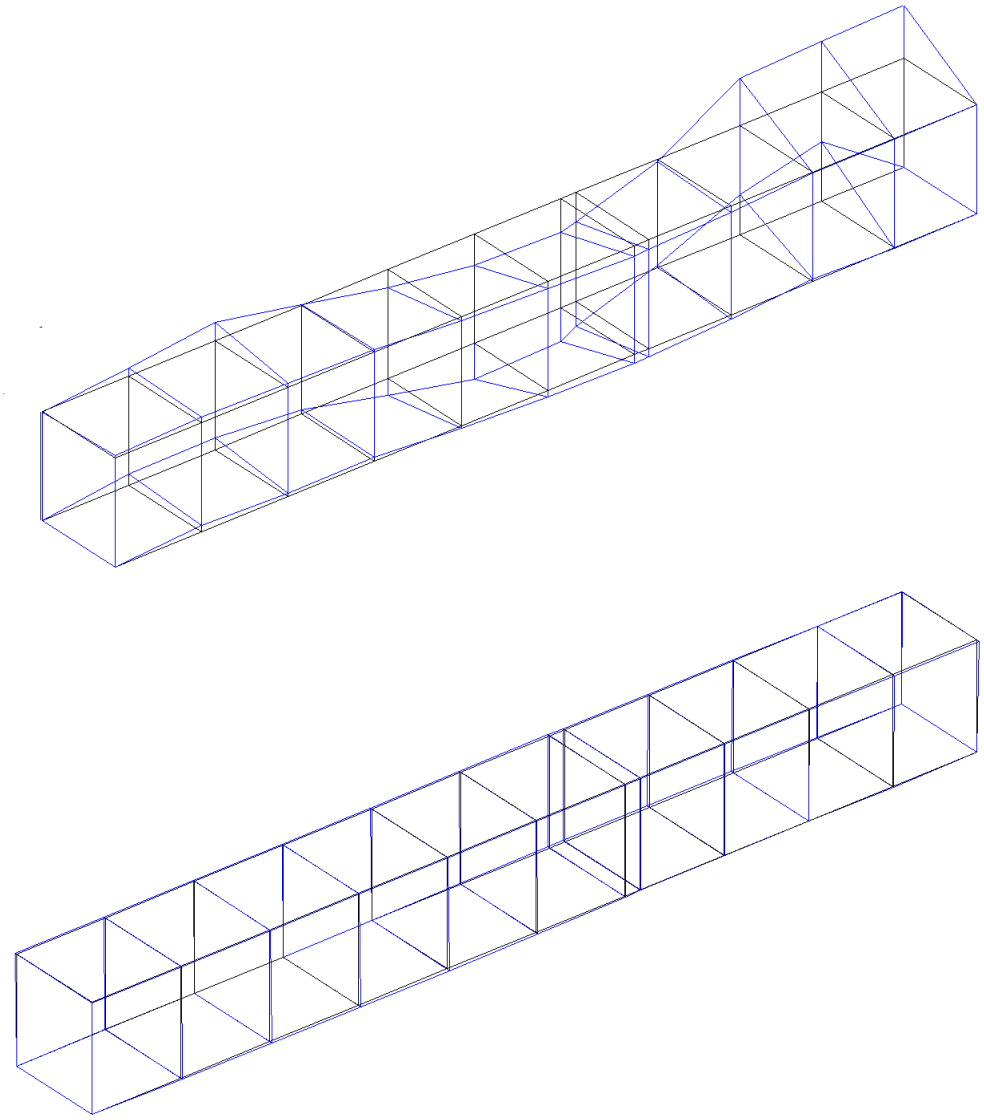

Figure A.8: Eighth mode shape identified at 38.07 Hz (a) Y direction mode, (b) Z direction mode.

The mode shapes begin to show third bending modes in the Y direction at the back panel. The magnitude of oscillation is larger than that of the front panel. The Z direction modes are negligibly small as compared to the Y direction.

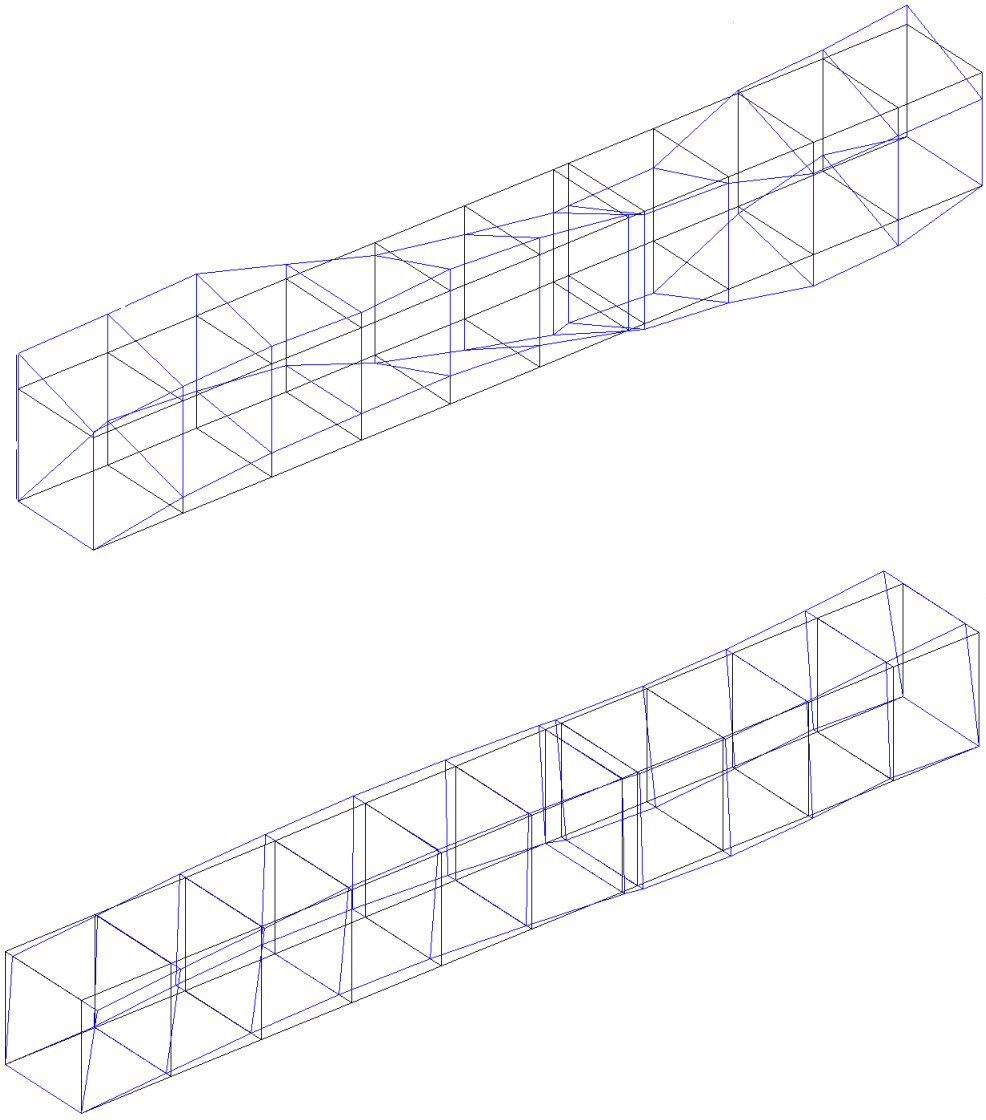

Figure A.9: Ninth mode shape identified at 39.1 Hz (a) Y direction mode, (b) Z direction mode.

In the ninth mode identified, the front panel is showing 2nd mode behavior while the back panel is showing 3rd mode behavior in the Y direction. The Z direction mode shows in phase 3rd bending mode for all the chords.